Hybrid Model for Characterization of Submicron Particles

Using Multiwavelength Spectroscopy

by

Alicia C. Garcia-Lopez

A dissertation submitted in partial fulfillment
of the requirements for the degree of
Doctor of Philosophy
Department of Electrical Engineering
College of Engineering
University of South Florida

Major Professor: Arthur David Snider, Ph.D.
Wilfrido Moreno, Ph.D.
Kenneth Buckle, Ph.D.
Stanley Deans, Ph.D.
Oscar D. Crisalle, Ph.D.

Date of Approval:
March 29, 2005

Keywords: Particle Analysis, Spherical Particles, Non-spherical Particles, In suspension
Particles, Rayleigh-Debye-Gans

© Copyright 2005, Alicia C. Garcia-Lopez

Dedication

I would like to dedicate this dissertation to my younger brother Rodrigo and my family.

Acknowledgments

I would like to acknowledge Prof. L. H. Garcia-Rubio for the permission to use his ideas for this research project, the vast amount of consultation time, and his expertise in the area of particle characterization. I would also like to acknowledge Prof. A. D. Snider for giving me a wonderful graduate experience in pursuing my Ph.D. I have greatly enjoyed working together and your guidance and mathematics expertise have greatly enhanced my life. Finally, I would like to acknowledge the PERC located at the University of Florida for their financial support.

Table of Contents

List of Tables

List of Figures

vii

List of Symbols

α	Angle of directional cosine
β	Angle of directional cosine
γ	Angle of directional cosine
ε	Extinction coefficient for a single chromophore
$\hat{\varepsilon}$	Average extinction coefficient for a single chromophore
ε_m	Molar extinction coefficient for a single chromophore
κ_c	Correction imaginary part of the refractive index
θ	Angle between scattering and incident beam
λ	Wavelength
λ_o	Wavelength in vacuo
π_n	Angle dependent function
φ	Solid angle
τ	Transmission/Turbidity
τ_n	Angle dependent function
ϕ	Rotational Euler angle around Z axis
ψ	Rotational Euler angle around Y axis
ω	Rotational Euler angle around new Z axis
χ	Size parameter

a	Radius
a_n	Mie coefficient
b_n	Mie coefficient
C_{abs}	Absorption cross section
C_{ext}	Extinction cross section
C_{sca}	Scattering cross section
D	Particle diameter
E	Extinction coefficient
$\hat{E}$	Average extinction coefficient
$\dot{E}$	Calculated Extinction coefficient
f	Form factor
G	Cross sectional area
h	Hypochromicity
h_n	Hankel functions
I_o	Incident intensity
I_s	Scattering intensity
k	Wave number
k	Quantity of chromophores
j_n	Bessel functions
l	Pathlength of sample
M_w	Molecular weight
m	Relative refractive index

N	Complex refractive index of particle
N_2	Complex refractive index of medium
N_A	Avogadro's number
N_p	Number of particles
n	Real part of the refractive index of particle
P	Probability of absorption by a photon
P_n	Legendre polynomial
Q_{abs}	Absorption efficiency factor
Q_{ext}	Extinction efficiency factor
Q_{sca}	Scattering efficiency factor
Q'_{ext}	Apparent extinction efficiency factor
Q'_{sca}	Apparent scattering efficiency factor
R	Correction factor
$\hat{R}$	Path averaged correction factor
r	Distance between Middle of Sample and Detector
S	Scattering Amplitude Function
s	Effective Geometric Area of Chromophore
V	Volume of Particle
vf	Volume fraction of

Hybrid Model for Characterization of Submicron Particles Using
Multiwavelength Spectroscopy

Alicia C. Garcia-Lopez

ABSTRACT

The area of particle characterization is expansive; it contains many technologies
and methods of analysis. Light spectroscopy techniques yield information on the joint
property distribution of particles, comprising the chemical composition, size, shape, and
orientation of the particles. The objective of this dissertation is to develop a hybrid
scattering-absorption model incorporating Mie and Rayleigh-Debye-Gans theory to
characterize submicron particles in suspension with multiwavelength spectroscopy.

Rayleigh-Debye-Gans theory (RDG) was chosen as a model to relate the
particle's joint property distribution to the light scattering and absorption phenomena for
submicron particles. A correction model to instrument parameters of relevance was
implemented to Rayleigh-Debye-Gans theory for spheres. Behavior of nonspherical
particles using RDG theory was compared with Mie theory (as a reference). A
multiwavelength assessment of Rayleigh-Debye-Gans theory for spheres was conducted
where strict adherence to the limits could not be followed. Reported corrections to the
refractive indices were implemented to RDG to try and achieve Mie's spectral prediction
for spheres.

The results of studies conducted for RDG concluded the following. The angle of acceptance plays an important role in being able to assess and interpret spectral differences. Multiwavelength transmission spectra contains qualitative information on shape and orientation of non-spherical particles, and it should be possible to extract this information from carefully measured spectra. There is disagreement between Rayleigh-Debye-Gans and Mie theory for transmission simulations with spherical scatterers of different sizes and refractive indices. Finally, it is not possible to adequately or realistically compensate for the differences between Mie and RDG through the use of hypochromicity models and/or effective refractive indices.

A hybrid model combining RDG and Mie theories was developed and tested for spheres of different sizes and refractive indices. The results of hybrid model is that it approximates Mie theory much better than Rayleigh-Debye-Gans for particle sizes smaller than the wavelength and for a broader range of optical properties in the context of multiwavelength spectroscopy. Overall, this new model is an improvement over Rayleigh-Debye-Gans theory in approximating Mie theory for submicron particles and is computationally more effective over other methods. The development of the hybrid spherical model constitutes a platform for developing nonspherical models.

Chapter One

Introduction and Methods

1.1 Introduction

Characterization of particles entails obtaining information about size, shape, orientation and chemical composition. Particle characterization is a broad area of undertaking which encompasses many technologies, among them light spectroscopy techniques. Light spectroscopy typically involves scattering and absorption methods. Scattering measurements are performed at a single wavelength but measured as a function of the direction of observation. For absorption, the light is measured in the forward direction as a function of wavelength. Light scattering techniques typically use highly collimated sources (lasers), whereas absorption spectrophotometric techniques use broadband sources to produce multiwavelength spectra. In either case the resulting spectra can be interpreted with the theory of electromagnetic radiation, which describes interaction of light with matter (Maxwell's Equations). Mie and Rayleigh-Debye-Gans theories are solutions to Maxwell's Equations that relate the particle's joint property distribution to the light scattering and absorption phenomena. This connection is made through the optical properties that are characteristic of the materials contained in the particle.

The objective of this study is to develop a hybrid scattering-absorption model incorporating both theories to characterize submicron particles with multiwavelength spectroscopy. To accomplish this objective Mie theory and Rayleigh-Debye-Gans theory

are revisited and extended to account for the field alteration predicted by Mie, and for the

dipole radiation mechanism employed by Rayleigh-Debye-Gans. Throughout this

dissertation Mie theory and Rayleigh-Debye-Gans theories are emphasized because at

this point they enable real time particle characterization for industrial and biomedical

applications. The largest area of application that would profit from this study is in the

biological and biomedical field in the subject of microbial and disease detection in tissue

and bodily fluids.

1.2 Materials and Methods

The programs for Mie theory, Rayleigh-Debye-Gans theory, instrument models and

hypochromicity were developed in Matlab v6.5.1. Computations for these programs

were conducted using a Dell Inspiron 4100 with 1GHz Pentium III processor and 512

MB RAM. The optical properties (refractive indices) utilized were provided by Dr.

Garcia-Rubio and the SAPD laboratory through the College of Marine Science at the

University of South Florida [17].

The computer codes developed for the analysis of Rayleigh-Debye-Gans and Mie

particles were tested against published values of the scattering functions [1, 14]. In

testing and exploring the algorithms for Rayleigh-Debye-Gans the refractive indices

selected were those of soft bodies and hemoglobin, where soft bodies are defined here as

particles whose relative refractive index is close to one with no absorption component.

The values of the index of refraction $n+i\kappa$ for biological particles commonly used are soft

bodies ($1.45 \leq n \leq 1.04$) and hemoglobin ($1.48 \leq n \leq 1.6$, $0.01 \leq \kappa \leq 0.15$) [17].

Polystyrene ($1.5 \leq n \leq 2.2$, $0.01 \leq \kappa \leq 0.82$), silver bromide ($2.6 \leq n \leq 3.5$,

$0.001 \leq \kappa \leq 1.6$) and silver chloride ($2 \leq n \leq 2.7$, $0.001 < \kappa \leq 0.85$) are materials found

in industrial applications whose properties are used as standards for optical instruments

[17]. Water ($1.3 \leq n \leq 1.4$) was used as the suspending medium. The refractive indices

as function of wavelength are reported in Appendix B.

The ranges of particle volumes were chosen between 12700 nm^3 and 87 μm^3. The

spherical diameter equivalents to the volume range are between 25 nm -5.5 μm. The

table below gives the simulation parameters used to define the suspensions for the

analyses conducted in this dissertation.

Table 1.1: Simulation Parameters

Light Source Wavelength	Particle Concentration	Particle Density
200-900 nm	1E-4 g/cc	1 g/cc

1.3 Overview of Chapters

This dissertation is divided into nine chapters. Chapter two presents a review of Mie and

Rayleigh-Debye-Gans theory, citing the resulting formulas for the scattered field and

their matrix formulations. For each theory the scattering intensity ratio that governs

scattering measurements/simulations and the turbidity formula that governs transmission

measurements/simulations are displayed. The latter formula contains a term proportional

to the scattering cross section, which takes different forms for the two models, and a term

proportional to the absorption cross section, which is the same for both models. Only

simulations of transmission are reported, at multiwavelength.

Chapter three describes aperture correction models that account for the fact that

actual transmission measurements are inevitably polluted by the presence of some near-

forward scattered radiation. The simulations of this effect are for the RDG model only,

for 1 μm hemoglobin spheres.

Chapter four reports a study of nonspherical scatterers, simulating soft body ellipsoids. Transmission curves are compared for two eccentricities, each with three different body orientations, using the RDG model.

Chapter five compares RDG theory and Mie theory for transmission with simulations for spherical scatterers of different sizes and refraction indices. Disagreement between the two theories is demonstrated. The rest of the dissertation is concerned with attempts to modify RDG to bring the transmission simulations into closer agreement with Mie (the exact solution for spheres).

In chapter six, two approaches are described to increase the computed RDG turbidity to that of Mie. The first approach is to use hypochromicity as a correction to RDG to account for absorption. The second approach is based on the observation that the RDG formula for the extinction cross section is (very nearly) a simple quadratic function of n and κ; therefore one can invert this function and find "effective" values of κ or n that will result in turbidity values calculated by RDG in agreement with those computed by Mie. Reasons for rejecting these approaches are cited.

Chapter seven presents the new hybrid model, based on the rigorous Mie calculation of the internal field and the Rayleigh-Debye-Gans approach for the scattering radiation. This theory is developed in full for spheres. In chapter eight the hybrid model is tested by simulated comparisons with Mie and Rayleigh-Debye-Gans theories, employing the span of optical properties of interest.

Finally, conclusions, contributions, and recommendations are covered in chapter nine.

4

Chapter Two

Scattering Theories and Models

This chapter describes light scattering theories and measurements of submicron particles in suspension. The first section provides information on scattering and turbidity measurements used to characterize particles. This section also provides a description of the models used to describe the observed measurement. The subsequent sections provide an outline of Mie theory and RDG theory. These theories describe the scattering phenomena observed in transmission and scattering measurements. Specifically, the scattering intensity ratio as a function of wavelength (in our case a broad wavelength range) and angle of observation, and the turbidity as a function of wavelength (again broad wavelength range) are quantified. Other more computationally intensive, techniques for solving light scattering and absorption problems are discussed. These techniques include the T-Matrix and the Purcell-Pennypacker methods.

2.1 Background

There are many types of spectroscopy measurement used to characterize particles in suspension. Most interest focuses on transmission and scattering measurements. In the former the electromagnetic energy of an incident wave is measured after interaction with a particle or suspension as it leaves the system in the forward direction. In contrast, scattering measurements capture the light after interacting with a particle as it leaves the

system at any angle of observation. They differ because transmission measurements capture both the (forward) scattered light and the unscattered portion of the incident beam. Information concerning the properties of the scattering and absorbing particle is contained in the measured spectra, which are plots of the power intensity versus frequency or wavelength (and, direction). Through the uses of the appropriate theories and models, it is possible to obtain estimates of the size, shape, chemical composition, internal structure, and surface charge from spectroscopic measurements [1].

A complete scheme for particle characterization must take into account various experimental conditions occurring in the lab system when spectroscopy measurements are conducted. These include the type of measurement, instrumentation setup, particle-light interaction, and other optical phenomena. Figure 2.1 illustrates how these components relate to one another. The scattering intensity ratio equation and the turbidity equation are energy balance equations that are developed from the scattering theories studied. A detailed description of the transmission measurement and analysis is provided in chapter three. Refractive indices and corrections are discussed in chapter six.

The desire to characterize particulate systems for real-time continuous monitoring has led to the selection of Rayleigh-Debye-Gans (RDG) theory and Mie theory. Computation time being the restricting factor, these theories provide light scattering solutions in a suitable time. The rest of this chapter is dedicated to the description of Mie and RDG theories along with the development of the corresponding scattering intensity ratio and turbidity formulas.

Complete Particle Characterization
|
Spectroscopy Measurement
|

Scattering Measurement
|
Scattering Intensity Ratio Equation

Transmission Measurement
|
Turbidity Equation

Light Scattering Theories and Models
|
Mie Theory
Rayleigh Theory
Rayleigh-Debye-Gans Theory
Anomalous Diffraction
Geometric Optics + Diffraction

Instrument Models
|
Pinhole Detector
Open Detector

Materials
|
Optical Properties

Kramers-Kronig
Beer-Lambert (in solution)
|
Optical Corrections

Hypochromicity

Figure 2.1: Diagram for Complete Particle Characterization Model

2.2 General Concepts and Equations

The emphasis of this section is the utilization of the scattering matrix formalism to evaluate the extinction of light predicted by the scattering intensity and turbidity equations. Throughout the recent course of light scattering history, the terms turbidity (or optical depth) and optical density have caused much confusion [4]. Turbidity has been traditionally defined as an attenuation coefficient due to scattering (only) for the transmission of the incident beam. Herein, turbidity is described as the *total* attenuation observed due to scattering and absorption. The term optical density (O.D.) was originally used synonymously with absorption; the units of O.D. are absorption unit per pathlength (*Au/cm*). Turbidity will be described in the units of optical density.

The amplitude scattering matrix is used to relate the incident and scattered fields.

$$\begin{pmatrix} E_{\|s} \\ E_{\perp s} \end{pmatrix} = \frac{e^{ik(r-z)}}{-ikr} \begin{pmatrix} S_2 & S_3 \\ S_4 & S_1 \end{pmatrix} \begin{pmatrix} E_{\|i} \\ E_{\perp i} \end{pmatrix}$$

2.1

where $E_{\|i}, E_{\perp i}, E_{\|s}, E_{\perp s}$ are the asymptotic incident and scattering fields parallel and perpendicular to the scattering plane; r is the distance from the scattering center to the detector, z is distance along the axis of propagation of the incoming wave, and k is the propagation constant or wave number in the medium surrounding the particle; $k = (2\pi n_o)/\lambda_o$, where λ_o is the wavelength in vacuo and n_o is the refractive index of the medium.

Van de Hulst [2] describes in detail various assumptions made for simplifying the scattering functions with regard to rotation and symmetry of particles. For a spherical particle S_3 and S_4 are equal to zero. S_1 and S_2 are complex amplitude scattering elements; they depend on the indices of refraction, particle size, and the scattering direction. S_1 and S_2 are given in the Mie model by formidable series expansions involving Bessel, Neumann, and Legendre functions. The expressions for S_1 and S_2 predicted by Mie and RDG theory are provided in subsequent sections.

If the detector is not situated in the forward direction, it is illuminated only by light that is scattered by the particle; its construction shields it from the incident beam. The term "scattering measurement" refers to this configuration. This scattered intensity I_s is given by

$$I_s = \frac{1}{2}\mathrm{Re}\left(\sqrt{\frac{\in}{\mu}}\right)|\vec{E}_s|^2$$

$$= \frac{1}{2}\mathrm{Re}\left(\sqrt{\frac{\in}{\mu}}\right)\left(|\vec{E}_{\parallel,s}|^2 + |\vec{E}_{\perp,s}|^2\right) \qquad 2.2$$

$$= \frac{1}{2}\frac{1}{k^2 r^2}\mathrm{Re}\left(\sqrt{\frac{\in}{\mu}}\right)\left(|S_s \vec{E}_{\parallel,i}|^2 + |S_1 \vec{E}_{\perp,i}|^2\right)$$

where $\in$ is the permittivity and μ is the permeability. If the incoming light is

unpolarized, $|E_{\parallel,i}|^2 = |E_{\perp,i}|^2 = \frac{1}{2}|E_o|^2$ so

$$I_s = \frac{1}{2}\frac{1}{k^2 r^2}\mathrm{Re}\left(\sqrt{\frac{\in}{\mu}}\right)\left(|S_2|^2 + |S_1|^2\right)\frac{|E_o|^2}{2}$$

$$= \frac{1}{2}\frac{|S_2|^2 + |S_1|^2}{k^2 r^2}\frac{1}{2}\mathrm{Re}\left(\sqrt{\frac{\in}{\mu}}\right)|E_o|^2 \qquad 2.3$$

$$= \frac{1}{2}\frac{|S_2|^2 + |S_1|^2}{k^2 r^2}I_o$$

I_s/I_o is known as the scattering intensity ratio.

On the other hand, if the detector is aligned with the incoming beam, it measures the forward scattered wave together with the transmitted incident wave. The analysis of such a "transmission measurement" is most easily conducted by accounting for the energy loss suffered by the original incident beam. There are two loss mechanisms which attenuate the incident beam, scattering and absorption. The power scattered out of the beam by a particle is evaluated by the integrating the scattered intensity over an enclosing sphere "at infinity" (in spherical coordinates).

$$scattered\ power = \int_0^\pi \int_0^{2\pi} I_s(\lambda, r, \theta, \phi)r^2 \sin\theta\, d\phi\, d\theta \qquad 2.4$$

9

It is convenient to define a scattering cross section C_{sca} as the area over which one would integrate the *incoming* intensity I_o to balance the scattered power; thus

$$I_o C_{sca} = scattered\ power \qquad 2.5$$

or

$$C_{sca} = \int_0^\pi \int_0^{2\pi} \frac{I_s(\lambda, r, \theta, \phi)}{I_o} r^2 \sin\theta\, d\phi\, d\theta \qquad 2.6$$

The scattering efficiency Q_{sca} is the ratio of the C_{sca} to the actual cross section G that the particle presents to the incoming beam:

$$Q_{sca} = \frac{C_{sca}}{G} \qquad 2.7$$

The power *absorbed* by the particle will be discussed in detail in chapter five; it too can be expressed using an equivalent area C_{abs}:

$$I_o C_{abs} = absorbed\ power \qquad 2.8$$

According to Van de Hulst [2], the absorption cross section for a particle of volume V and relative refractive index of refraction $m = (n + i\kappa)/n_o$ is given (in both theories) by

$$C_{abs} = 3kV\,\mathrm{Im}\left(\frac{m^2 - 1}{m^2 + 2}\right) \qquad 2.9$$

The absorption efficiency is expressed analogously:

$$Q_{abs} = \frac{C_{abs}}{G} \qquad 2.10$$

Thus one can mathematically characterized the power loss in the incident light as if an area ($C_{sca} + C_{abs}$) were blocked out of the incident beam by each particle. The extinction cross section and efficiency , then, are given by

10

$$C_{ext} = C_{sca} + C_{abs}, \quad Q_{ext} = \frac{C_{ext}}{G} \tag{2.11}$$

If the particle density in the medium is N_p, then in an infinitesimal length dz there are N_pdz particles per unit area; each effectively depletes the beam power by $C_{ext}I$. Therefore the attenuation of the beam intensity $I(z)$ as a function of pathlength z is governed by

$$I(z + dz) - I(z) = -N_p(dz)C_{ext}I(z) \tag{2.12}$$

or

$$\frac{dI_z}{dz} = -N_p C_{ext}I(z) \tag{2.13}$$

The solution to the differential equation is

$$I(z) = I(o)e^{-N_p C_{ext}z} \tag{2.14}$$

The optical theorem [1] states that the extinction cross section can be expressed in terms of the elements of the scattering amplitude matrix in the forward direction

$$C_{ext} = \frac{4\pi}{k^2}\mathrm{Re}[S_1(\theta = 0)] = \frac{4\pi}{k^2}\mathrm{Re}[S_2(\theta = 0)] \tag{2.15}$$

The terms turbidity, or optical density τ are used to characterize the total attenuation in a sample of length l.

$$\tau = N_p C_{ext} l = N_p G Q_{ext} l \tag{2.16}$$

In practice, a detector placed in the forward direction will have a finite aperture, and thus capture some of the radiation scattered at small angles; corrections for this effect are discussed in chapter three.

2.3 Mie Theory and Model

The exact solution to the boundary value problem for light scattering by a sphere is generally referred to as Mie Theory [1]. Mie theory assumes that the spherical scattering object is composed of a homogeneous, possibly absorbing isotropic and optically linear material irradiated by an infinitely extending plane wave.
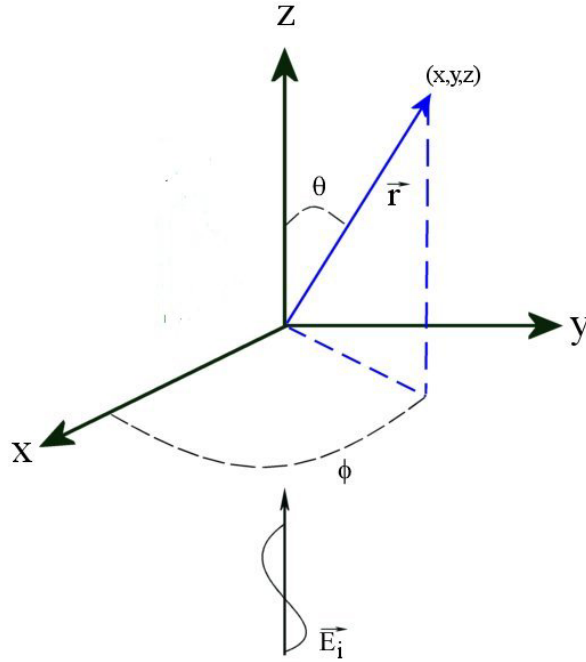
Figure 2.2: Diagram of Coordinate System used in the Mie and RDG Models

In figure 2.2 (x,y,z) refer to Cartesian coordinates and ($\theta,\phi,\vec{r}$) refer to spherical coordinates. The amplitude scattering matrix elements S_1 and S_2 are expressed explicitly as

$$S_1(\theta) = \sum_{n=1}^{\infty} \frac{2n+1}{n(n+1)} \{a_n \, \pi_n(\cos\theta) + b_n \, \tau_n(\cos\theta)\}$$

$$S_2(\theta) = \sum_{n=1}^{\infty} \frac{2n+1}{n(n+1)} \{b_n \, \pi_n(\cos\theta) + a_n \, \tau_n(\cos\theta)\}$$

2.17

where $\pi_n(\cos\theta)$ and $\tau_n(\cos\theta)$ are defined in terms of the associated Legendre polynomial P_n^1;

$$\pi_n(\cos\theta) = \frac{1}{\sin\theta}P_n^1(\cos\theta)$$
$$\tau_n(\cos\theta) = \frac{d}{d\theta}P_n^1(\cos\theta)$$

2.18

Note that there is no ϕ dependence in the Mie model. To calculate the scattering intensity ratio using Mie theory, the equations in 2.17 for the amplitude scattering matrix elements can be substituted into equation 2.2

The amplitude scattering matrix elements for Mie theory at $\theta = 0$ are given by:

$$S(0°) = S_1(0°) = S_2(0°) = \frac{1}{2}\sum_{n=1}^{\infty}(2n+1)(a_n + b_n)$$

2.19

The turbidity formula for Mie theory is calculated by substituting 2.19, into equations 2.15 and 2.16.

Through the direct calculation of the turbidity and scattering intensity ratio equations, Mie theory has been shown to be an effective tool for determining particle size distributions of nonspherical shapes, internal structures, and optical properties [4].

2.4 Rayleigh-Debye-Gans Theory and Model

The basis of the theory for Rayleigh-Debye-Gans scattering is Rayleigh scattering. Rayleigh presented an approximate theory for particles of any shape and size having a relative refractive index near unity, Debye and Gans later added refinements. Kerker [5] states that the fundamental approximation in the Rayleigh-Debye-Gans approach is that the "phase shift", the change of the phase of a light ray that passes through the sphere is

13

negligible. A restriction is therefore put upon the particle size, the wavelength, and the refractive index. For a particle of radius a the restriction is $2ka|m-1| << 1$.

The physical assumption of Rayleigh-Debye-Gans scattering is that each infinitesimal volume element of the particle gives rise to Rayleigh scattering and does so independently of the other volume elements. The waves scattered in a given direction by these elements interfere due to the different positions of the volume elements in space. For spherical and non-spherical particles, a form factor

$$f(\theta) = \frac{1}{V} \int e^{i\delta} dV \qquad\qquad 2.20$$

is introduced that averages the phase difference δ throughout the volumes V of the (spherical and nonspherical) particle; the scattering amplitude elements S_1 and S_2 then take the form of

$$S_1 = \frac{3ik^3}{4\pi}\left(\frac{m^2-1}{m^2+2}\right)V f(\theta) \qquad\qquad 2.21$$

$$S_2 = \frac{3ik^3}{4\pi}\left(\frac{m^2-1}{m^2+2}\right)V f(\theta)\cos\theta \qquad\qquad 2.22$$

were $S_3 = S_4 = 0$. Kerker lists form factors from various shapes, of which some are quoted in this dissertation. In subsequent sections the specific derivation of the form of f is given, as well as a discussion for utilizing f to deduce orientation. A detailed derivation of the scattering intensity ratio equation and the turbidity equation for RDG is developed in Appendix A. The scattering intensity ratio is easily obtained by substituting equations 2.20 and 2.21 for the amplitude scattering elements into equation 2.2. For unpolarized light, 2.3 becomes

$$\frac{I_s}{I_o}(\lambda,\theta) = \frac{9k^4}{32r^2\pi^2}\left|\frac{m^2-1}{m^2+2}\right|^2 V^2 f^2(\theta)(1+\cos^2\theta)$$ 2.23

The scattering cross section C_{sca} is expressed from 2.6 as

$$C_{sca} = \frac{9k^4V^2}{16\pi}\left|\frac{m^2-1}{m^2+2}\right|^2 \int_0^\pi f^2(\theta)(1+\cos^2\theta)\sin\theta\,d\theta$$ 2.24

The general expression for the absorption cross section is, from equation 2.9,

$$C_{abs} = 3kV\,\mathrm{Im}\left(\frac{m^2-1}{m^2+2}\right)$$ 2.25

The extinction cross section is the sum of these two (equation 2.24 and 2.25):

$$C_{ext} = \frac{9k^4V^2}{16\pi}\left|\frac{m^2-1}{m^2+2}\right|^2 \int_0^\pi f^2(\theta)(1+\cos^2\theta)\sin\theta\,d\theta + 3kV\,\mathrm{Im}\left(\frac{m^2-1}{m^2+2}\right)$$ 2.26

The expression for the turbidity for a monodispersed system can then be explicitly expressed by the following equation.

$$\tau = N_p\ell\left(\frac{9k^4V^2}{16\pi}\left|\frac{m^2-1}{m^2+2}\right|^2 \int_0^\pi f^2(\theta)(1+\cos^2\theta)\sin\theta\,d\theta + 3kV\,\mathrm{Im}\left(\frac{m^2-1}{m^2+2}\right)\right)$$ 2.27

2.5 Hybrid Theory and Model

The new scattering model proposed in this dissertation is a hybrid combination of Mie theory and Rayleigh-Debye-Gans theory. Chapter six is dedicated to the description and development of the hybrid theory and model.

2.6 Methods Review

In sections 2.3 and 2.4 the models presented for characterizing particles have been Mie

theory for spherical particles and Rayleigh-Debye-Gans theory for arbitrary shaped

particles. To summarize, Mie theory is an exact mathematical solution to Maxwell's

Equations for light scattered by spheres. It has been used extensively to characterize non-

spherical particles approximately for a broad range of sizes and optical properties.

Although Mie theory provides good estimates of the size and chemical composition it

does not posses the ability to estimate the actual shape and orientation of non-spherical

particles. Rayleigh-Debye-Gans theory provides information on shape and orientation

for spherical and nonspherical particles; however, its applicability has limitations with

regards to size and optical properties of systems.

For the case of nonspherical particles, many exact and approximate methods have

been developed. Singham and Bohren discuss advantages and disadvantages of several

[6, 7]. Two methods considered significant to this investigation are the T-Matrix and

Purcell-Pennypacker method. The T-Matrix is the linear transformation connecting the

coefficients of the eigenfunctions in the scattered field and those for the incident field. It

is through the linearity of Maxwell's equations and the boundary condition satisfied by

the electromagnetic field that these coefficients are linearly related. Bohren states that in

principle the coefficients of the T-matrix are obtainable by integration; however,

computational difficulties arise if the particles are highly absorbing or their shapes

extreme. Recent progress has been made for computing the T-matrix as discussed by

Mishchenko et. al [8]. Mishchenko provides a review and description of several

numerical techniques developed for single and aggregated particles. The scope of this dissertation is on single particles and as such a brief overview follows.

The standard approach for computing the T-matrix for single scatterers is based on the extended boundary condition method developed by Waterman for homogenous particles. Nearly all numerical results computed by the T-matrix relates to bodies of revolution. The first computational advance of the T-matrix is using nonspherical particles of *fixed* orientation using the extended boundary condition method. This method proved to be faster than the conventional separation of variables method for spheroids and discrete dipole approximation integral equation formulation. The disadvantage to using the extended boundary condition method is its poor numerical stability for particles with very large real and/or imaginary parts of the refractive index, large size compared to the wavelength, and/or large extreme geometries.

Mishchenko discusses the iterative extended boundary condition as another approach for overcoming the problem of numerical instability in computing the T-matrix for highly elongated spheroids. The disadvantage of this technique is that the numerical stability comes at the expense of considerable increase in computation code, complexity, and CPU time. The last computational approach discussed by Mishchenko is that of using extended precision instead of double precision floating point variables. This technique provides an increase in size parameter for spheroids and better accuracy. The use of the extended precision variable requires only a negligibly small additional memory and its approach is simple with little additional programming. The disadvantage to the extended precision is the CPU time.

In the Purcell-Pennypacker method a particle is approximated by a lattice of dipoles, each small compared with the wavelength but still large enough to contain many atoms. Each dipole is excited by the incident field and by the fields of all the other dipoles. Two methods are used to solve for these equations; either iteration or matrix inversion. The iterative method is slow for large parameters, dipoles and values of the refractive index. The matrix inversion method, although useful for calculating scattering by a particle in more than one orientation and for orientational averaging over an ensemble of particles, is limited to small number of dipoles.

An embedding method using a scattering-orders approach was developed by Singham and Bohren [6]. The scattering-orders perturbation method is an extension of the series for the perturbation method which looks upon a nonspherical particle as a sphere, the boundary of which is distorted or perturbed by different amounts at different points [1]. In the case of Singham and Bohren, the scattering-order perturbation method is used to formulate the coupled dipole method. This method uses the dipolar interactions as infinite series in scattering-orders. Two interactions exist, those between dipoles within the sphere and all others. The scattering fields resulting in the dipole interaction within the sphere are described by Mie theory or any other equivalent theory. It was demonstrated that this method worked and shortened computation time. However, it was limited by the scattering-order series, which can diverge. The greater the refractive index, the smaller the particle size for which it diverges.

The endeavor to characterize bioparticulates in the context of engineering application requires identifying the problem, finding solutions, analyzing, designing and testing of the solution all taking place in real-time. Mie, Rayleigh-Debye-Gans, and the new hybrid theory provide a more palatable means to characterize biological systems as compared to those aforementioned. The rest of this dissertation describes how these theories are utilized and explored.

Chapter Three

Instrumentation Correction Model for Transmission

The research presented in this document utilizes many models to represent those

conditions present when taking experimental measurements. As stated in the previous

chapter and illustrated in figure 2.1, light scattering, instrumentation and optical formulas

are integrated to make up a complete model for experimental conditions observed when

taking turbidity measurements. The previous chapter described the light scattering

equations for the intensity ratio and transmission spectroscopy measurements. This

chapter is dedicated to discussing the instrument formulas available for simulating

transmission measurements and implementation of the formulas to RDG theory.

3.1 Instrumentation Correction Model

Deepak et al. [9] defines the expression "forward scattering for a single scattering

phenomenon" as scattered radiation reaching the detector after being scattered only once

by a scatterer situated within the path of the direct radiation. Ideally, the conditions for

turbidity measurements entail a non-divergent beam illuminating a homogeneous

medium and a detector directly, opposite the light source, possessing an acceptance angle

close to zero (to capture light solely in the forward direction). The turbidity equation

presented in the previous chapter does not account for the instrument setup, therefore an

instrument model or correction to the turbidity is introduced in this chapter. On the basis

of the scattering theories presented and the instrument setup used for transmission

measurements, the correction factor provided by Deepak et al. was chosen.

The correction factor is dependent upon the geometry of the transmission

measurement through the angle θ, subtended at the scatterer by the detector window

(figure 3.1). Therefore the instrument design has to be taken into account. For

completeness the two designs provided by Deepak et al. were implemented [9]: the open

detector and pinhole detector. The geometries are illustrated in figure 3.1 (a) and (b).

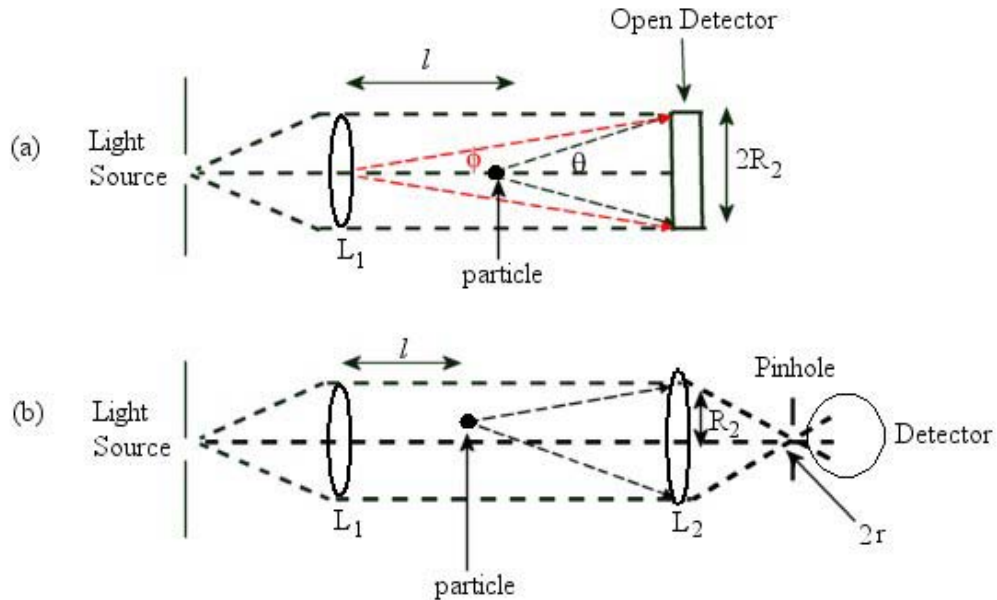Figure 3.1: Transmission System (a) Open Detector (b)Pinhole Detector

Deepak et al. states that the true optical depth τ from transmission measurements

cannot be obtained directly. Deepak et al. notes that the finite aperture of the detector, in

a transmission measurement, picks up some additional light that has been scattered into

the aperture. As seen in chapter two the turbidity formula (equation 2.16)

$$\tau = N_p l(C_{sca} + C_{abs}) = N_p lG(Q_{sca} + Q_{abs}) = N_p lQ_{ext} \qquad 3.1$$

accounts for light that has been scattered out of, or absorbed from, the incident beam.

Recall that the power scattered by a particle equals (equation 2.4)

$$scattered\ power = \int_0^\pi \int_0^{2\pi} I_s(\lambda, r, \theta, \phi) r^2 \sin\theta d\phi d\theta = C_{sca} I_o \qquad 3.2$$

However, if the finite aperture captures scattered light within a cone of half-angle δ in the

forward direction, then the beam depletion due to scattering only

$$\int_\delta^\pi \int_0^{2\pi} I_s(\lambda, r, \theta, \phi) r^2 \sin\theta d\phi d\theta\ , \qquad 3.3$$

giving an effective scattering cross section of

$$C'_{sca} = C_{sca} - \int_\delta^\pi \int_0^{2\pi} \frac{I_s(\lambda, r, \theta, \phi)}{I_o} r^2 \sin\theta d\phi d\theta \qquad 3.4$$

The apparent extinction cross section of the particle can be written

$$C'_{ext} = C'_{sca} + C_{abs} = C_{sca} + C_{abs} - \int_\delta^\pi \int_0^{2\pi} \frac{I_s(\lambda, r, \theta, \phi)}{I_o} r^2 \sin\theta d\phi d\theta \qquad 3.5$$

or

$$\frac{C_{ext}}{C'_{ext}} = 1 - \frac{1}{C_{ext}} = \int_\delta^\pi \int_0^{2\pi} \frac{I_s(\lambda, r, \theta, \phi)}{I_o} r^2 \sin\theta d\phi d\theta \equiv P(\delta) \qquad 3.6$$

In the open detector system (figure 3.1a) a radiation source is placed at the focal

length of the transmitter lens L_1, which transmits a parallel beam through the medium of

thickness l, which is in turn measured by an open detector of radius R_2. The path

averaged correction factor $\hat{P}$ for particles on axis is defined as

$$\hat{P} = \tan\delta \int_{\phi}^{\frac{\pi}{2}} R(\chi,\delta)\csc^2\phi \, d\phi \qquad 3.7$$

where the angle δ for the scatters satisfies $\tan\delta = R_2/L_1$. The pinhole detector system (Figure 3.1b) consists of a radiation source placed at the focal point of a lens L_1. A second lens L_2, with focal length f, focuses the light through an aperture of radius r in the focal plane and onto the detector. The path averaged correction factor $\hat{P}$ for the pinhole detector is simply

$$\hat{P} = P(\delta) \qquad 3.8$$

The result of equation 3.2 stems from the fact that δ is determined by $\tan\delta = r/f$, which stays constant.

The correction factor corresponding to the design set up can be introduced into the turbidity equation, equation 2.11, by multiplying through by $\hat{P}(\delta)$:

$$\tau(\lambda) = N_p l \, \pi a^2 Q_{ext}(\chi,m)\hat{P}(\delta) \qquad 3.9$$

3.2 Implementation of Instrument Corrections

The corrections for scattering developed by Deepak [9] have been evaluated for RDG theory for hemoglobin spheres. Hemoglobin spheres are hypothetical spheres whose refractive indices are those of hemoglobin. The refractive indices of hemoglobin were used to test these effects for strong scattering and absorption relative refractive indices ($1 \le n/n_o \le 1.2$, $0.001 \le \kappa/n_o \le 0.1$). The acceptance angle for spectrometer detectors are typically less than or equal to 2 degrees. The acceptance angles studied for both detector

23

configurations were 1, 2, and 5 degrees for a spherical particle of 1 μm. The parameters used to conduct the simulations are provided in table 1.1.

Figures 3.2 and 3.3 show the simulated transmissions using Rayleigh-Debye-Gans theory with and without acceptance angle corrections for each detector configuration. The (uncorrected) Mie theory simulation is included as a reference. The pinhole detector setup (figure 3.2) shows smaller subtle changes in the corrected spectra for all angles (RDG_1, RDG_2, RDG_5) compared to uncorrected (RDG) spectra. The open detector setup (figure 3.3) shows dramatic changes in the spectra as the aperture angle increases. It is evident that the angle of acceptance plays an important role in being able to assess and interpret spectral differences. Bohren has made similar statements concerning the angle of acceptance though here calculations have been provided.

Having demonstrated the methodology for correcting for finite detector apertures in transmission measurements, we next turn to a study of the effects of particle shape and orientation. Aperture corrections are omitted in the simulations reported in the remainder of the dissertation, except where noted.
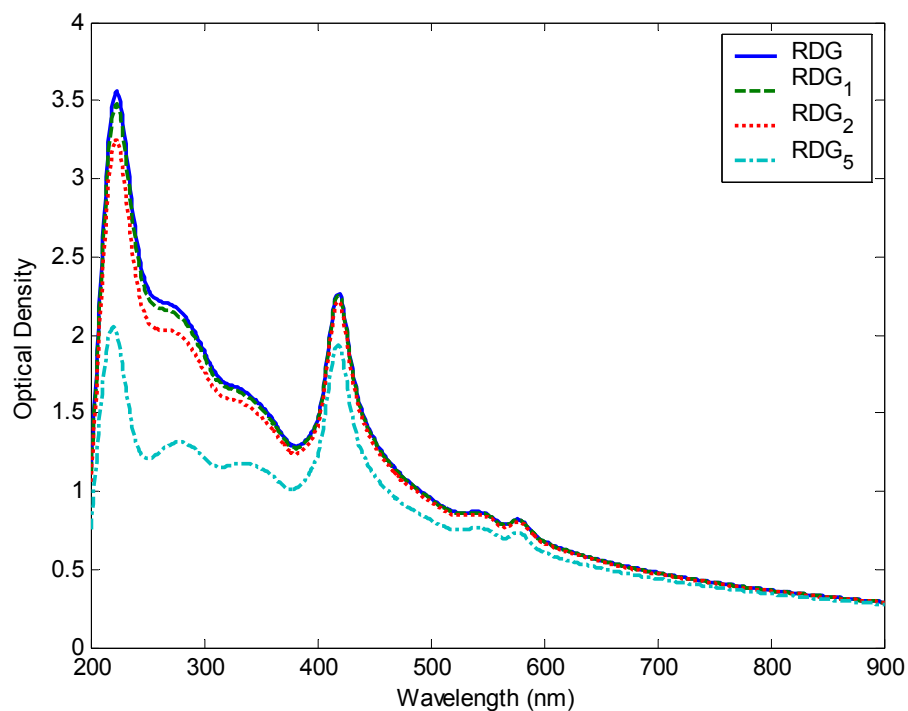
Figure 3.2: Calculated Transmission of Rayleigh-Debye-Gans for 1 μm Hemoglobin Spheres with Pinhole Detector Setup
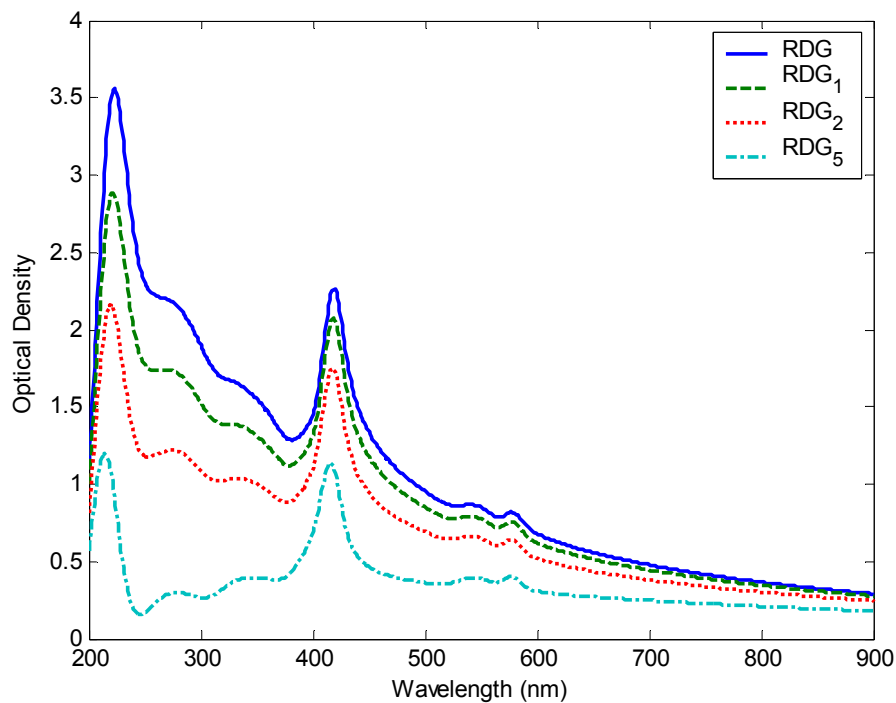
Figure 3.3: Calculated Transmission of Rayleigh-Debye-Gans for 1 μm Hemoglobin Spheres with Open Detector Setup

Chapter Four

Nonspherical Particles

Form factors have been developed for many shapes such as cylinders, disks, rods,

spheres, and ellipsoids. We are interested in biological systems, whose particles are best

represented by ellipsoids.

4.1 Geometry and Notation for Ellipsoids

It is convenient to carry out the present analysis in two non-standard, left handed

coordinate systems, the laboratory and particle frame. The laboratory frame establishes

the position and orientation of the particle relative to the source and detector. The

particle frame exploits the convenience of particle coordinates in describing the

scattering. Therefore scattering calculations are in the particle frame and related back to

the laboratory frame. Unit vectors along the x_L, y_L, and z_L axes in the lab frame are

denoted by $\vec{i}_L, \vec{j}_L$, and $\vec{k}_L$; and similarly for the particle frame.
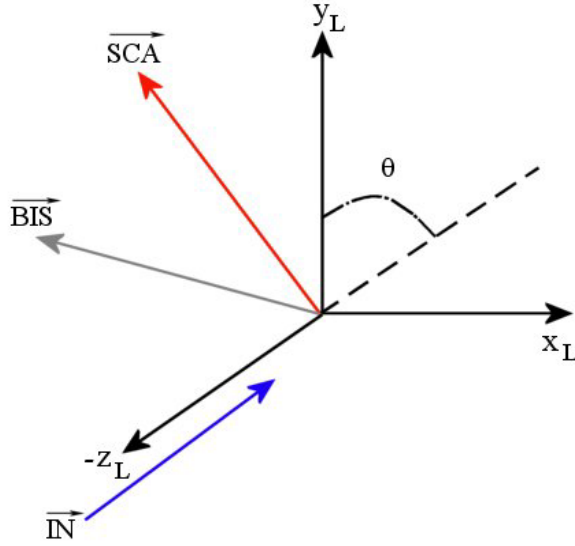
Figure 4.1: Light Scattering in Laboratory Frame
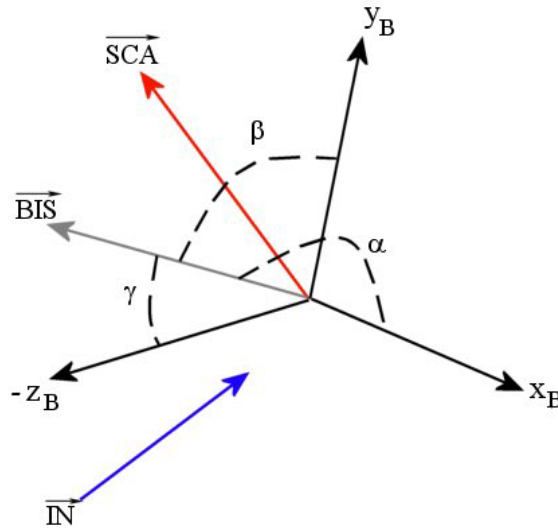
Figure 4.2: Light Scattering in Particle Frame

The behavior of light scattered from the particle is dependent upon its size, shape,

orientation and chemical composition. Figure 4.1 illustrates the incident beam

approaching the particle in the z_L-direction in the laboratory frame. The light scattered

from the particle can radiate in all directions. The line in the scattering plane that bisects

the angle $\pi-\theta$ between the incident and scattered beam is called the bisectrix [2], denoted

by $\overrightarrow{BIS}$ in figures 4.1 and 4.2. The plane through the bisectrix ($\overrightarrow{BIS}$) and perpendicular

to the plane of the scattering ($\overrightarrow{SCA}$) will be called the bisectrix plane.

Equation 4.1 describes the directions of incident light, scattered light and the

bisectrix from the laboratory frame.

$$
\begin{aligned}
\overrightarrow{IN} &= \vec{k}_L \\
\overrightarrow{SCA} &= \sin\theta \vec{i}_L - \cos\theta \vec{k}_L \\
\overrightarrow{BIS} &= \overrightarrow{SCA} - \overrightarrow{IN} = \sin\theta \vec{i}_L - (\cos\theta + 1)\vec{k}_L
\end{aligned}
\qquad 4.1
$$

The description can also be expressed in the particle frame. Figure 4.2 shows the angles

α, β, γ used to relate the bisectrix to the particle axes. Calculation of the scattered light

intensity at different angles in the laboratory frame can be reconstructed through its

relation to the particle frame.

$$
\begin{vmatrix} i_L \\ j_L \\ k_L \end{vmatrix} = E \begin{vmatrix} i_p \\ j_p \\ k_p \end{vmatrix}
\qquad 4.2
$$

where $i_p = |1\ 0\ 0|$, $j_p = |0\ 1\ 0|$, $k_p = |0\ 0\ 1|$ in the particle frame, the Euler angles ψ, ϕ, ω are

used to relate the frames using the zyz' Euler rotation sequence, and E is given by .

$$
E = \begin{vmatrix} \cos\psi \cos\omega \cos\phi - \sin\psi \sin\phi & \sin\psi \cos\omega \cos\phi + \cos\psi \sin\phi & -\sin\omega \cos\phi \\ -\cos\psi \cos\omega \sin\phi - \sin\psi \cos\phi & -\sin\psi \cos\omega \sin\phi + \cos\psi \cos\phi & \sin\omega \sin\phi \\ \cos\psi \sin\omega & \sin\psi \sin\omega & \cos\omega \end{vmatrix}
$$

$$
4.3
$$

Using this relationship, the directional cosines of angles α, β, γ can be found in the

laboratory frame to mathematically describe the bisectrix (equation 4.1).

$$
\cos\alpha = \frac{\overrightarrow{BIS}}{\left|\overrightarrow{BIS}\right|} \cdot \vec{i}_L, \quad \cos\beta = \frac{\overrightarrow{BIS}}{\left|\overrightarrow{BIS}\right|} \cdot \vec{j}_L, \quad \cos\gamma = \frac{\overrightarrow{BIS}}{\left|\overrightarrow{BIS}\right|} \cdot \vec{k}_L
\qquad 4.4
$$

In the case of an ellipsoid with a fixed orientation, we can see the use of the directional

cosines in the form factor computed by Kerker:

$$f^2(\theta) = \frac{9\pi J_{3/2}^2(u)}{2u^3}$$

$$u = hA \tag{4.5}$$

$$A = a^2 \cos^2 \alpha + b^2 \cos^2 \beta + c^2 \cos^2 \gamma$$

where A is a vector described by the directional cosines and a, b, c are the semiaxes for

ellipsoid. The variable h equals $h = \frac{4\pi}{\lambda} \sin\left(\frac{\theta}{2}\right)$.

The following is a short table of various form factors, pertinent to this work, taken

from Kerker [4]. The equations presented in this section were programmed; simulations

conducted are reported in the next section.

Table 4.1: Table of Form Factors

Shapes	Definition of variables	Form factor $f^2(\theta)$
Sphere	Radius=a $u=ha$	$\dfrac{9\pi J_{3/2}^2(u)}{2u^3}$
Concentric Sphere with spherical shell	Inner radius=a Outer radius=b $u=ha$ $v=hb$ Inner refractive index=m1 Inner refractive index=m2	$\dfrac{9\pi}{2}\left[\dfrac{J_{3/2}(v)}{v^{3/2}} + \left(\dfrac{m^1-m2}{m^2-1}\right)\left(\dfrac{a^3}{b^3}\right)\dfrac{J_{3/2}(u)}{u^{3/2}}\right]$
Ellipsoid of Revolution	Semi axes are a,b, β is angle between figure axis & bisectrix $u=h(a^2\cos^2\beta+b^2\sin^2\beta)^{1/2}$	$\dfrac{9\pi J_{3/2}^2(u)}{2u^3}$
Ellipsoid	Semi axes are a,b,c $u=hA$ $A^2=a^2\cos^2\alpha+b^2\cos^2\beta+$ $c^2\cos^2\gamma$ α,β,γ are the directional cosines of the bisectrix	$\dfrac{9\pi J_{3/2}^2(u)}{2u^3}$

4.2 Ellipsoid Simulations

For the simulation of the effects of shape and orientation on the multiwavelength transmission spectra, prolate ellipsoids with refractive indices of soft particles have been selected. Ellipsoids have been used to model the scattering behavior of a large variety of biological systems such as microorganisms and red blood cells, and offer the possibility of exploring geometrical extremes between spheres and needle-like particles. The semimajor and semiminor axes for prolate ellipsoid were determined for a volume equivalent to 1 μm diameter sphere.

For absorption it is apparent from equation 2.9 that the pathlength for the particle is not relevant since the absorbed power is proportional to the volume. Nevertheless, scattering is proportional to the cross sectional area and therefore orientation. For a prolate ellipsoid with length a along its semimajor axis and lengths $b=c$ ($<a$) along its semiminor axes, the eccentricity ($\varepsilon = c/a$) values tested were 0.3 and 0.8. Figure 4.3 illustrates three orientations studied for the ellipsoid. Consider the extinction cross sectional area of the particle as the shadow projected on the forward plane (Geometrical Optics). Orientation A illuminates the ellipsoid along a semiminor axis, here the largest cross sectional area (football shape) is projected with the light passing through the shortest pathlength of the ellipsoid. Orientation B illuminates the ellipsoid along the semimajor axis; here the smallest cross sectional area (circle) is projected with the light passing through at the longest pathlength of the particle. Finally, orientation C illuminates across the ellipsoid along a nonaxial direction, here the projection of the particle and the light passing through are intermediate to those of orientation A and B. The orientations stated represent extreme cases for a particle fixed in space.

30

Orientation A

Orientation B
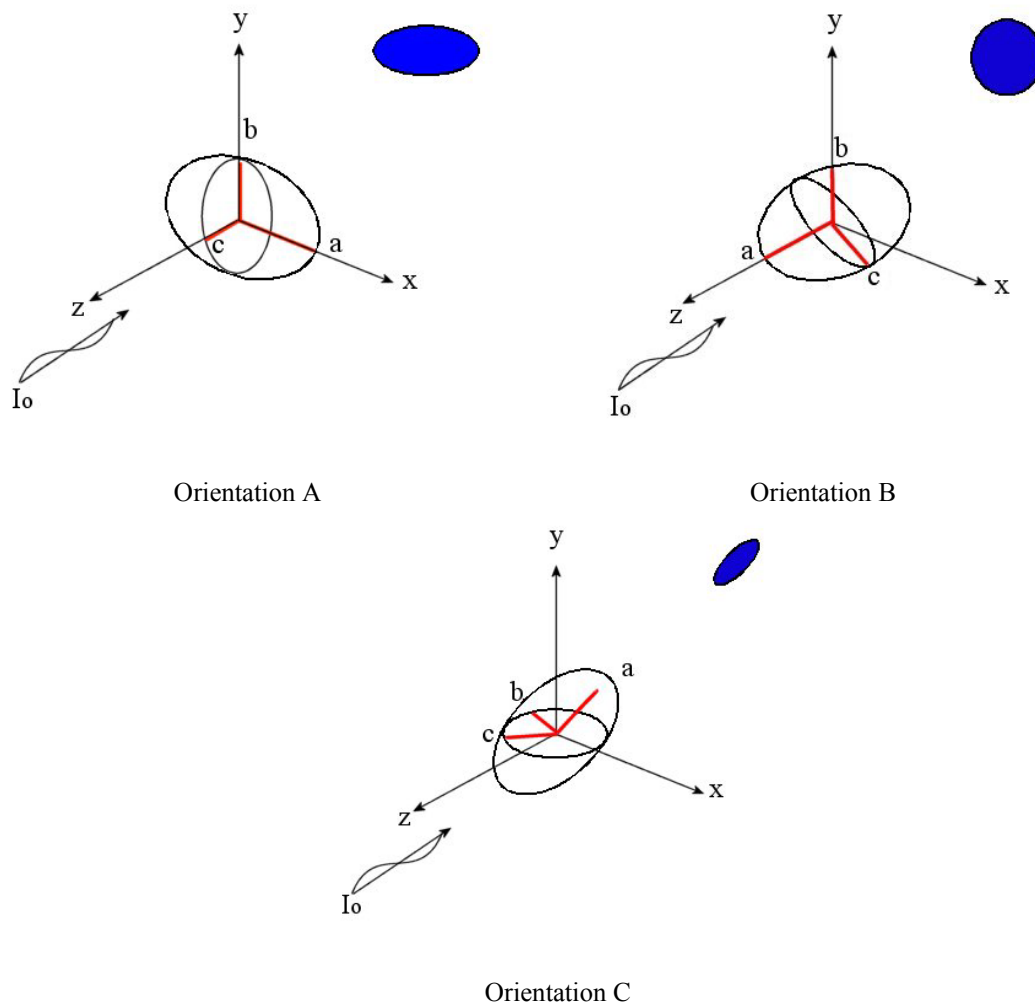
Orientation C

Figure 4.3: Fixed Orientations A, B, and C for an Ellipsoid

For each of these orientations the projected cross sectional area in the laboratory

xy plane and average pathlength along the laboratory z axis were calculated. These

projected values were used to compute the transmission (using the RDG form factors as

presented earlier). The algorithms for Rayleigh-Debye-Gans calculations for non-

spherical particles with volumes equivalent to that of a 1 μm diameter sphere, were tested

against Mie calculations for the sphere, using the relative refractive indices in the range

where the RDG assumptions are met; for these case studies the refractive indices of soft

31

bodies were used. The multiwavelength turbidity spectra were calculated for soft body ellipsoids for two eccentricity values and three fixed orientations.

The multiwavelength turbidity spectra for the soft body ellipsoids are plotted along side the calculated turbidity using Mie theory. Figure 4.4 shows the effect of the particle orientation (A, B, C) for a prolate ellipsoid with an eccentricity of 0.3. Figure 4.5 shows the turbidity for an ellipsoid with an eccentricity of 0.8. (An eccentricity of 1 for an ellipsoid results in a sphere; thus the predicted spectra for RDG should be the same as for Mie theory.) Comparison of ellipsoids with varying eccentricities (figures 4.4 and 4.5) shows that particle orientation and shape have a significant effect on the features and amplitude of the multiwavelength turbidity, in the RDG model.

Multiwavelength transmission spectra contain quantitative and qualitative information on shape and orientation of non-spherical particles, and it should be possible to extract this information from carefully measured spectra. This conclusion is in agreement with the results reported in Buehler [18].
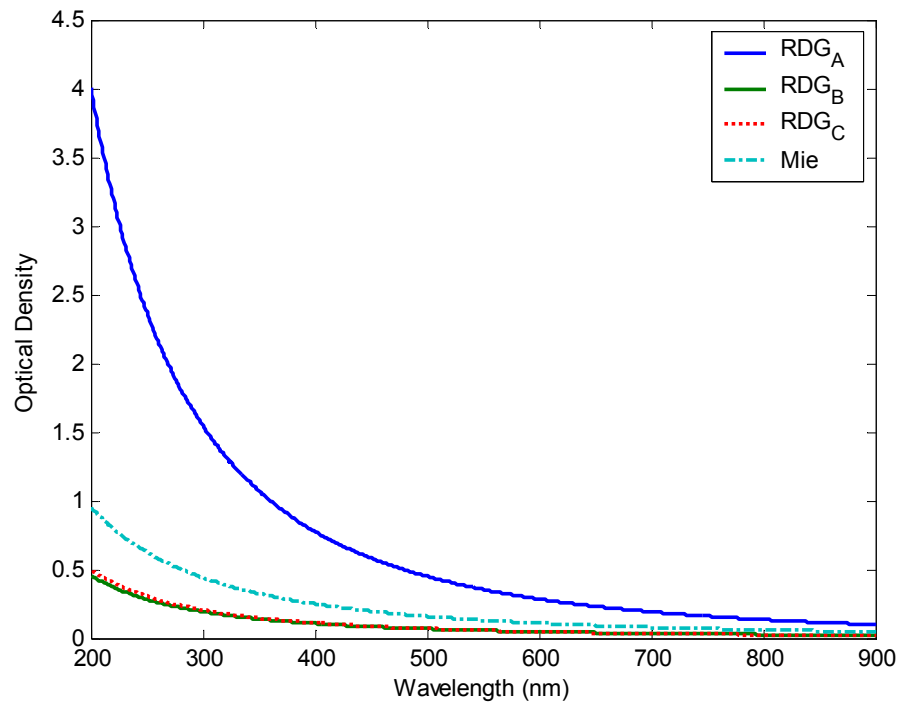
Figure 4.4: Calculated Transmission of Soft Body Prolate Ellipsoid $\varepsilon=0.3$ with a Volume Equivalent to a 1 μm Sphere
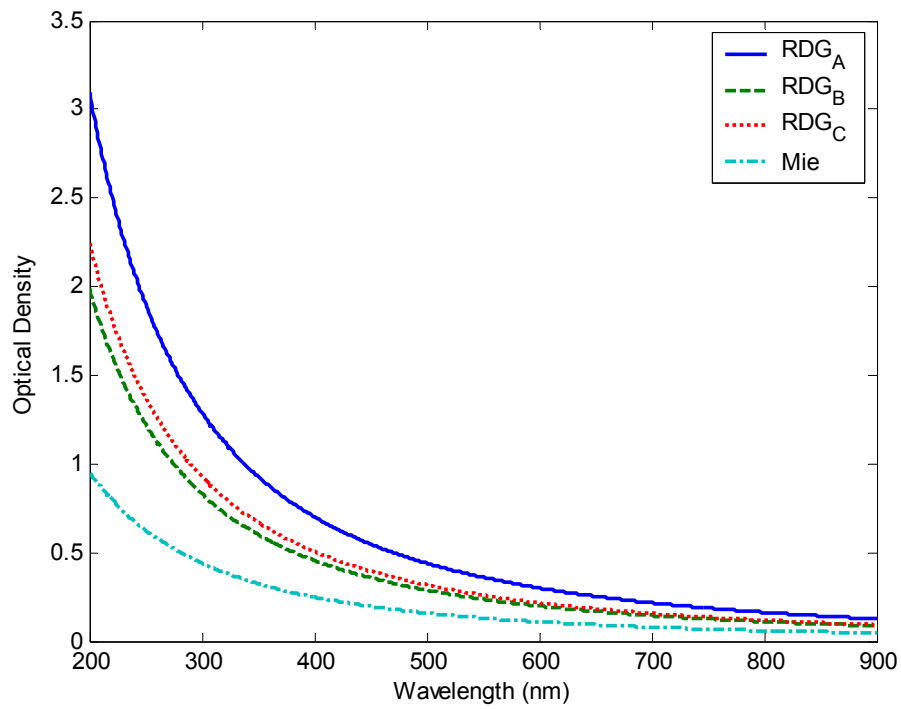

Figure 4.5: Calculated Transmission of Soft Body Prolate Ellipsoid $\varepsilon=0.8$ with a Volume Equivalent to a 1 μm Sphere

Chapter Five

Validation Study of Rayleigh-Debye-Gans Theory

This chapter scrutinizes Rayleigh-Debye-Gans theory by simulating a broad range of

refractive indices and particle sizes, probing the limitations imposed by the assumptions

and approximations implicit in the theory.

5.1 Exploration of Theoretical Limits

The limits of Rayleigh-Debye-Gans model were discussed in chapter two. To

summarize: the relative refractive index m must be close to one and the size of the

particle must be much smaller than $\lambda/|m-1|$. There exists a trade off for the limits of

RDG theory; first, if m is close to one and no absorption is present then the size of the

particle can be the same order of magnitude as the wavelength. Conversely, if absorption

is present and m is greater than one, the particle size must be smaller than the wavelength.

Although these assumptions are invoked in the derivation of the theory, scope of the

present research and the complexity of its models calls for a reevaluation of these

restrictions for multiwavelength measurements where strict adherence to the limits cannot

be followed. Three approaches were taken to explore, through simulation, the constraints

of this theory for spheres. First, the sizes of the spherical particles were kept small

compared to the wavelengths, but the wavelength-dependent relative refractive index was

allowed to significantly exceed one , typical of actual materials.

Second, the relative refractive index was kept close to one while the absorption was held at zero, and particle sizes comparable to the wavelengths were considered. Third, the contribution of absorption in the relative refractive index, kept close to 1, was investigated for particle sizes comparable to the wavelengths. The following subsections describe in more detail the parameters used and the conclusions and observations drawn.

5.2 Particle Diameter << Wavelength

The first of the sensitivity studies conducted tested the limits of Rayleigh-Debye-Gans for relative refractive indices greater than one and the absorption greater than zero, while keeping small sized spherical particles, compared to the wavelengths (200 nm-900 nm). The multiwavelength transmission spectra were calculated for Mie and Rayleigh-Debye-Gans using spheres of silver bromide ($1.1 \leq n/n_o \leq 2.4$, $0.0001 \leq \kappa \leq 0.85$) and spheres of silver chloride ($1.1 \leq n/n_o \leq 2.4$, $0.0001 \leq \kappa \leq 0.6$). The spherical diameter sizes chosen were 25 nm and 50 nm. Particle concentration, particle density, and wavelength range were kept constant

Figures 5.1, 5.2 show that Rayleigh-Debye-Gans gives an adequate approximation to Mie for particle sizes much smaller than the wavelength. Figures 5.3, 5.4 reveals that for slightly larger particles Rayleigh-Debye-Gans no longer closely follows Mie Theory. Notice that in the spectral region where absorption is small (300-900 nm) both theories coincide even though n/n_o>1. However, where strong absorption is present, the theories rapidly diverge (see the optical properties of AgBr and AgCl reported in Appendix B), clearly suggesting that absorption plays an important role in the disparity between the theories.

Figure 5.1: Calculated Transmission of Mie and Rayleigh-Debye-Gans for a Suspension of 25 nm AgBr Spheres

Figure 5.2: Calculated Transmission of Mie and Rayleigh-Debye-Gans for a Suspension of 25 nm AgCl Spheres
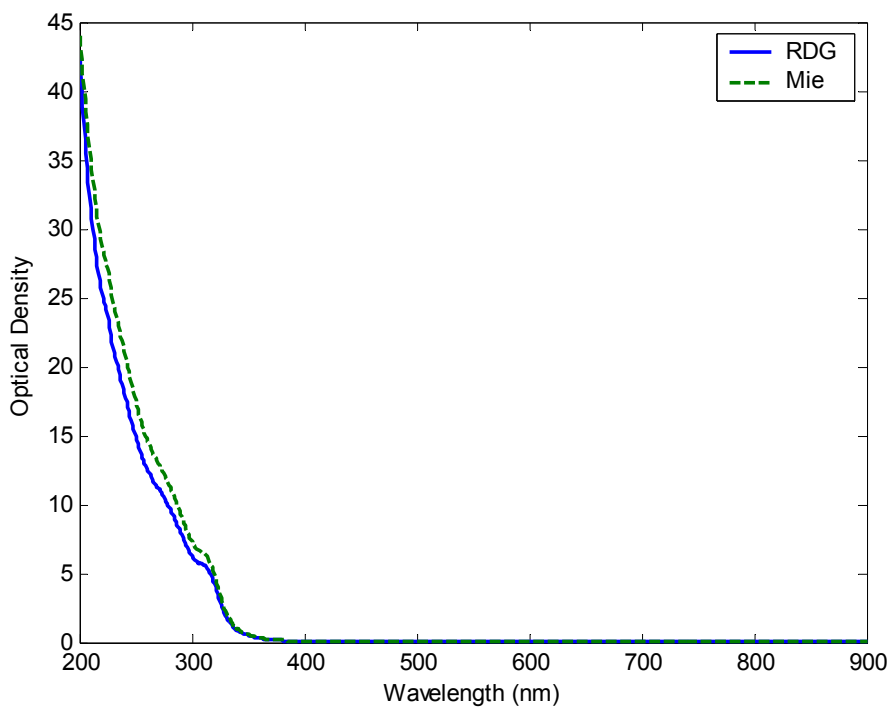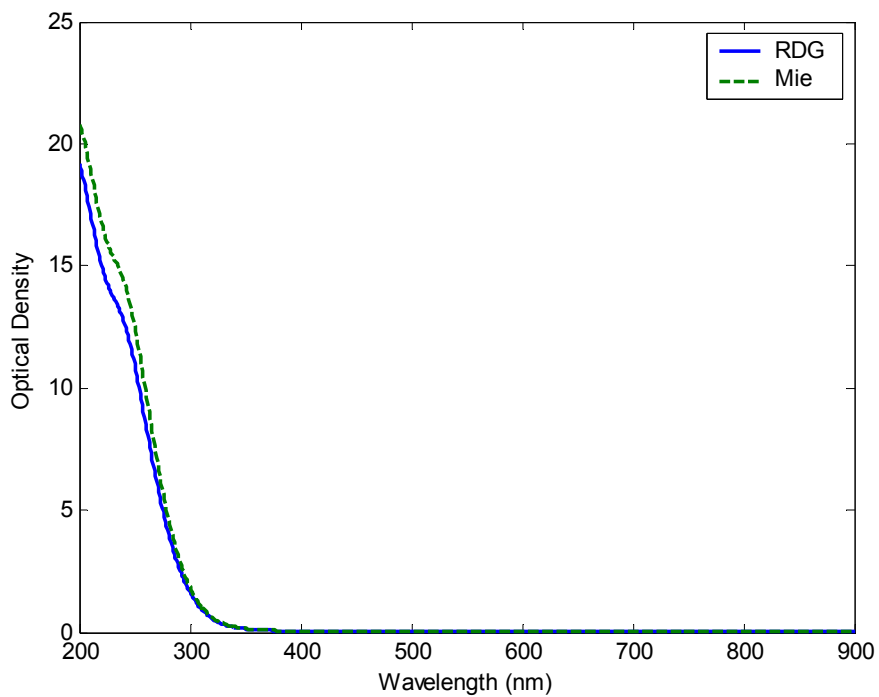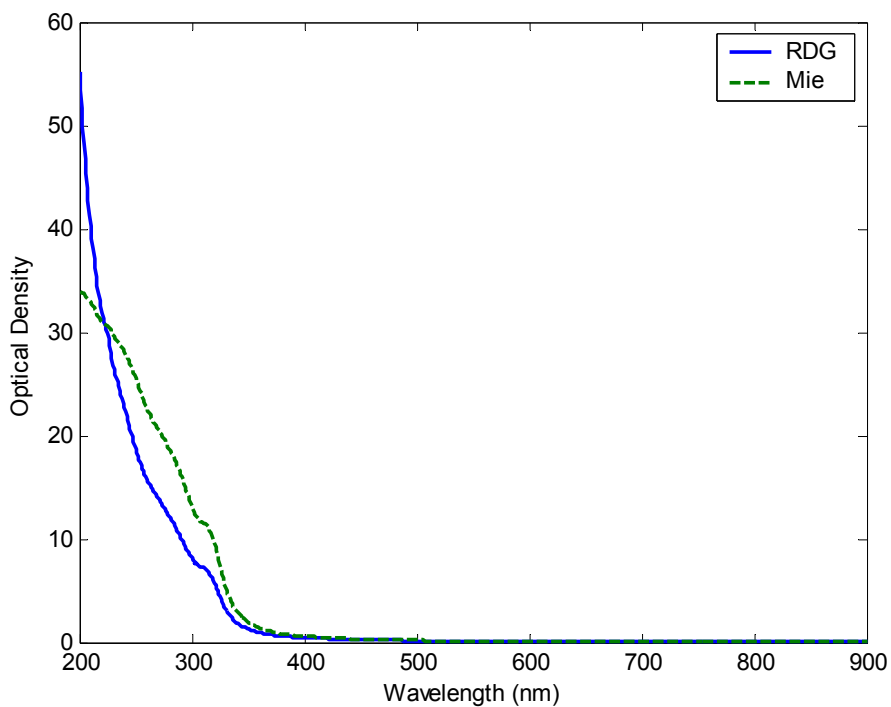
Figure 5.3: Calculated Transmission of Mie and Rayleigh-Debye-Gans for a Suspension of 50 nm AgBr Spheres
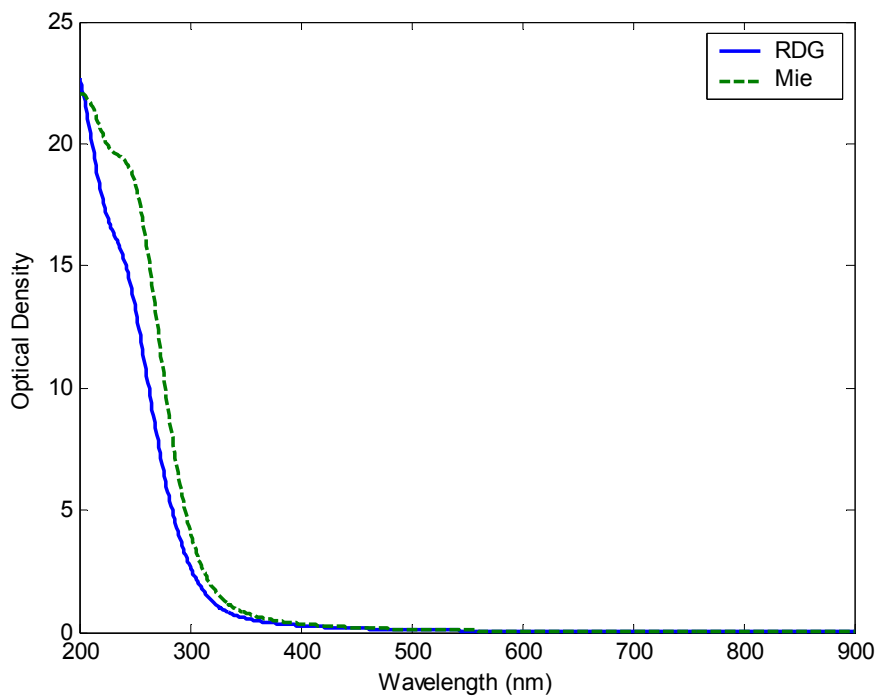

Figure 5.4: Calculated Transmission of Mie and Rayleigh-Debye-Gans for a Suspension of 50 nm AgCl Spheres

37

5.3 Particle Diameter ~ Wavelength, No Absorption

The restriction of Rayleigh-Debye-Gans theory with respect to size was tested through the calculation of transmission spectra for nonabsorbing spherical particles with relative refractive index close to one. The refractive indices chosen were soft bodies ($n = 1.04$) and hemoglobin ($1.01 \leq n/n_o \leq 1.2$). Only the real part of the refractive index was used for hemoglobin. Particle diameters used were 500 nm, 1 μm, and 5.5 μm.

Figures 5.5 and 5.6 show that Rayleigh-Debye-Gans theory approximates Mie theory for 500nm and 1μm. Figure 5.7 shows that for a particle size of 5.5 μm Rayleigh-Debye-Gans and Mie no longer coincide. The combination of zero absorption and refractive index ratio close to 1 increases considerably the particle size ranges for which RDG is applicable; this is in agreement with the results reported in Kerker [5].
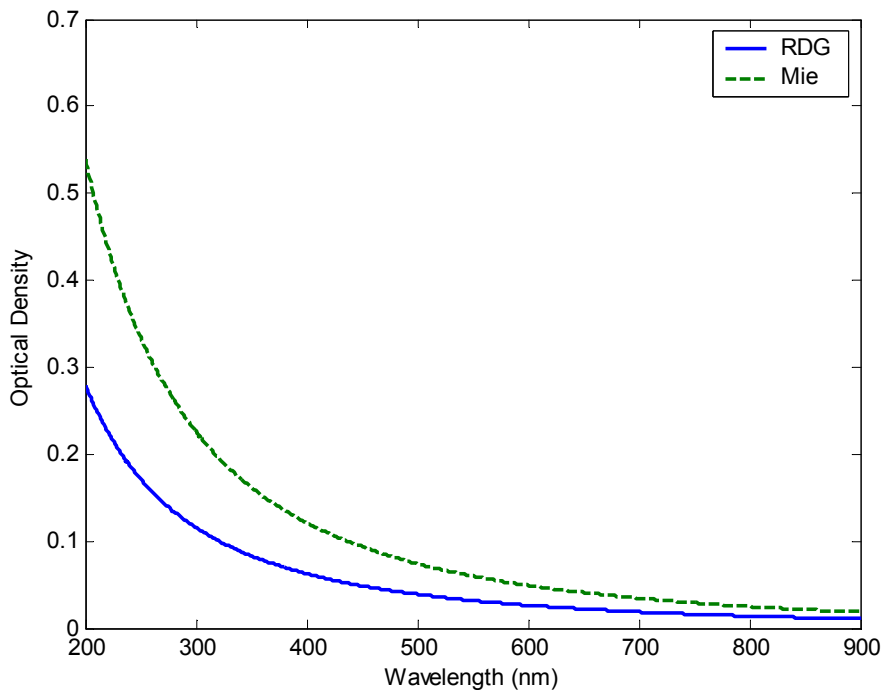

Figure 5.5: Calculated Transmission of Mie and Rayleigh-Debye-Gans for a Suspension of 500 nm Soft Body Spheres
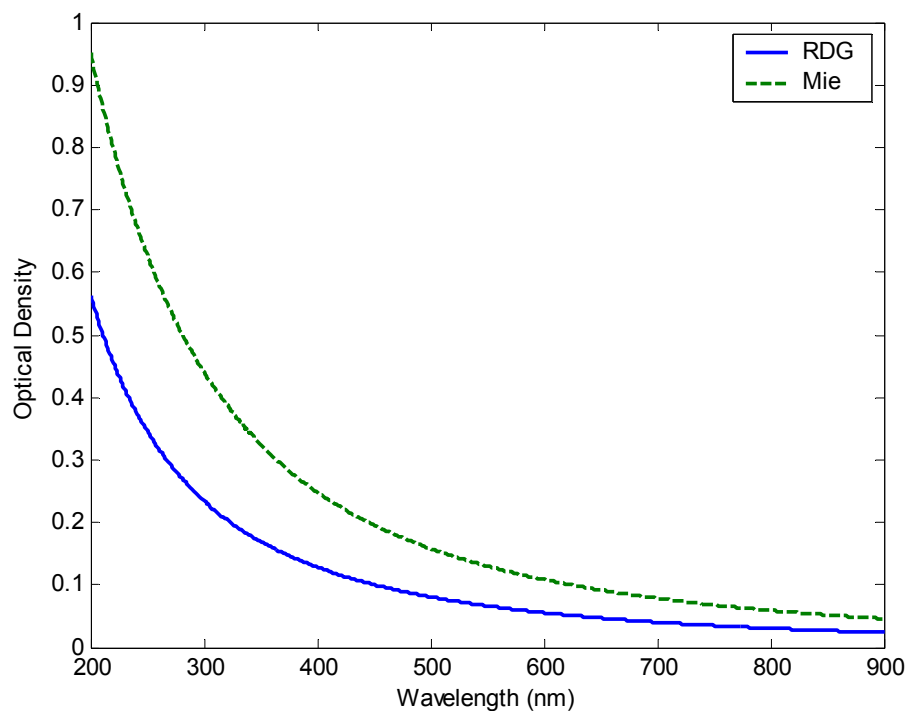
Figure 5.6: Calculated Transmission of Mie and Rayleigh-Debye-Gans for a Suspension of 1 µm Soft Body Spheres
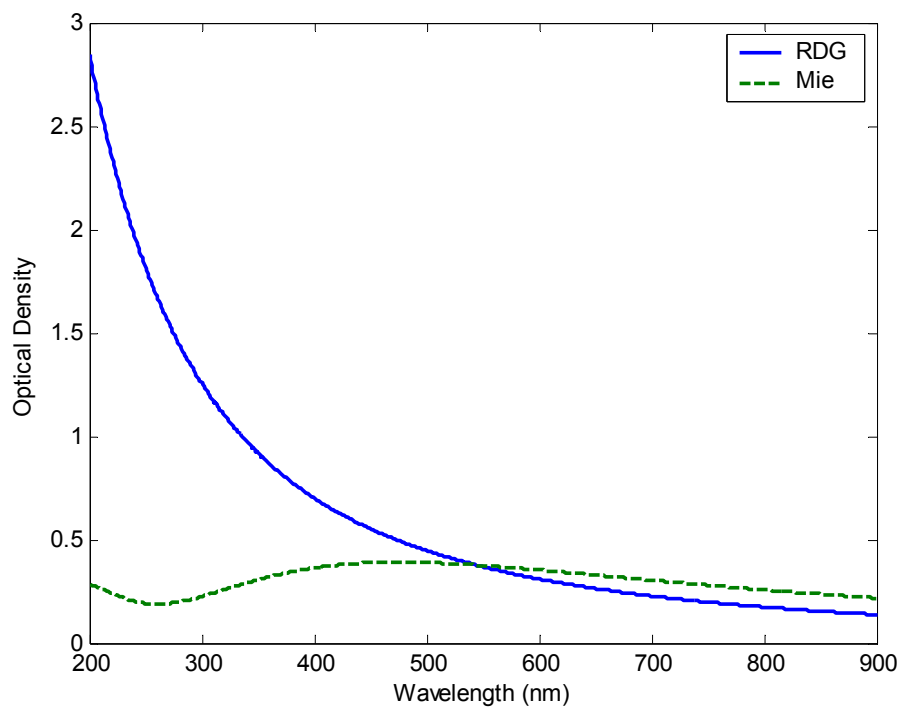
Figure 5.7: Calculated Transmission of Mie and Rayleigh-Debye-Gans for a Suspension of 5.5 µm Soft Body Spheres

The multiwavelength transmission calculations conducted with only the real part of the refractive index of hemoglobin show that for 500 nm diameter particles (figure 5.8), the theories follow one another closely in spectral shape but there are quantifiable differences in amplitude. If the turbidity is used for analysis the spectral differences between the two theories would result in considerable variation in the estimate of particle size and concentration. With increasing of the particle diameter to 1 μm (figure 5.9), the spectral shape for Mie theory relative to Rayleigh-Debye-Gans flattens considerably at the shorter wavelengths. Figure 5.10 shows a semi-logarithmic turbidity plot of 5.5 μm particles to show the differences in shape and amplitude for the two theories. The effect of a relative refractive index greater than one with no absorption results in a limited particle size range for RDG theory, in contrast to particles with a refractive index close to one with no absorption.

Figure 5.8: Calculated Transmission of Mie and Rayleigh-Debye-Gans for a Suspension of 500 nm Hemoglobin Spheres with κ=0

Figure 5.9: Calculated Transmission of Mie and Rayleigh-Debye-Gans for a Suspension of 1 μm Hemoglobin Spheres with κ=0
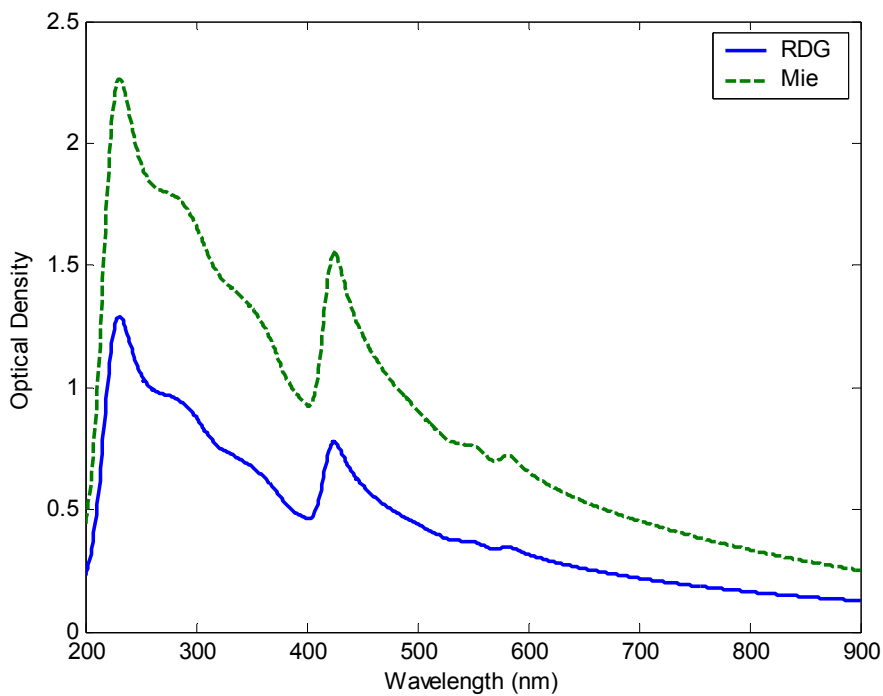
41

Figure 5.10: Calculated Transmission of Mie and Rayleigh-Debye-Gans for a Suspension of 5.5 µm Hemoglobin Spheres with κ=0

5.4 Particle Diameter ~ Wavelength, Absorption $\kappa > 0$

The limits of validity Rayleigh-Debye-Gans theory with a relative refractive index close to one and an absorption value greater than zero were tested through the calculation of the transmission spectra for spherical particles whose sizes are comparable to those of the multiwavelength range. The refractive indices of whole hemoglobin ($1.01 \leq n/n_o \leq 1.2$, $0.001 \leq \kappa \leq 0.1$), meaning the real and imaginary part of the complex refractive index were considered. The particle diameter sizes used were: 100 nm, 500 nm, and 1 µm. Figure 5.11 shows that Rayleigh-Debye-Gans and Mie closely follow one another for a 100 nm sphere. As the particle size was increased to 500 nm and 1 µm the calculated turbidity from Rayleigh-Debye-Gans slowly deviates from Mie (see figures 5.12 and

42

5.13). As the size increases, the features of the spectra calculated with Mie theory flatten. This observed difference appears to be caused by absorption cross section C_{abs} which is proportional to the volume in case for RDG theory, but not in the case of Mie theory.
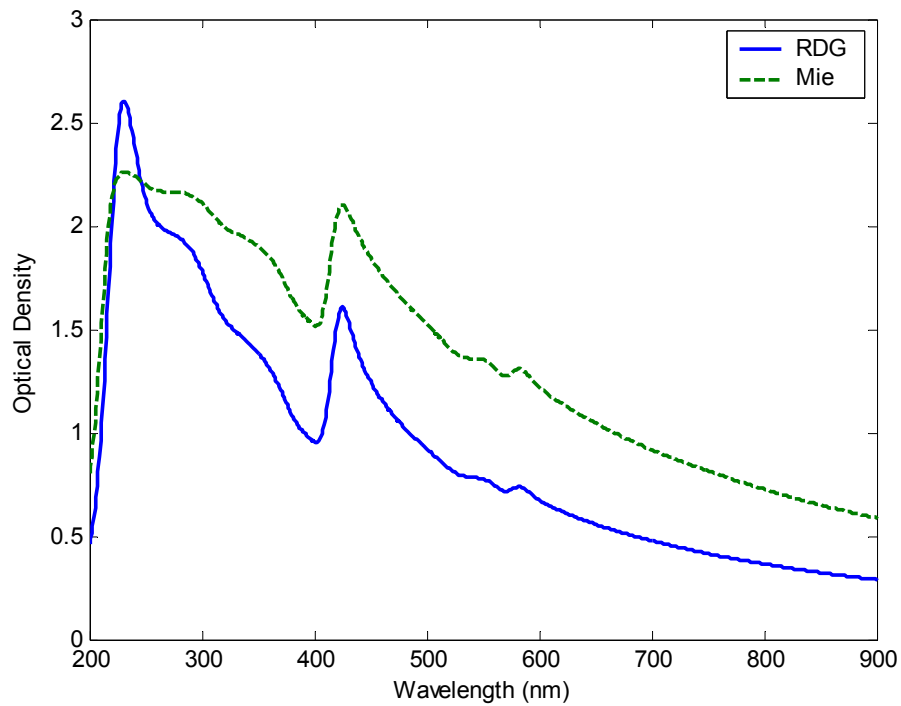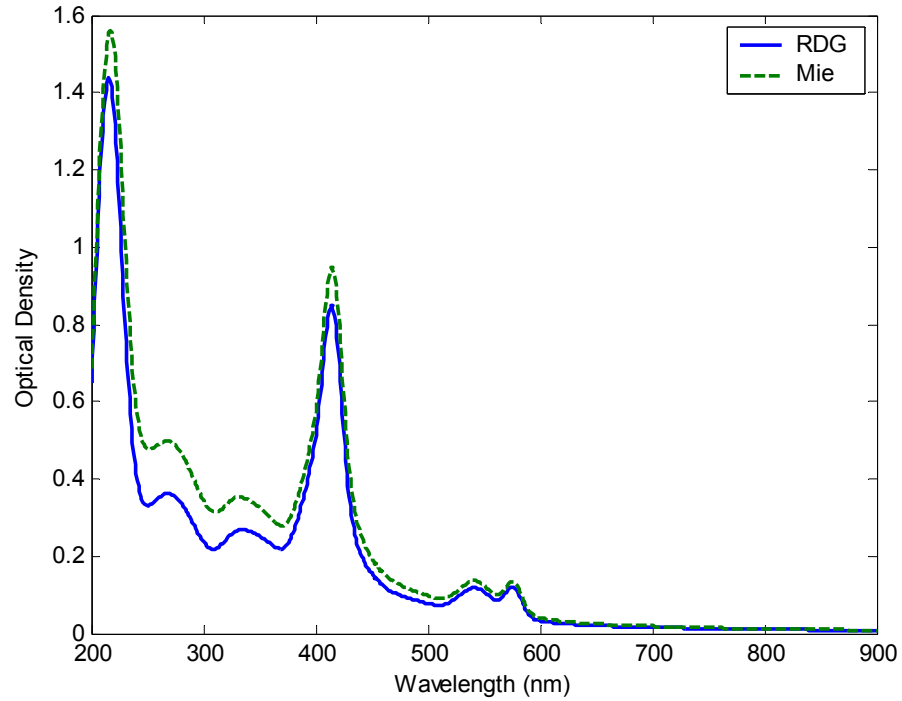

Figure 5.11: Calculated Transmission of Mie and Rayleigh-Debye-Gans for a Suspension of 100 nm Hemoglobin Spheres

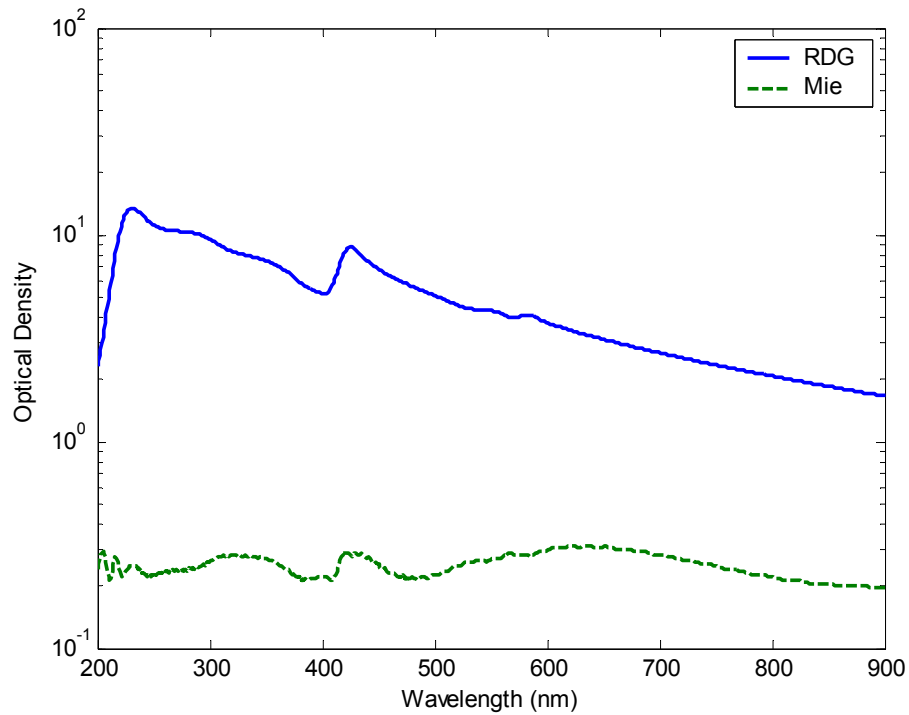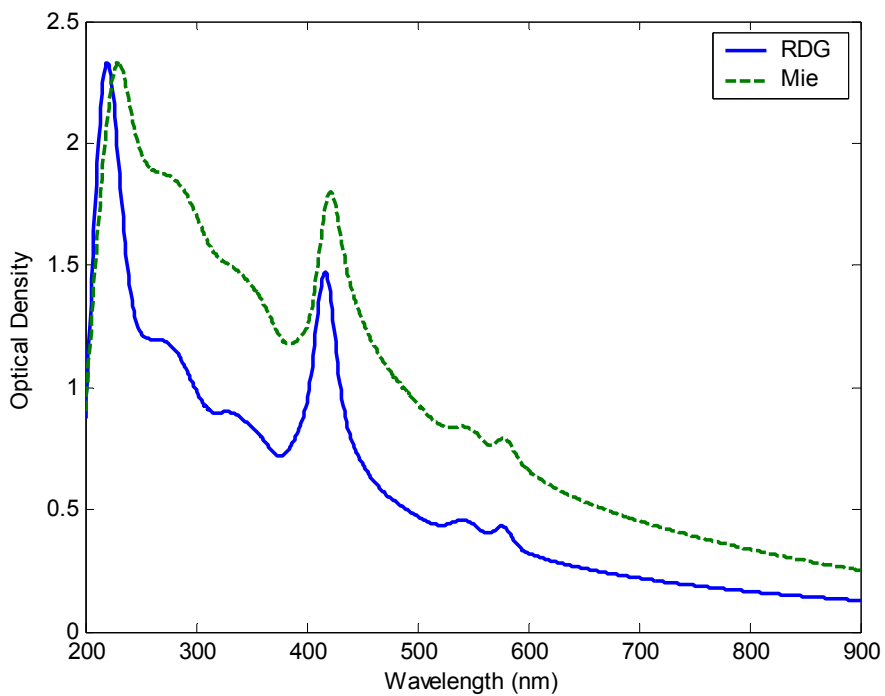*Figure 5.12: Calculated Transmission of Mie and Rayleigh-Debye-Gans for a Suspension of 500 nm Hemoglobin Spheres*
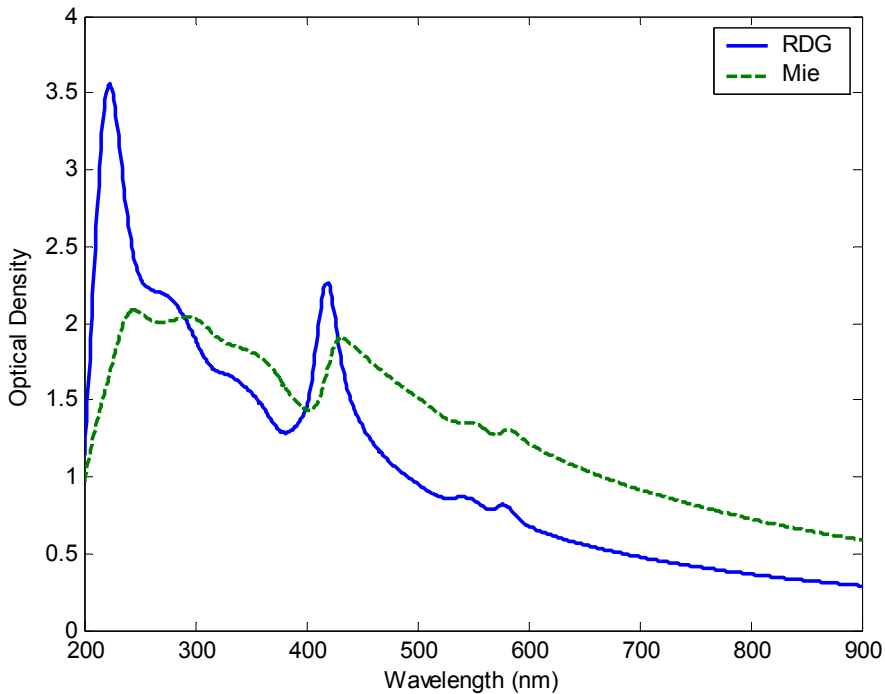
Figure 5.13: Calculated Transmission of Mie and Rayleigh-Debye-Gans for a Suspension of 1 μm Hemoglobin Spheres

5.5 Conclusion

There is disagreement between Rayleigh-Debye-Gans and Mie theory for transmission simulations with spherical scatterers of different sizes and refractive indices. The disagreement is most severe when absorption is present. The rest of this dissertation will be concerned with attempts to modify RDG theory to bring the transmission simulations into closer agreement with Mie.

Chapter Six

Corrections to the Refractive Index

This chapter is dedicated to examining the effect of the complex index of refraction on

the transmission characteristics of a particle. Schemes for adjusting the complex

refractive index to bring RDG predictions into agreement with Mie theory are presented.

6.1 Refractive Index

The complex refractive index is given by

$$N = n + i\kappa \qquad\qquad 6.1$$

where n and κ are non negative values ,n is the refractive index (real), κ is the absorption

coefficient (imaginary). The scattering of light is due to differences in refractive indices

between the medium and the particle. The refractive index of the particle (N_1) relative to

the suspending medium (N_0) is,

$$m = \frac{N_1}{N_0} = \frac{n_1 + i\kappa_1}{n_0 + i\kappa_0} \qquad\qquad 6.2$$

referred to as the relative refractive index, as presented in chapter two

The real and imaginary parts of the complex refractive index expressed as

function of frequency, are related through the integral Kramers-Kronig relations.

$$n(\omega) - 1 = \frac{2}{\pi} P \int_0^\infty \frac{\Omega k(\Omega)}{\Omega^2 - \omega^2} d\Omega \qquad\qquad 6.3$$

$$\kappa(\omega) = \frac{-2\omega}{\pi} P \int_0^\infty \frac{n(\Omega,)}{\Omega^2 - \omega^2} d\Omega \qquad\qquad 6.4$$

here ω is the angular frequency measured and P is the principal value of the integral [1].

In principle, if either $n(\omega)$ or $\kappa(\omega)$ is known or can be measured, the other can be

calculated directly through equations 6.3 and 6.4. Measurements over the complete range

of frequency (0 to ∞) are required when applying this transform.

6.2 Hypochromic Effect

The observable light scattering phenomena depends on the instrumentation configuration

and optical properties of the material. The optical properties (real and imaginary parts of

the refractive index) are intrinsic properties of matter. It is known that the optical

properties depend on the state of aggregation [1]. However, under certain conditions (i.e.

infinite dilution) the optical properties are additive and independent of concentration.

The presence of absorbing groups (chromophors) in high concentration within particles

gives rise to a concentration dependence of the observed optical phenomena. This

phenomenon generally results in a decrease of the imaginary component of the refractive

index κ relative to its value in solution (hypochromicity).

Hypochromicity is a phenomenon in which an individual molecule, containing

several chromophores, has a certain absorptivity at a given wavelength that is less than

the sum of the absorptivities of the individual chromophores at that same wavelength.

When analyzing particulate systems, the state of aggregation of chromophores within the

47

particles may result in hypochromic effects that bias the estimation of their concentration. For this reason, hypochromism was used to determine a correction factor for the imaginary part κ of the refractive index. The most recent models for hypochromicity are those developed by Veshkin [11,12,and 13] and take into consideration the molecular structure and the number of chromophoric groups per unit volume of particle. The procedure of Veshkin was extended to the multiwavelength scenario and implemented; details are given in Appendix D.

The differences in behavior observed between the spectra calculated with Mie and with RDG theory suggests, in agreement with the work of Latimer [15], that it may be possible to compensate RDG theory through the use of "effective" optical properties estimated from particles of known shape and composition.

6.3 Implementation of Optical Correction for Absorption

Rayleigh-Debye-Gans is limited to small changes in refractive index $n(\lambda)$ close to one and small values of absorption $\kappa(\lambda)$. Rayleigh-Debye-Gans theory assumes each dipole absorbs and scatters independently and only considers the interference of the scattering wave. As a result, the angular scattering intensity is shape and orientation dependent, whereas the absorption cross-section is independent of the particle shape (equation 2.9); in other words, the total absorption is only dependent on the particle volume (the total number of chromophoric groups in the particle). When compared with Mie the latter causes a large discrepancy where the absorption efficiencies calculated with Mie theory always smaller (hypochromic) than the values calculated with RDG for large absorption coefficients (i.e., Hemoglobin, DNA). This apparent hypochromicity suggests that the

48

theoretical models developed to account for hypochromic or "screening" effects may be able to bring RDG into a better agreement with Mie.

To explore the potential application of Veshkin's correction the volume fraction of chromophoric groups (v_f in equations 6.12- 6.21) is treated as an adjustable parameter. Two cases are considered: $v_f=0$ corresponds to 100% hypochromicity which translates to the corrected $\kappa_c(\lambda)$ being equal to zero; and $v_f=1$ corresponds to using the value of $\kappa(\lambda)$ directly. Spherical hemoglobin particles with a diameter of 1 μm were where Veshkin's correction was applied only to $\kappa(\lambda)$. The volume fraction values used in this study were 0.15, 0.20, 0.33, and 0.50. The molecular diameter of hemoglobin is 68 Å with the cross sectional area of 20 Å and a molecular weight of 16100 [16]. The orientation value q was set to one, meaning the molecules are randomly oriented [12].

The results of the hypochromicity corrections implemented in RDG theory are shown in figures 6.1 and 6.2. Figure 6.1 shows the spectra calculated with RDG and Mie without any corrections for hypochromicity, together with the spectra calculated with RDG and several levels of hypochromicity (i.e., volume fractions). Notice that, although intermediate levels of hypochromicity result in improved RDG-calculated spectra, Veshkin's model is not very effective in reducing the differences between Mie and RDG theories. This point is demonstrated more dramatically when 100% hypochromicity is considered. Figure 6.2 shows the extreme cases of 0% and 100% hypochromicity applied to both theories.

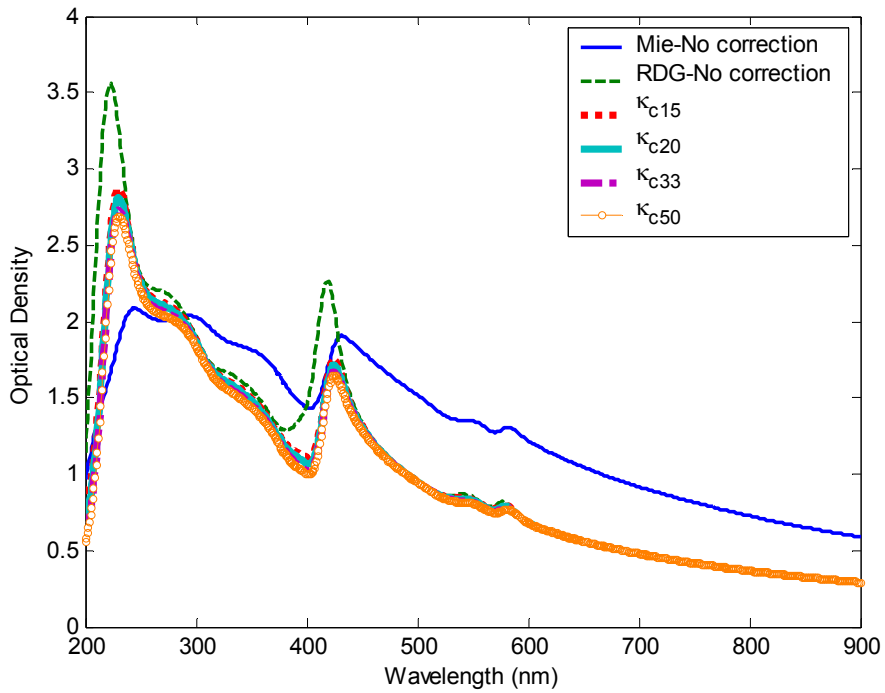*Figure 6.1: Calculated Transmission of Mie and Rayleigh-Debye-Gans for 1 μm Hemoglobin Sphere with Veshkin Correction*

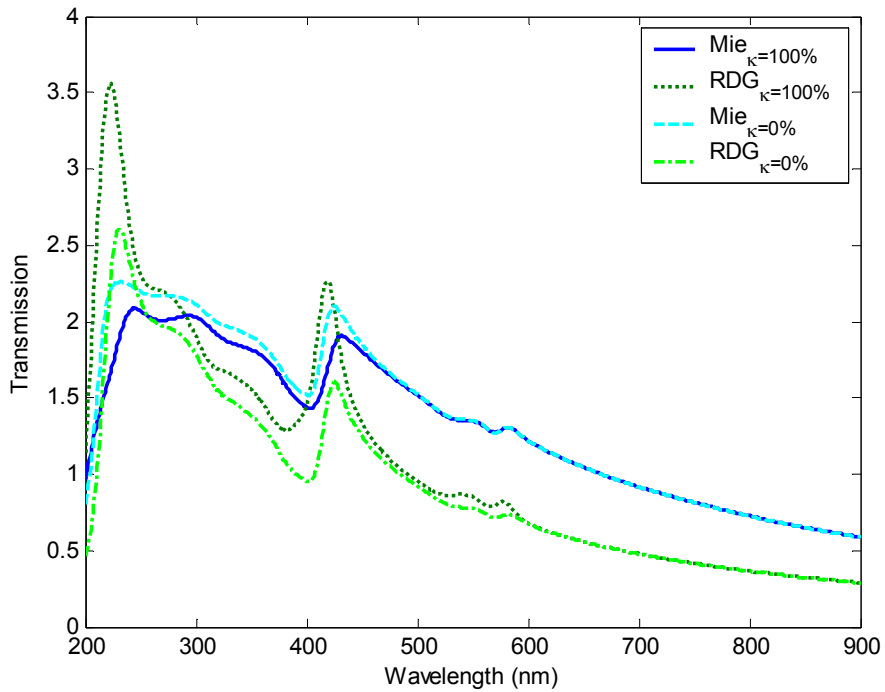*Figure 6.2: Calculated Transmission of Mie and Rayleigh-Debye-Gans for 1 μm Hemoglobin Sphere with 0% and 100% Hypochromicity*

The use of Veshkin's model for the correction of the absorption coefficient brings about the problem of the inconsistency in terms of the Kramers-Kronig transforms since, after the correction, equations 6.3 and 6.4 will no longer hold. To demonstrate this inconsistency, an effective value of $n_{eff}(\lambda)$ was calculated through the Kramer-Kronig transform after $\kappa(\lambda)$ was corrected, using Veshkin's model. All the conditions were kept the same for calculating the transmission as previously in this section. Figure 6.3 shows the results of calculating the transmission for Rayleigh-Debye-Gans with an effective n_{eff} and a corrected κ_c using Veshkin's model compared, to uncorrected values of κ and n for RDG and Mie theory.

Figure 6.3: Calculated Transmission of Mie and Rayleigh-Debye-Gans for 1 μm Hemoglobin Sphere with Veshkin Correction to k_c and an Effective n_{eff} Calculated through Kramers-Kronig Transform
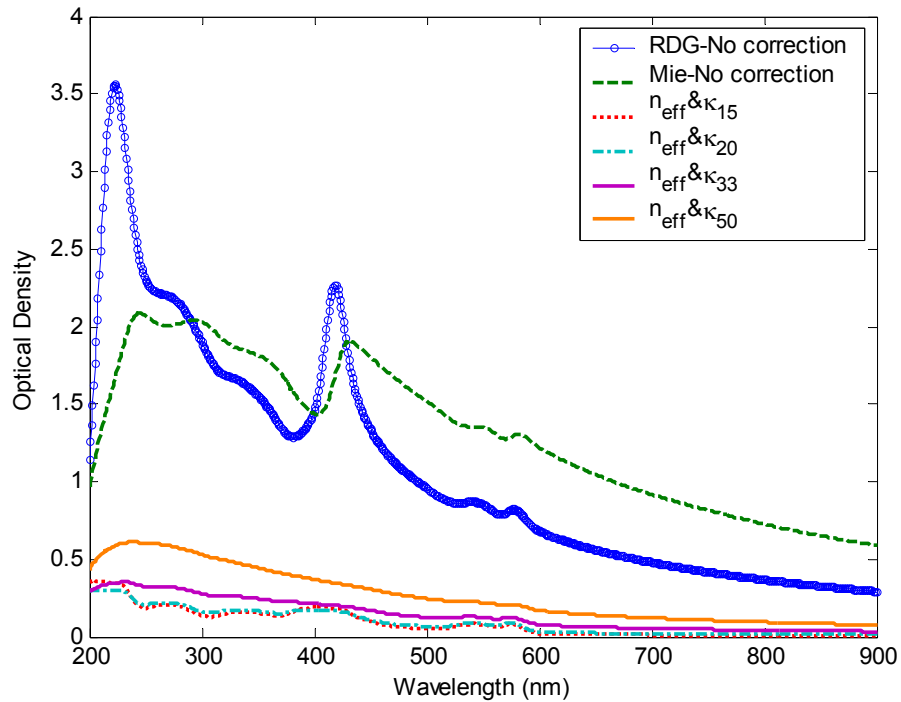
51

Using the effective *n* calculated from corrected κ_c, one would expect the transmission by RDG more closely the transmission calculated by Mie; however, the contrary is observed. A close look at the transmission values of figure 6.3 can be seen in figure 6.4. At different volume fractions of the chromophore relating to k_c and n_{eff} values, there are distinct differences in the shape of the spectra. The differences in the spectra are rooted in determining the values *n* from a revised κ using the Kramers-Kronig transform.
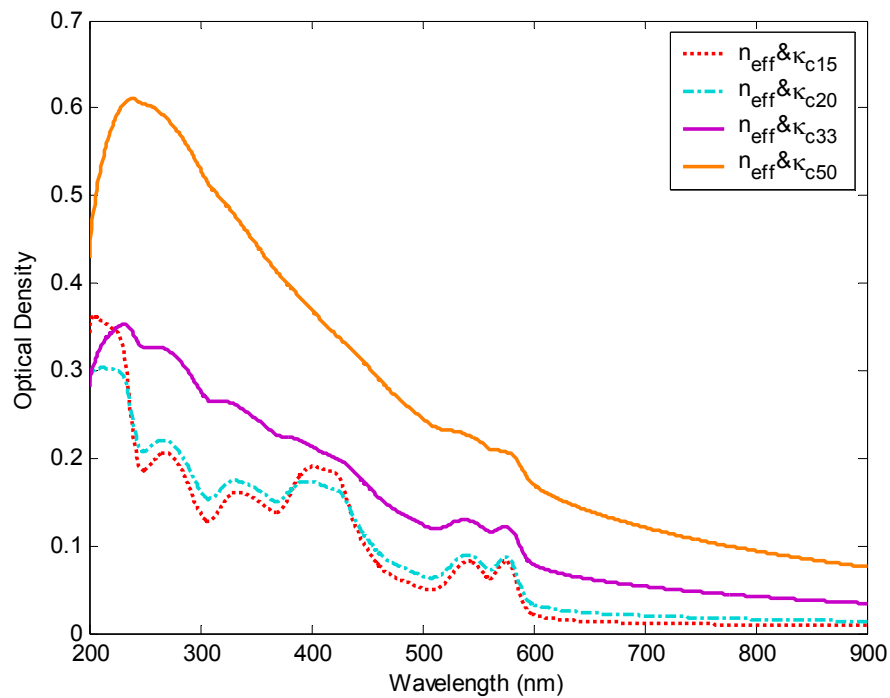
Figure 6.4: Zoom in of Figure 6.4 of Calculated Transmission of Rayleigh-Debye-Gans for 1 μm Hemoglobin Sphere with Veshkin Correction to k_c and an Effective n Calculated through Kramers-Kronig Transform

An alternate approach for bringing together Mie and RDG theories is the mathematical adjustment of the refractive indices at each wavelength. This is explored in the next section.

6.4 Effective Refractive Index Estimation

The concept behind calculating effective refractive indices is that given the absorption efficiency Q_{abs} determined by Mie theory there is a set of $n(\lambda)$ and $\kappa(\lambda)$ values that would allow Rayleigh-Debye-Gans to predict some extinction efficiency Q_{ext} to coincide with the extinction efficiency calculated by Mie. The absorption efficiency for either Rayleigh-Debye-Gans or Mie theory was expressed in chapter two as:

$$Q_{abs} = 4ka\operatorname{Im}\left(\frac{m^2-1}{m^2+2}\right) \approx 4ka\operatorname{Im}\left(\frac{2}{3}(m-1)\right) = \frac{8}{3}ka\kappa \qquad 6.5$$

The scattering efficiency Q_{sca} in RDG is expressed (equation 2.24):

$$Q_{sca} = (ka)^4\left|\frac{m^2-1}{m^2+2}\right|^2 \int_0^\pi f^2(\theta)(1-\cos^2\theta)\sin\theta\,d\theta \qquad 6.6$$

For simplification introduce $\Lambda = \int_0^\pi f^2(\theta)(1-\cos^2\theta)\sin\theta\,d\theta$, which is independent of n and κ for $m\approx 1$,

$$Q_{sca} \approx (ka)^4\Lambda\left|\frac{2}{3}(n-1)+i\frac{2}{3}\kappa\right|^2 = \frac{4}{9}(ka)^4\Lambda\left((n-1)^2+\kappa^2\right) \qquad 6.7$$

Therefore, the extinction efficiency can then be expressed as the sum of equations 6.5 and 6.7

$$\begin{aligned}
Q_{ext} &= \frac{8}{3}(ka)\kappa + \frac{4}{9}(ka)^4\Lambda\left((n-1)^2+\kappa^2\right) \\
&= \frac{4}{9}(ka)^4\Lambda(n-1)^2 + \frac{4}{9}(ka)^4\Lambda\kappa^2 + \frac{8}{3}(ka)\kappa
\end{aligned} \qquad 6.8$$

If we assume Q_{ext} and n are known, then we can solve for κ explicitly using the quadratic formula.

53

The same type of algebra manipulation can be done to solve for the refractive index n if Q_{ext} and κ are known.

$$n_1 = \left(\sqrt{\frac{Q_{ext,ko}}{q_1} + 1} \right) n_o \qquad 6.9$$

$$\kappa_1 = \left(\frac{-q_2 \pm \sqrt{q_2^2 + 4q_1 Q_{ext,no}}}{2q_1} \right) n_o \qquad 6.10$$

Equations 6.9 and 6.10 are written in terms of relative values. Note that for equations 6.9 and 6.10 to give real effective values for n_1 and κ_1; $Q_{ext,no}$, $Q_{ext,ko}$, q_1, and q_2 must always be positive. The artificiality of this mathematical juggling is clear; changing only κ or n, and not the other, would lead to a violation of the Kramer-Kronig relations. Therefore the implementation of this adjustment is rejected.

6.5 Conclusion

The effect of changes in the refractive indices has been explored as a means to extend the range of application of RDG and to bring it into better agreement with Mie theory for larger particles and for particles containing strong chromophoric groups. It was concluded that, it is not possible to adequately or realistically compensate for the differences between Mie and RDG through the use of hypochromicity models and/or effective refractive indices. Therefore, a different type of approach is required. The following chapter discusses exploiting the internal field calculation of Mie theory as a vehicle to improve the Rayleigh-Debye-Gans and Mie conflict in the presence of absorption.

Chapter Seven

New Hybrid Theory

The hybrid theory developed in this chapter uses the Mie solution to compute the internal

field of a sphere, and the Rayleigh-Debye-Gans approach to solve for the scattering

fields. The induced Rayleigh-Debye-Gans dipole moment is computed from the internal

Mie field, rather than the incoming field. From this we solve for the scattering fields in

terms of the parallel and perpendicular components of the incoming light. Form factors

were generated through the scattering amplitude functions. The following is the

mathematical development of the hybridized theory for a spherical particle.
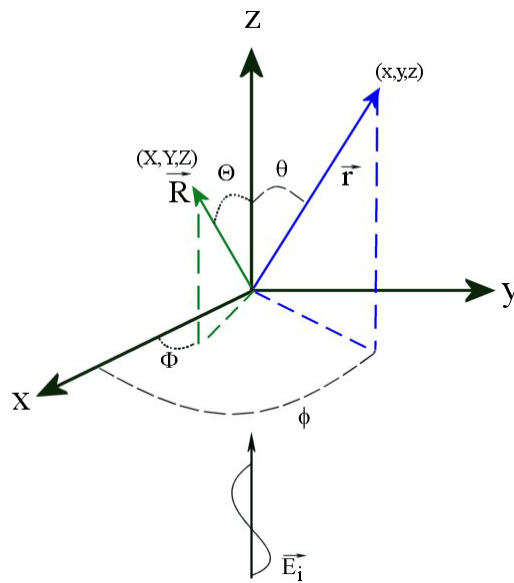

7.1 Geometry and Notation

Figure 7.1: Diagram of Scatterer Point and Detector Location

For describing the electric field scattered by a particle in the laboratory system there are two objects of interest, the detector and scatterer. Figure 7.1 illustrates the detector located at $\vec{r}$ with spherical coordinates (r,θ,ϕ) or Cartesian coordinates (x,y,z). Points within the scatterer are identified by $\vec{R}$ with coordinates (R,Θ,Φ) or (X,Y,Z).

The curvilinear unit vectors attached to the detector in figure 7.2 can be expressed in rectangular coordinates through the following equations:

$$x = r\sin\theta\cos\phi$$
$$y = r\sin\theta\sin\phi \qquad\qquad 7.1$$
$$z = r\cos\theta$$

$$\vec{e}_r = \sin\theta\cos\phi\,\vec{e}_x + \sin\theta\sin\phi\,\vec{e}_y + \cos\theta\,\vec{e}_z$$
$$\vec{e}_\theta = \cos\theta\cos\phi\,\vec{e}_x + \cos\theta\sin\phi\,\vec{e}_y - \sin\theta\,\vec{e}_z \qquad\qquad 7.2$$
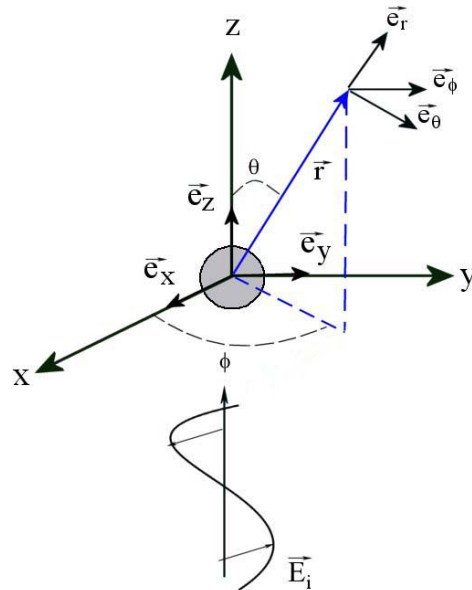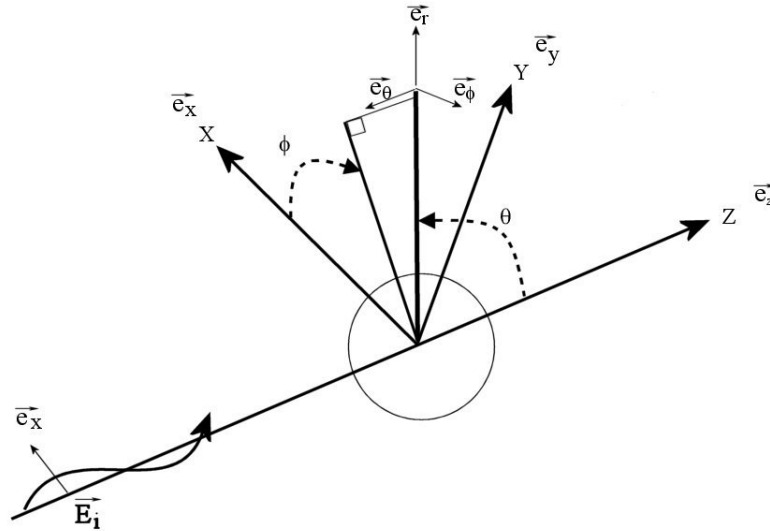$$\vec{e}_\phi = -\sin\phi\,\vec{e}_x + \cos\theta\,\vec{e}_y$$

Figure 7.2: Local Unit Vectors with Respect to the Detector

Figure 7.3 similarly depicts the unit vectors attached to a point inside the scatterer. The

transformation equations for these vectors are identical to equations 7.1 and 7.2, with

corresponding subscripts and angles.

Figure 7.3: Local Unit Vectors with Respect to the Scatterer

As indicated**,** the incident wave moves in the z-direction and is presumed to be plane-

polarized in the x-direction. It impinges upon the particle and is scattered. The scattered

wave is detected at some angle θ and ϕ measured from the direction of propagation of the

incident wave; see figure 7.1. The following section provides a mathematical description

of the fields induced by the particle. As will be seen, the scattering dynamics are best

described using the vectors $\vec{e}_R, \vec{e}_\Theta, \vec{e}_\Phi$; the scattered radiation is best described by

$\vec{e}_r, \vec{e}_\theta, \vec{e}_\phi$. Therefore the transformation equations play an important role in unifying the

description.

7.2 Internal Field

The incoming field for light illuminating a spherical particle, propagating in the z-direction, and polarized in the x-direction, is described in generic Cartesian coordinates as

$$\vec{E}_i(\xi,\eta,\varsigma,t) = E_o e^{ik\varsigma} e^{-i\omega t} \vec{e}_x \qquad 7.3$$

where k is the wave number in the medium. The time factor $e^{-i\omega t}$ will be omitted in the following.

The resulting field inside the sphere is given by Mie theory as

$$\vec{E}(\vec{R}) = E_o \sum_{n=1}^{\infty} \frac{2n+1}{n(n+1)} \left(c_n \vec{M}_{O1n}^1 - i d_n \vec{N}_{E1n}^1 \right) \qquad 7.4$$

where $\vec{M}$ and $\vec{N}$ are the solutions to the vector wave equation in terms of Bessel functions and spherical harmonics [1]. We truncate the series above in the following manner

$$\frac{\vec{E}(\vec{R})}{E_o} \approx \frac{3}{2} c_1 \vec{M}_{O11} - \frac{3}{2} i d_1 \vec{N}_{E11} - \frac{5}{6} i d_2 \vec{N}_{E12} + O\left(\left[\frac{a}{\lambda}\right]^2\right) \qquad 7.5$$

where a is the radius of the spherical particle and λ is the wavelength. Bohren and Huffman provide the general expressions for the terms $\vec{M}$ and $\vec{N}$ as series themselves, which we also truncate as:

$$\vec{M}_{O11}(\vec{R}) \approx \frac{k_1}{3} R \cos\Phi \, \vec{e}_\Theta - \frac{k_1}{3} R \sin\Phi \, \cos\Theta \, \vec{e}_\Phi + O\left(\left[k_1 R\right]^2\right) \qquad 7.6$$

$$\vec{N}_{E11}(\vec{R}) \approx \frac{2}{3} \cos\Phi \, \sin\Theta \, \vec{e}_R + \frac{2}{3} \cos\Phi \, \cos\Theta \, \vec{e}_\Theta - \frac{2}{3} \sin\Phi \, \vec{e}_\Phi + O\left(\left[k_1 R\right]^2\right) \qquad 7.7$$

$$\vec{N}_{E12}(\vec{R}) \approx \frac{6}{5} k_1 R \cos\Phi \sin\Theta \cos\Theta \, \vec{e}_R + \frac{3}{5} k_1 R \cos\Theta \left(2\cos^2\Theta - 1\right) \vec{e}_\Theta$$
$$- \frac{3}{5} k_1 R \sin\Phi \cos\Theta \, \vec{e}_\Phi + O\left([k_1 R]^2\right) \qquad \text{7.8}$$

where k_1 is the wave number inside the sphere. The coefficients for c_n and d_n are

calculated through

$$c_n = \frac{\mu_1 j_n(ka)\left[kah_n^1(ka)\right]' - \mu_1 h_n^1(ka)\left[kaj_n(ka)\right]'}{\mu_1 j_n(mka)\left[kah_n^1(ka)\right]' - \mu h_n^1(ka)\left[mkaj_n(mka)\right]'} \qquad \text{7.9}$$

$$d_n = \frac{\mu_1 m j_n(ka)\left[kah_n^1(ka)\right]' - \mu_1 m h_n^1(ka)\left[kaj_n(ka)\right]'}{\mu m^2 j_n(mka)\left[kah_n^1(ka)\right]' - \mu_1 h_n^1(ka)\left[mkaj_n(mka)\right]'} \qquad \text{7.10}$$

where μ_1 is the permeability of the sphere and is presumed to equal μ, the permeability

of the medium, and k is the wave number in the medium. The primes denote

differentiation with respect to ka.

The expressions of 7.6, 7.7 and 7.8 are translated to rectangular coordinates as

$$\vec{M}_{O11} \approx \frac{k_1}{3} Z \, \vec{e}_x + \frac{k_1}{3} X \, \vec{e}_z \qquad \text{7.11}$$

$$\vec{N}_{E11} \approx \frac{2}{3} \vec{e}_x \qquad \text{7.12}$$

$$\vec{N}_{E12} \approx \frac{3}{5} k_1 Z \vec{e}_x + \frac{3}{5} k_1 X \vec{e}_z \qquad \text{7.13}$$

resulting in

$$\frac{\vec{E}(\vec{R})}{E_o} = \left[d_1 + \frac{(d_1 + c_1)}{2} ik_1 Z \right] \vec{e}_x + \frac{(d_1 - c_1)}{2} ik_1 X \vec{e}_z + O\left([k_1 R]^2\right) \qquad \text{7.14}$$

This expression can be written in exponential form to the same order of accuracy; since

$$e^x = 1 + x + O(x^2) \qquad \text{7.15}$$

we implement the following,

$$\frac{(d_1 - c_1)}{2} ik_1 X = e^{\frac{(d_1 - c_1)}{2} ik_1 X} - 1 + O\left(\left[k_1 R\right]^2\right)$$

$$d_1 + \frac{(d_1 + c_1)}{2} ik_1 Z = d_1 e^{\frac{(d_1 + c_1)}{2d_1} ik_1 Z} + O\left(\left[k_1 R\right]^2\right),$$

7.16

resulting in the following approximation for the Mie field inside the sphere.

$$\frac{\vec{E}(\vec{R})}{E_o} = d_1 e^{ik_1 \frac{(d_2 + c_1)}{2d_1} Z} \vec{e}_x + \left(e^{ik_1 \frac{(d_2 - c_1)}{2} X} - 1 \right) \vec{e}_z$$

7.17

Note that in the limit as $k_1 \to k$, if we have $d_1 \to 1, c_1 \to 1, d_2 \to 1$ then

$\vec{E}(\vec{R}) \to E_o e^{ikZ} \vec{e}_x$, the incoming field value. In chapter eight we demonstrate by computer

studies that, indeed, c_1, d_1, and d_2 all equal 1 when $k_1 = k$. This is consistent; if the

dielectric properties of the scatterer match those of the medium the incoming field is

unaltered.

7.3 Dipole Scattering Approach

Electromagnetic theory states that a dipole located at $\vec{R}$ of intensity $\vec{p}(\vec{R}) e^{-i\omega t}$ radiates in

the far field according to the following [2]:

$$\vec{E}_s = \left(\frac{e^{ik|\vec{r} - \vec{R}|}}{-ik|\vec{r} - \vec{R}|} \frac{ik^3}{4\pi\varepsilon} e^{-i\omega t} \right) \vec{e}_{\vec{r} - \vec{R}} \times \left[\vec{e}_{\vec{r} - \vec{R}} \times \vec{p}(\vec{R}) \right]$$

7.18

where $\vec{E}_s$ is the scattered electric field radiated by the dipole and ε is the permittivity or

dielectric constant of the medium. It also states that a small dielectric sphere of radius ρ

placed in a *uniform static* electric field $\vec{E}$ generates a dipole moment. The induced

dipole moment is proportional to the field and is given by

60

$$\vec{p} = 3\varepsilon \frac{m^2 - 1}{m^2 + 2} \left(\frac{4}{3} \pi \rho^3 \right) \vec{E}$$

$$= 3\varepsilon \frac{m^2 - 1}{m^2 + 2} \vec{E} dV$$

7.19

where ε is the permittivity, m is the relative refractive index, and dV is the volume of the scatterer.

Rayleigh scattering assumes that an *oscillating, nonuniform* field $\vec{E}(\vec{R})e^{-i\omega t}$ generates a dipole moment in a spherical volume given by the same expression in equation 7.19 and that the dipole re-radiates according to equation 7.18. Following the RDG approach, we assume that each *infinitesimal* volume within the scatterer (not the entire scatterer itself) behaves in this fashion. By substituting equation 7.19 into 7.18 we obtain the following expression for the incremental electric field radiated by the infinitesimal dipole located at $\vec{R}$:

$$d\vec{E}_s = \left(\frac{e^{ik|\vec{r} - \vec{R}|}}{-ik|\vec{r} - \vec{R}|} \frac{ik^3}{4\pi\varepsilon} \right) \vec{e}_{\vec{r} - \vec{R}} \times \left[\vec{e}_{\vec{r} - \vec{R}} \times 3\varepsilon \frac{m^2 - 1}{m^2 + 2} \vec{E}(\vec{R}) dV \right]$$

7.20

For $|\vec{R}| << |\vec{r}|$, Rayleigh approximates $1/|\vec{r} - \vec{R}| \approx 1/r$, $\vec{e}_{\vec{r} - \vec{R}} \approx \vec{e}_r$, and

$e^{ik|\vec{r} - \vec{R}|} \approx e^{ik\{(r - \vec{R} \cdot \vec{e}_r)\}} = e^{ikr} e^{-ik\vec{R} \cdot \vec{e}_r}$. When substituting these approximations into equation 7.20 the following expression is obtained.

$$d\vec{E}_s = -\left(\frac{3k^2}{4r\pi} \frac{m^2 - 1}{m^2 + 2} e^{ikr} e^{-ik\vec{R} \cdot \vec{e}_r} dV \right) \vec{e}_r \times \left[\vec{e}_r \times \vec{E}(\vec{R}) \right]$$

7.21

7.4 Hybrid Theory

The difference between Rayleigh-Debye-Gans theory and the hybrid theory

presented herein is as follows: RDG assumes that the local field $\vec{E}(\vec{R})$ generating the

infinitesimal dipole in equation 7.21 is given by the *incoming field*, whereas the hybrid

theory takes the *internal field* that Mie theory gives for the sphere as the field inducing

the dipole moment. By using the internal Mie field, we are taking some account of the

effect of the surrounding dipole field alterations to the incoming field (such as

attenuation, which is highlighted in chapter five as a major shortcoming in RDG theory).

The validity of either approach presumes that the incoming electric field is roughly

uniform over the sphere, so that the radius a of the sphere must be a small fraction of the

wavelength ($a << \lambda$).

If we substitute the expression for the internal electric field, equation 7.17, into

equation 7.21 an explicit formula for the scattered electric field is obtained.

$$d\vec{E}_s = -\left(\frac{3k^2}{4r\pi} \frac{m^2-1}{m^2+2} e^{ikr} e^{-ik\vec{R}\cdot\vec{e}_r} dV \right) \vec{e}_r \times \left[\vec{e}_r \times \left(d_1 e^{ik_1 \frac{d_2+c_1}{2d_1} Z} \vec{e}_x + \left(e^{ik_1 \frac{d_1-c_1}{d_1} Z} - 1 \right) \vec{e}_z \right) E_o \right] \quad 7.22$$

In order to evaluate $\vec{e}_r \times [\vec{e}_r \times \vec{e}_x]$ and $\vec{e}_r \times [\vec{e}_r \times \vec{e}_z]$ one has to use the identities in

equations 7.1,2. The following expression is a result of the conversion and mathematical

manipulation, with the identifications $Z = \vec{R}\cdot\vec{e}_z$ and $X = \vec{R}\cdot\vec{e}_x$.

$$d\vec{E}_s = -E_o \left(\frac{3k^2}{4r\pi} \frac{m^2-1}{m^2+2} e^{ikr} e^{-ik\vec{R}\cdot\vec{e}_r} dV \right) \begin{pmatrix} d_1 e^{ik_1 \frac{d_2+c_1}{2d_1} \vec{R}\cdot\vec{e}_r} \left(\sin\phi\vec{e}_\phi - \cos\phi\cos\theta\vec{e}_\theta \right) \\ + \left(e^{ik_1 \frac{d_1-c_1}{d_1} \vec{R}\cdot\vec{e}_x} - 1 \right) \sin\theta\vec{e}_\theta \end{pmatrix} \quad 7.23$$

As in Rayleigh-Debye-Gans theory, we sum (integrate) this over the total scatterer volume. We introduce f_1 and f_2 as "form factors" for the sphere:

$$\vec{E}_s = \int d\vec{E}_s = -E_o e^{ikr}\left(\frac{3k^2}{4\pi r}\frac{m^2-1}{m^2+2}V\right)\left[-f_1\cos\theta\cos\phi\vec{e}_\theta + f_2\sin\theta\vec{e}_\theta - f_1\sin\phi\vec{e}_\phi\right] \quad 7.24$$

where

$$f_1(\theta,\phi)=\frac{1}{V}d_1\int e^{ik_1\frac{(d_2+c_1)}{2d_1}\vec{R}\cdot\vec{e}_z}e^{-ik\vec{R}\cdot\vec{e}_r}dV = \frac{1}{V}d_1\int e^{i\vec{R}\cdot\left(k_1\frac{(d_2+c_1)}{2d_1}\vec{e}_z-k\vec{e}_r\right)}dV \quad 7.25$$

$$f_2(\theta,\phi)=\frac{1}{V}\int\left(e^{ik_1\frac{(d_2-c_1)}{2}\vec{R}\cdot\vec{e}_x}-1\right)e^{-ik\vec{R}\cdot\vec{e}_r}dV$$

$$=\frac{1}{V}\int e^{i\vec{R}\cdot\left(k_1\frac{(d_2-c_1)}{2}\vec{e}_x-k\vec{e}_r\right)}dV -\frac{1}{V}\int e^{i\vec{R}\cdot(-k\vec{e}_r)}dV \quad 7.26$$

Note that if $k_1 = k$, since (as noted above) $c_1 = d_1 = d_2 = 1$, f_1 reduces to

$\frac{1}{V}\int e^{ik\vec{R}\cdot(\vec{e}_z-\vec{e}_R)}dV$, the form factor "$f$" in the RDG theory. Furthermore observe that the factor f_2, which does not appear in the RDG theory, goes to zero when $k_1 = k$.

The problem now becomes how to calculate the integrals in equations 7.25 and 7.26. They all have the form $\int e^{i\vec{R}\cdot\vec{S}}dV$ with constant $\vec{S}$. Consider a local coordinate system in the sphere with its z' axis aligned with $\vec{S}$. If we look at figure 7.4, the element of volume at height z' is

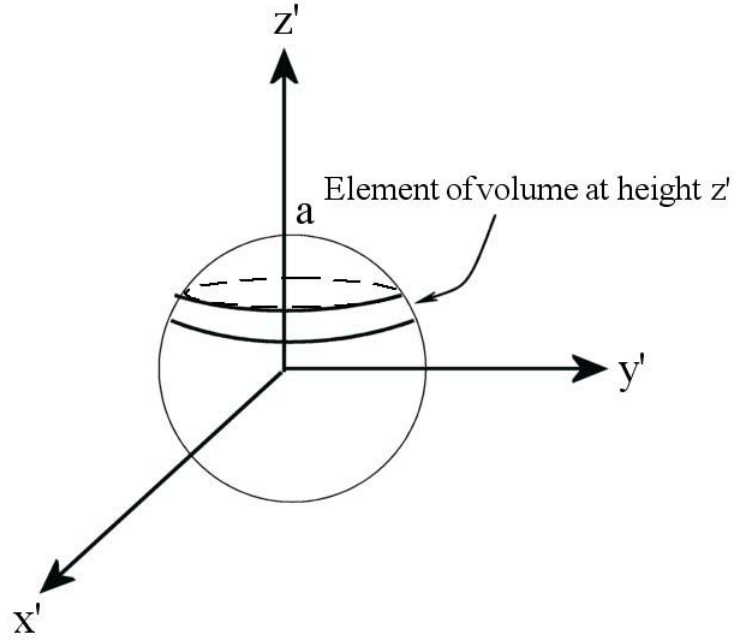$$dV = base \times height = \pi\left(x'^2+y'^2\right)dz' \quad 7.27$$

Figure 7.4: Diagram of the Volume at Height z' for a Sphere

However $x'^2 + y'^2 + z'^2 = a^2$ and z' runs from $-a$ to a; therefore,

$$\int e^{i\vec{R}\cdot\vec{S}}dV = \int e^{i|\vec{S}|\vec{R}\cdot\vec{e}_{z'}}dV = \int_{z'=-a}^{a} e^{i|\vec{S}|z'}\pi\left(a^2 - z'^2\right)dz' \qquad 7.28$$

We can use Maple to perform these integrals. The results are

$$f_1 = \frac{1}{V}d_1 2\pi\left(\frac{iAae^{iAa} - e^{iAa} + iAae^{-iAa} + e^{-iAa}}{i^3 A^3}\right) \qquad 7.29$$

$$f_2 = \frac{1}{V}2\pi\left[\left(\frac{iBae^{iBa} - e^{iBa} + iBae^{-iBa} + e^{-iBa}}{i^3 B^3}\right) - \left(\frac{iCae^{iCa} - e^{iCa} + iCae^{-iCa} + e^{-iCa}}{i^3 C^3}\right)\right] \qquad 7.30$$

$$A = \sqrt{k^2 + \frac{k_1^2\left(d_2 + c_1\right)^2}{4d_1^2} - \frac{kk_1\left(d_2 + c_1\right)}{d1}\cos\theta}$$

$$B = \sqrt{k^2 + \frac{k_1^2\left(d_2 - c_1\right)^2}{4} - kk_1\left(d_2 - c_1\right)\cos\phi\sin\theta} \qquad 7.31$$

$$C = \sqrt{k^2} = k$$

Observe from figure 7.2 that θ and ϕ are the detector angles and that $\vec{e}_\theta$ is in the scattering plane while $\vec{e}_\phi$ is perpendicular. Therefore parallel and perpendicular components of the scattered field, equation 7.24, are expressed in terms of the form factors as

$$E_{\|,s} = - E_o e^{ikr} \frac{3k^2}{4r\pi} \frac{m^2 - 1}{m^2 + 2} V \left[- f_1 \cos\theta\cos\phi + f_2 \sin\phi \right] \qquad 7.32$$

$$E_{\perp,s} = - E_o e^{ikr} \frac{3k^2}{4r\pi} \frac{m^2 - 1}{m^2 + 2} V \left[- f_1 \sin\phi \right] \qquad 7.33$$

The scattering intensity is given by

$$I_s = \frac{1}{2} \mathrm{Re}\left(\sqrt{\frac{\epsilon}{\mu}} \right) \left[\left| E_{\|,s} \right|^2 + \left| E_{\perp,s} \right|^2 \right] \qquad 7.34$$

7.5 Scattering Amplitude Matrix Formulation for the Hybrid Model

Note that in this new model the scattered field can still be expressed using a scattering matrix in the manner of Van de Hulst, Bohren and Huffman, and Kerker. To do so, the incoming field must be expressed in terms of its components parallel and perpendicular to the scattering plane. In spherical coordinates the incoming field is given by

$$\vec{E}_i = E_o e^{ikz} \left(\sin\theta\cos\phi\,\hat{e}_r + \cos\theta\cos\phi\,\hat{e}_\theta - \sin\phi\,\hat{e}_\phi \right) \qquad 7.35$$

Here $\vec{e}_\phi$ is perpendicular to the scattering plane while the unit vector $\cos\theta\vec{e}_\theta + \sin\theta\vec{e}_r$ lies in the plane. As a result the incoming field can be written as:

$$\begin{aligned} E_{\|,i} &= E_o e^{ikz} \cos\phi \\ E_{\perp,i} &= E_o e^{ikz} \sin\phi \end{aligned} \qquad 7.36$$

65

After some manipulation the scattered field (equations 7.32, 7.33) can be related to the incident field in a scattering matrix format:

$$\begin{pmatrix} E_{\parallel,s} \\ E_{\perp,s} \end{pmatrix} = -\frac{3k^2}{4\pi r}\left(\frac{m^2-1}{m^2+2}\right)V \begin{vmatrix} -f_1\cos\theta + f_2\dfrac{\sin\theta}{\cos\phi} & 0 \\ 0 & -f_1 \end{vmatrix} \begin{pmatrix} E_{\parallel,i} \\ E_{\perp,i} \end{pmatrix} \qquad 7.37$$

7.6 Scattering Intensity Ratio and Turbidity

The scattering intensity ratio is expressed using equation 7.24.

$$\frac{I_s}{I_o} = \frac{|E_s|^2}{|E_o|^2} = \frac{9k^4}{32\pi^2 r^2}\left|\frac{m^2-1}{m^2+2}\right|^2 V^2\left[\left|-f_1\cos\theta\cos\phi + f_2\sin\theta\right|^2 - |f_1\sin\phi|^2\right] \quad 7.38$$

It can be written in terms of the scattering amplitude matrix equation 7.37; however this is not recommended due to the singularity $(\cos\theta)^{-1}$.

The formula for turbidity in the hybrid model is derived by calculating C_{sca} from insertion of equation 7.38 into equation 2.6 from chapter two; the absorption cross section C_{abs} remains as in equation 2.9:

$$C_{abs} = 3kV\,\mathrm{Im}\left(\frac{m^2-1}{m^2+2}\right) \qquad 7.39$$

the turbidity is finally determined by (equation 2.16)

$$\tau = N_p l\left(C_{sca} + C_{abs}\right) = N_p l G Q_{ext} \qquad 7.40$$

Chapter Eight

Validation and Sensitivity of Hybrid Theory

The previous chapter gave a detailed mathematical description of the hybrid model. This

chapter is dedicated to performance evaluation of the model in comparison to those of

Rayleigh-Debye-Gans and of Mie through a series of transmission simulation studies.

First the hybrid model was tested with the propagation constant of the medium equal to

that of the particle to verify correct programming implementation. Second the validity of

the hybrid theory using various particle sizes was tested for relative refractive indices

close to one. The third study tests the hybrid theory's effectiveness by introducing

absorption through the imaginary part of the refractive index. The last study investigates

the behavior of the hybrid theory for refractive indices exceeding the conditions required

for Rayleigh-Debye-Gans theory, that is, having strong scattering *and* absorption

components, for various diameter sizes. The other parameters (concentration, pathlength,

etc.) required to calculate the transmission were kept constant ,as listed in table 5.1.

8.1 Validation of Hybrid Theory Implementation

As we indicated in chapter six, when $k_1 \rightarrow k$ the internal Mie field approaches

the incoming field; c_1, d_1, and d_2 all approach 1. The calculations displayed by figure 8.1
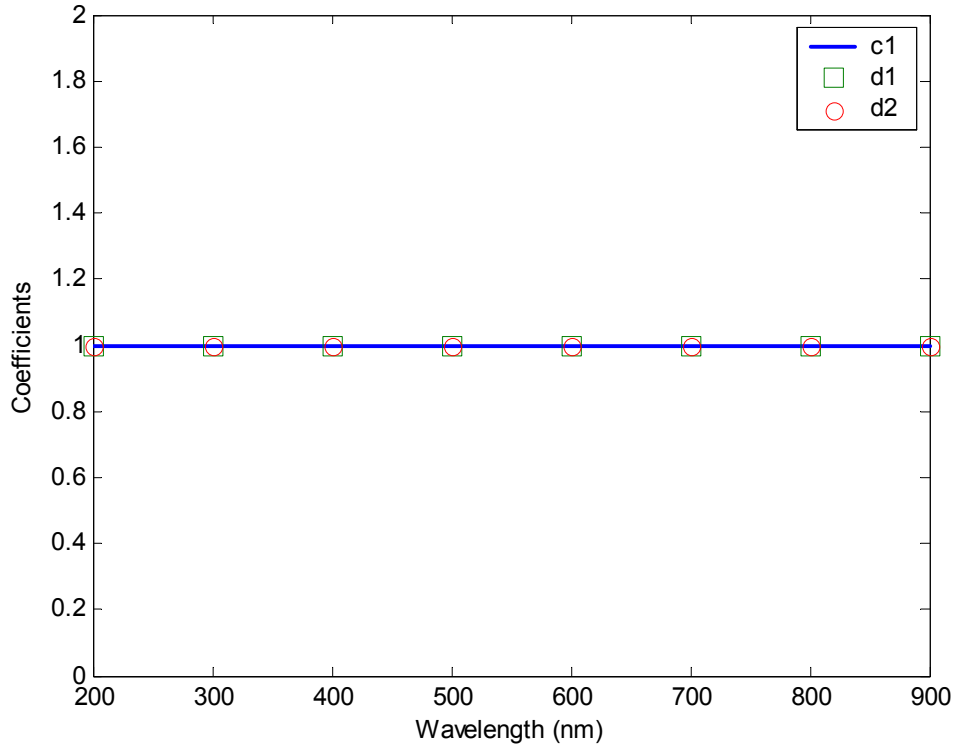
confirm that $c_1 = d_1 = d_2 = 1$ when $k_1 = k$.

Figure 8.1: Coefficients c_1, d_1, and d_2 Versus λ at the Limit when $k_1=k$

Another effect of taking k_1 equal to k is that the form factor f_1 of the hybrid model for spheres reduces to the form factor f of Rayleigh-Debye-Gans for spheres (and f_2 goes to zero). Figures 8.2 and 8.3 are 3-D images of these form factors graphed by wavelength λ and azimuthal angle of observation θ (with $\phi = 0$). Figure 8.2 shows f_1 of the hybrid model. The form factor f of Rayleigh-Debye-Gans is shown in figure 8.3.

As an example of the case where k_1 (particle) is different from k (medium), the refractive indices of polystyrene ($0.01 \leq \kappa_1 \leq 0.6$) in water ($\kappa = 0$) were used to illustrate the behavior of the form factors for the hybrid model compared to that of Rayleigh-Debye-Gans. Figures 8.4, 8.5, 8.6, and 8.7 are the real and imaginary parts of the form factors f_1 and f_2 for the hybrid model. Figure 8.8 is the form factor for Rayleigh-

Debye-Gans. Note that the hybrid model's factors contain real and imaginary parts even if $\kappa = 0$ (nonabsorbing).

Therefore our working program for the hybrid theory has been validated. The next sections will reveal the superiority of the hybrid theory in approximating the exact (Mie) solution, for different particle diameters and relative refractive indices.
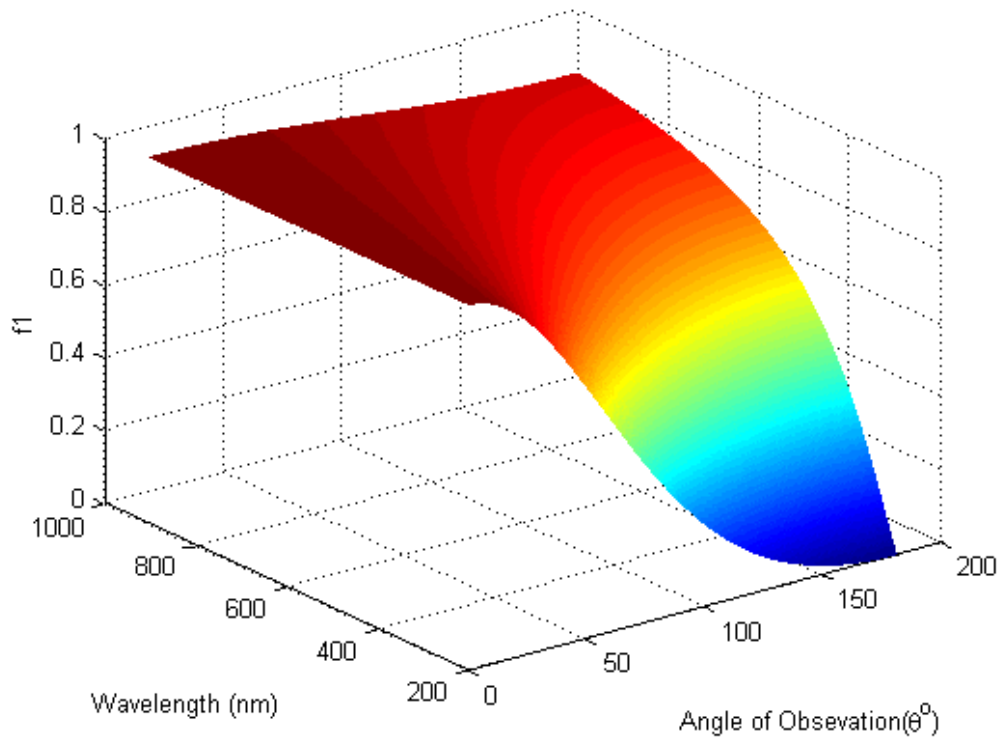
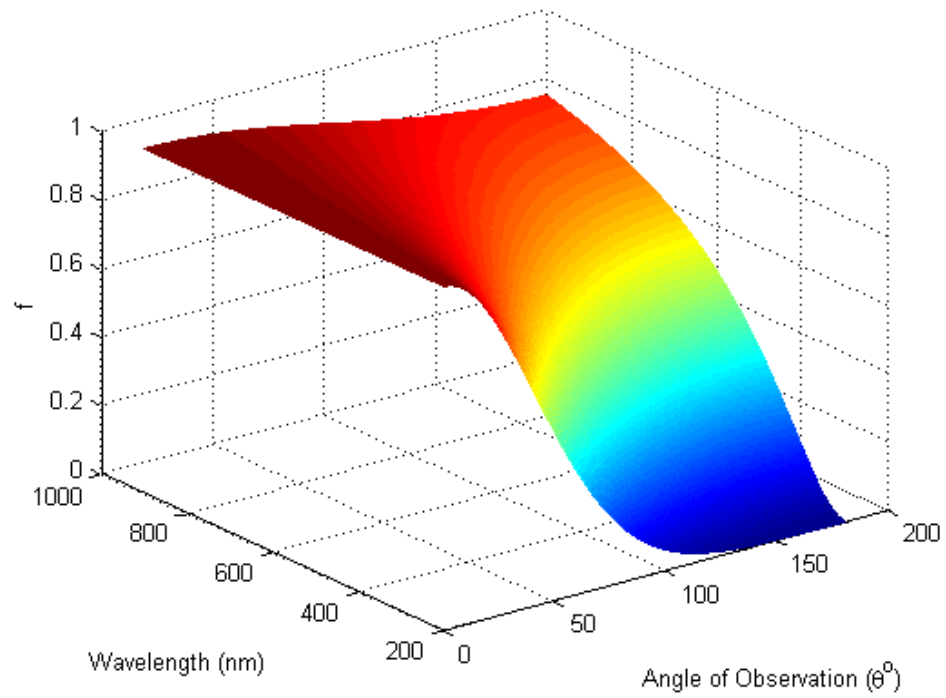*Figure 8.2: Form Factor f_1 for Hybrid Theory at $k_1=k$*
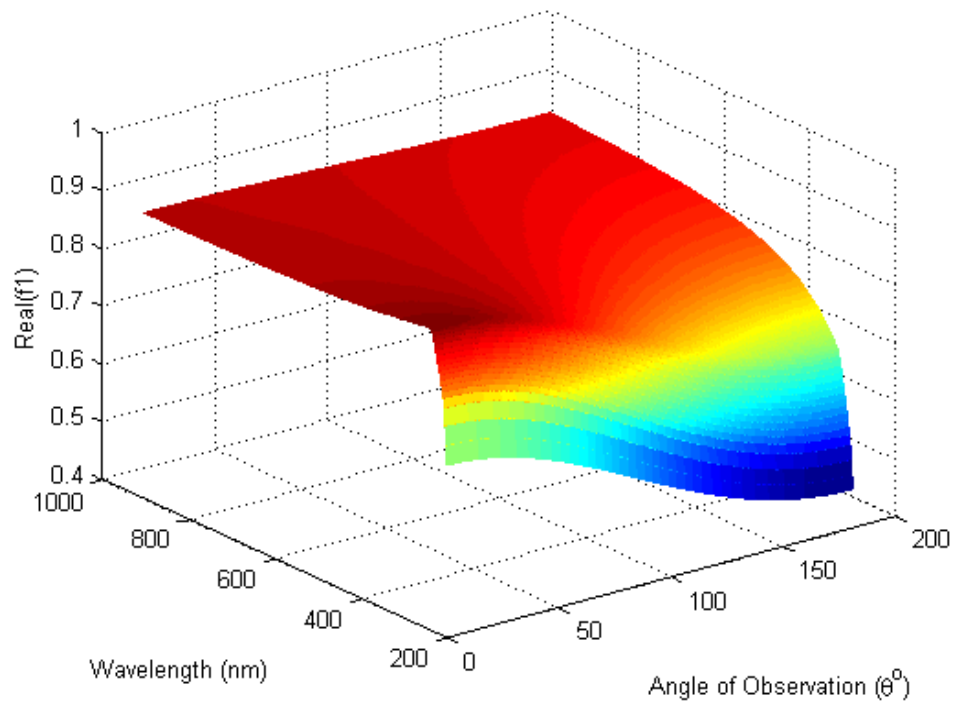
Figure 8.3: Form Factor f for Rayleigh-Debye-Gans Theory

Figure 8.4: Real Part of Form Factor f_1 for Hybrid Theory using Polystyrene
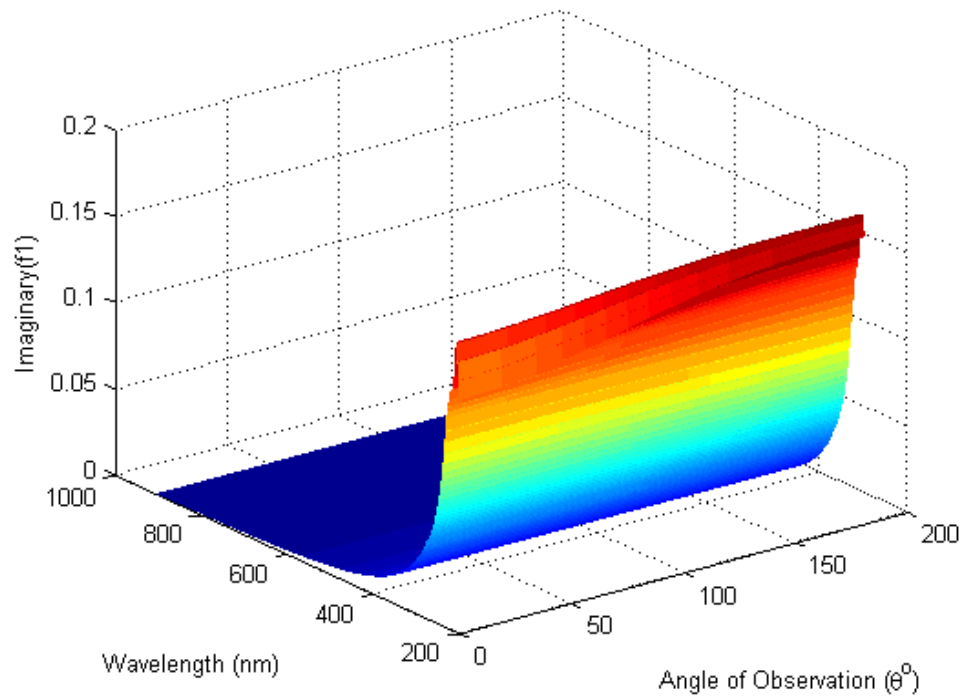
Figure 8.5: Imaginary Part of Form Factor f_1 for Hybrid Theory using Polystyrene
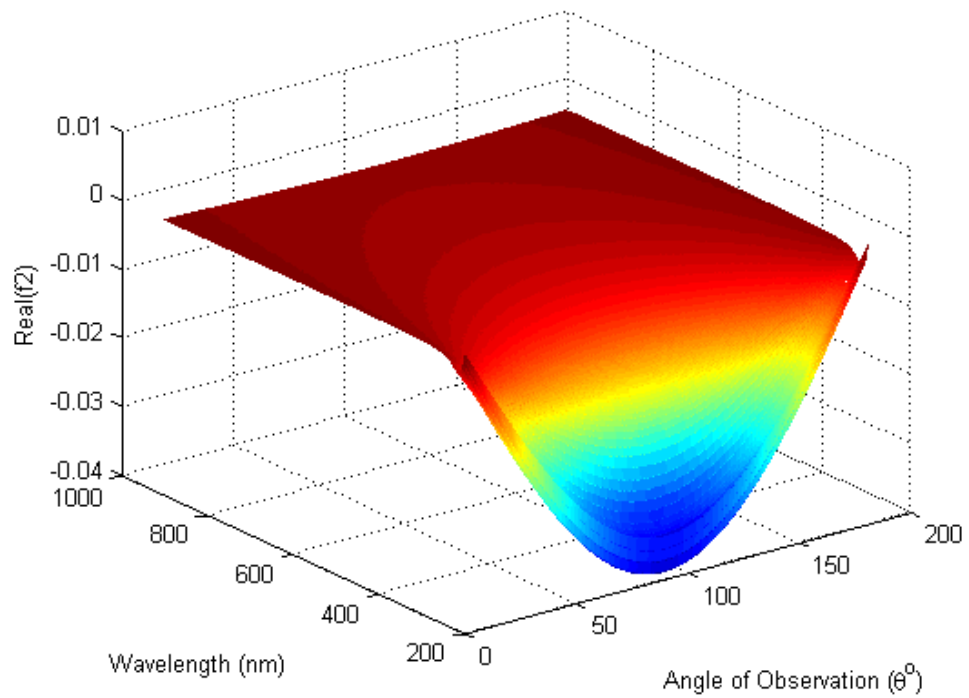
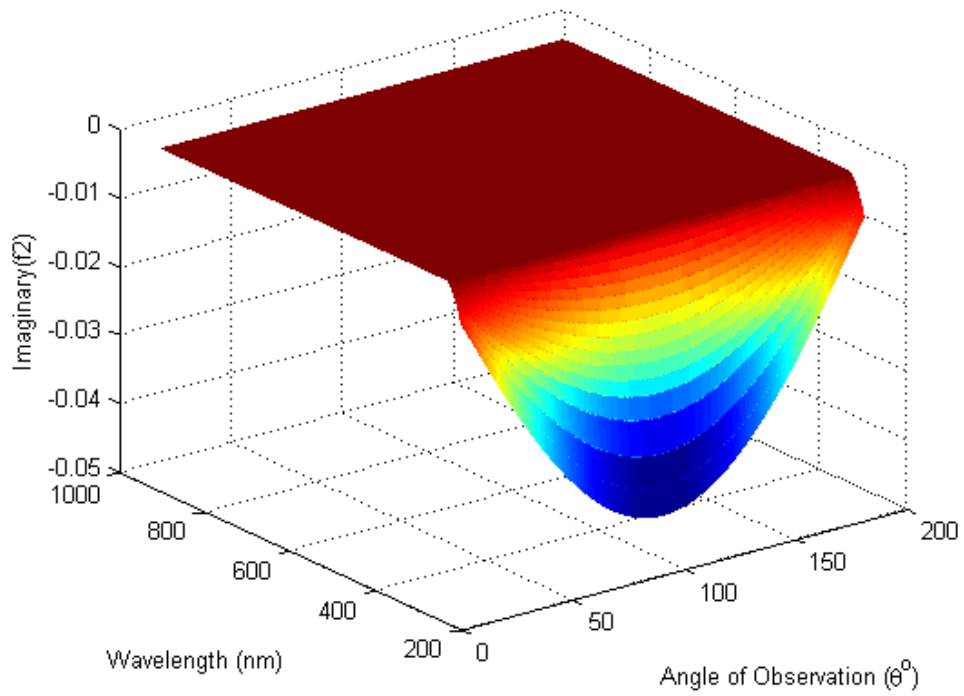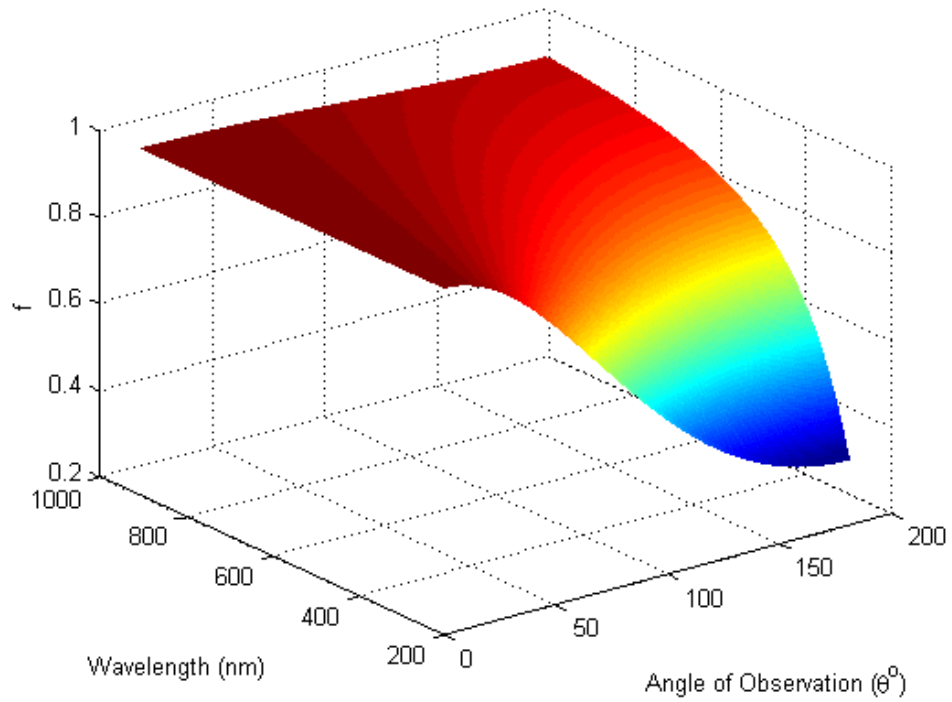*Figure 8.6: Real Part of Form Factor f_2 for Hybrid Theory using Polystyrene*

71

Figure 8.7: Imaginary Part of Form Factor f_2 for Hybrid Theory using Polystyrene

Figure 8.8: Form Factor f for Rayleigh-Debye-Gans Theory using Polystyrene

8.2 Case 1: Relative Refractive index n/n_0 ~1 and Absorption $\kappa = 0$

The validity of the hybrid theory was tested against Rayleigh-Debye-Gans and Mie theory using the relative refractive indices of soft bodies ($n/n_o = 1.04$) to calculate the transmission. The spherical diameter sizes used were 50, 100, 250, and 500 nm. The results of this study are shown in transmission spectral plots provided in figures 8.9, 8.10, 8.11 and 8.12. Figures 8.9 (50 nm) and 8.10 (100 nm) show that the hybrid theory for very small particles at the shorter wavelengths is a much better approximation to Mie theory than is RDG theory. At wavelengths much larger than the particle size, the hybrid spectrum is still superior to Rayleigh-Debye-Gans. In figure 8.11 the hybrid model for 250 nm particles closely estimates Mie theory above 300nm wavelength and outperforms RDG even down to 200 nm wavelength (which is shorter than the diameter).

A significant change in the calculated transmission spectra is observed in figure 8.12, where the diameter size is 500 nm. Here the hybrid spectrum no longer resembles that of Mie theory or RDG at wavelengths shorter than half the diameter. Nonetheless, for larger wavelengths the hybrid model again is a better approximation to the exact Mie theory than Rayleigh-Debye-Gans. The inset of figure 8.12 is a zoom in of the spectra between 500 nm to 900 nm wavelength showing the hybrid model approximating better than RDG at the longer wavelengths.

In summary, the hybrid theory is seen to be a vastly improved model for estimating the transmission for nonabsorbing soft particles whose diameter is smaller than the wavelength. The following section will explore the effect of including absorption in the hybrid model.
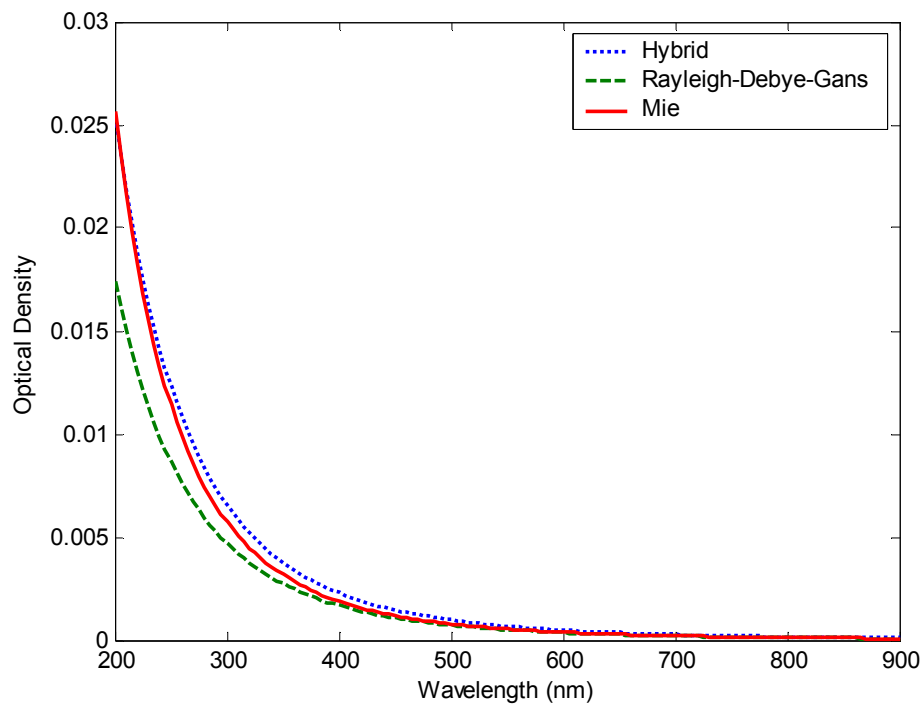
73

Figure 8.9: Comparison of Calculated Transmission for 50 nm Soft Body Spheres using RDG, Mie, and Hybrid Theories
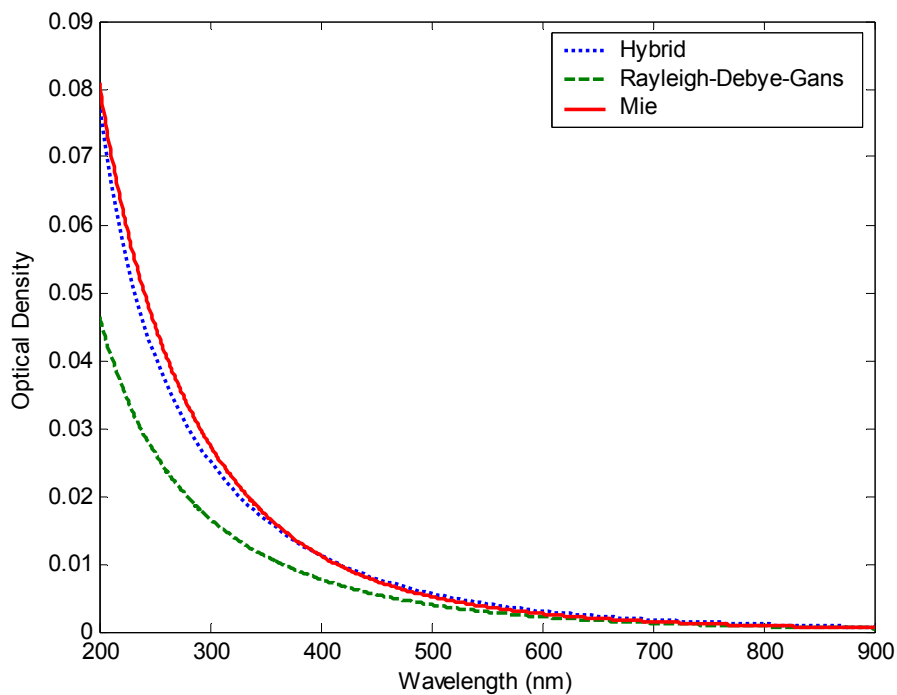

Figure 8.10: Comparison of Calculated Transmission for 100 nm Soft Body Spheres using RDG, Mie, and Hybrid Theories
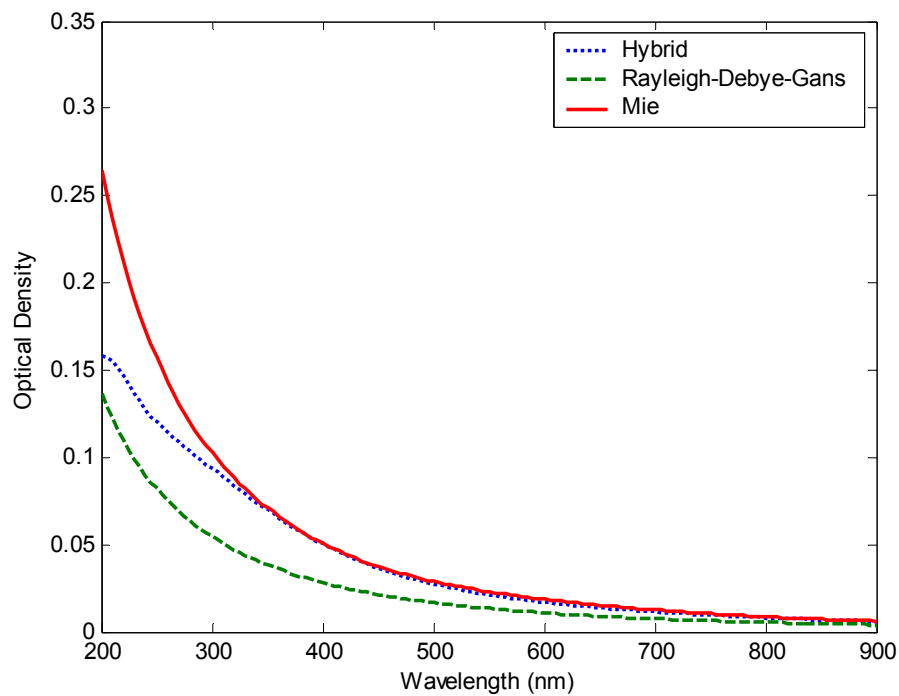
Figure 8.11: Comparison of Calculated Transmission for 250 nm Soft Body Spheres using RDG, Mie, and Hybrid Theories
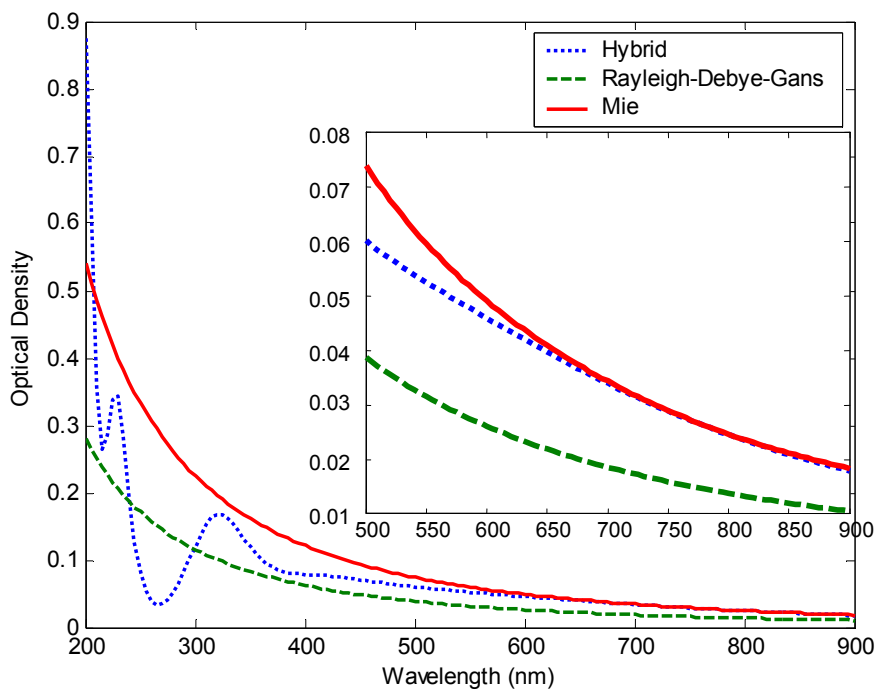

Figure 8.12: Comparison of Calculated Transmission for 500 nm Soft Body Spheres using RDG, Mie, and Hybrid Theories

75

8.3 Case 2: Relative Refractive index $n/n_0 \geq 1$ and Absorption $\kappa > 0$

The previous section showed that the hybrid model provided an improved approximation to Mie theory for nonabsorbing particles and whose relative refractive index is greater than or equal to one. In this section the contribution of absorption κ is included in the refractive index n, while the relative refractive n/n_0 was kept close to one. The optical properties of polystyrene ($1.1 \leq n/n_o \leq 1.5, 0.01 \leq \kappa \leq 0.6$) were chosen in keeping with the requirements aforementioned. The diameter sizes selected for the transmission calculations were, again, 50, 100, 250, and 500 nm. Figures 8.13 and 8.14 are plotted on a semi log scale to enhance the features of the spectra. For particles diameters of 50 and 100 nm, figures 8.13 and 8.14, the calculated transmission by the hybrid model continues to approximate Mie theory closer than Rayleigh-Debye-Gans.

As the particle diameter is increased to 250 nm and 500nm, figure 8.15 and 8.16, interestingly the hybrid spectra qualitatively mimics the reduced transmission features displayed by Mie theory at wavelengths shorter than the diameter. At wavelengths comparable to or larger than the diameter, the hybrid model remains the better estimate to Mie theory. The insets of figures 8.15 and 8.16 show the spectra where the particle diameter is that of the wavelength and emphasize how well the hybrid model behaves compared to RDG in approximating Mie theory.

Evidently from the graphs, the differences between the incoming field and the Mie field are quite significant when absorption is present. The results demonstrate that the hybrid model provides an improved approximation over Rayleigh-Debye-Gans theory for absorbing scatterers whose relative refractive index is close to one, over a very large

range of wavelengths. The next section studies the behavior of the hybrid model for absorbing scatterers whose relative refractive index is approximately 1.
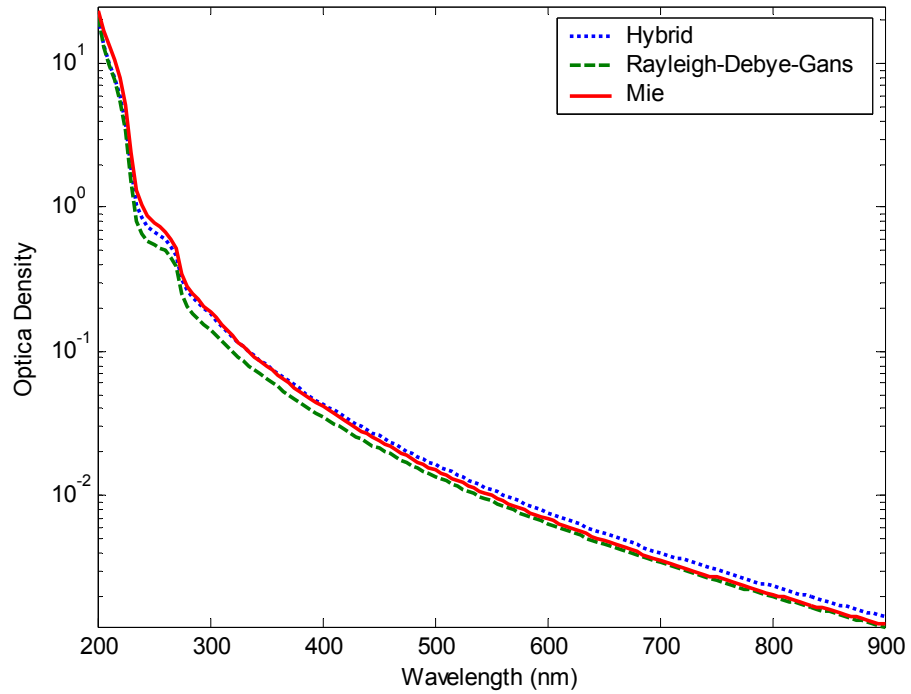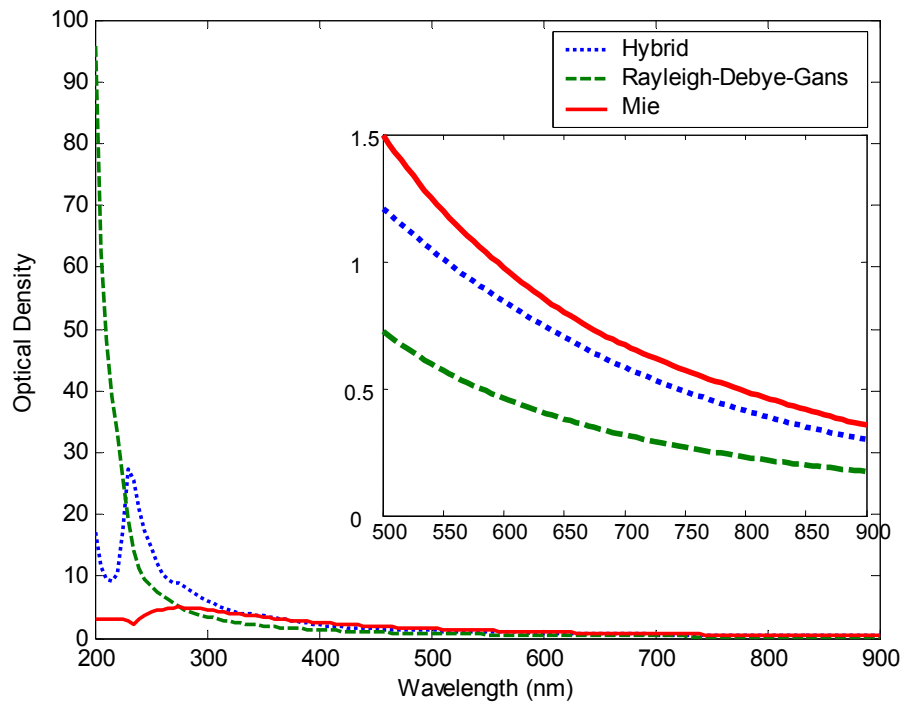

8.13: Comparison of Calculated Transmission for 50 nm Polystyrene Spheres using RDG, Mie, and Hybrid Theories
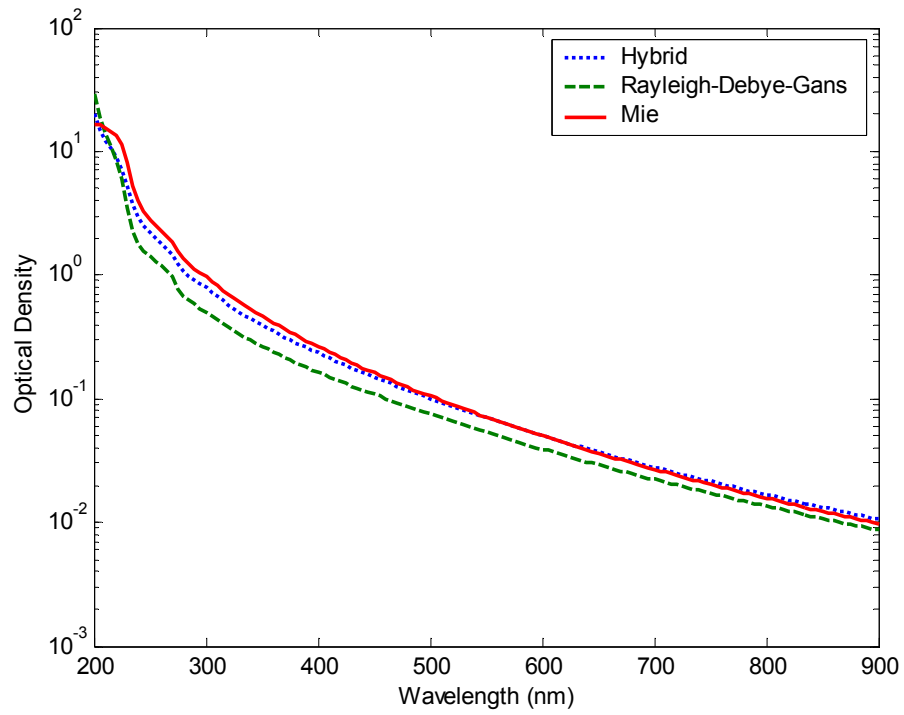
8.14: Comparison of Calculated Transmission for 100 nm Polystyrene Spheres using RDG, Mie, and Hybrid Theories
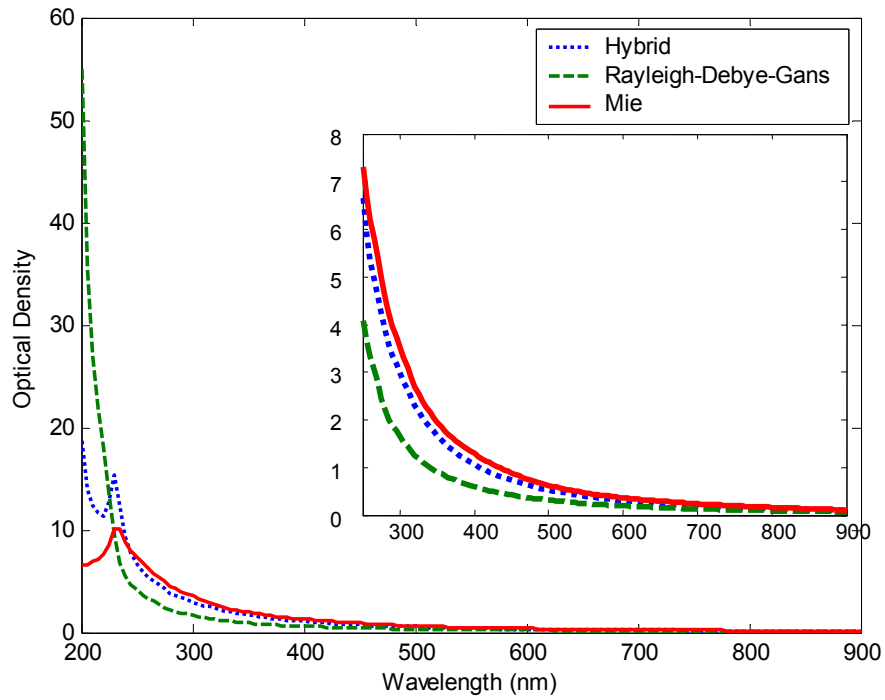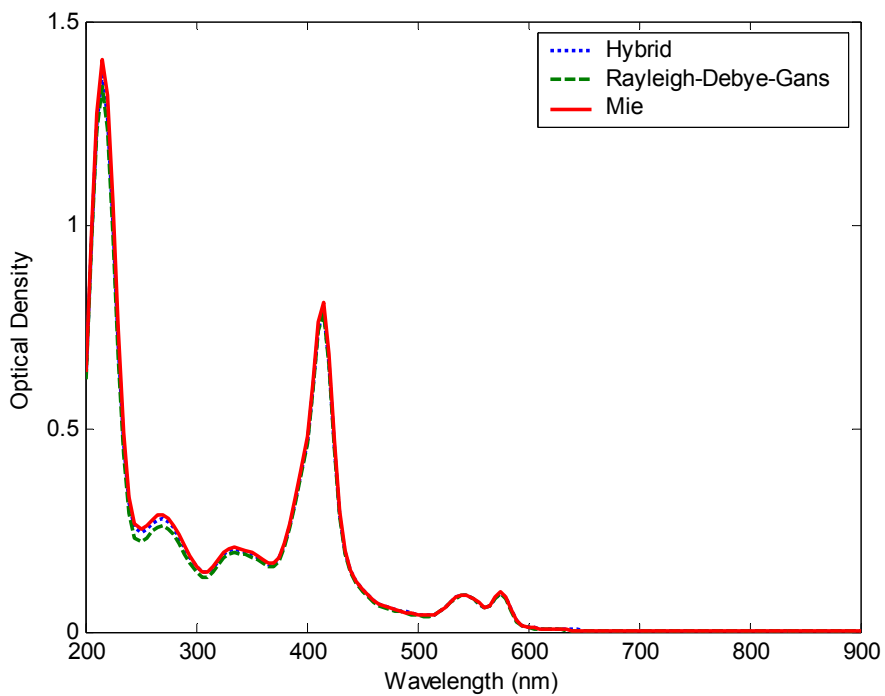

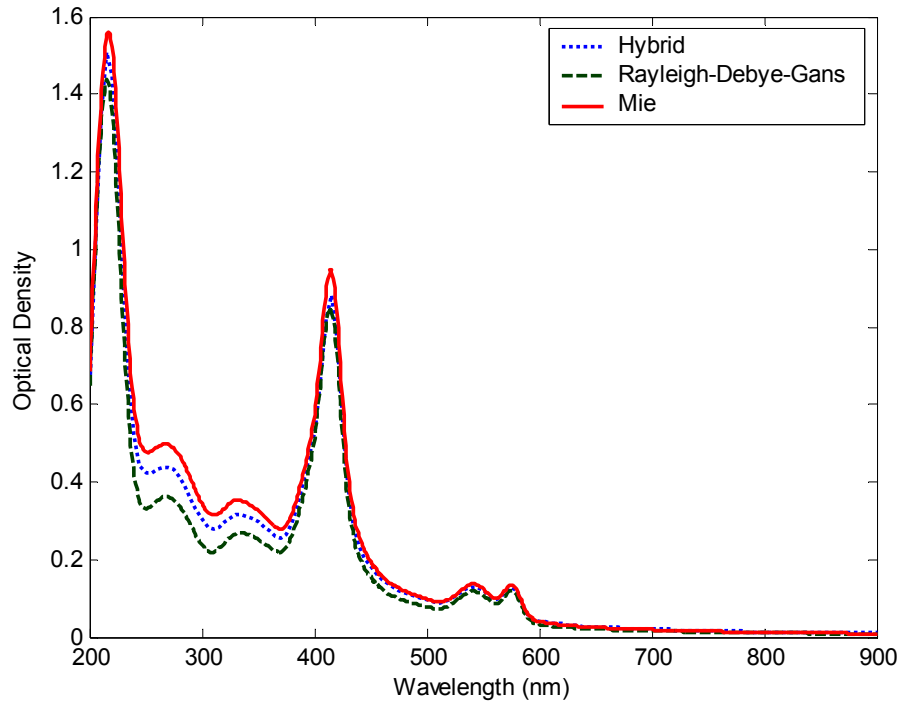*8.15: Comparison of Calculated Transmission for 250 nm Polystyrene Spheres using RDG, Mie, and Hybrid Theories*

8.16: Comparison of Calculated Transmission for 500 nm Polystyrene Spheres using RDG, Mie, and Hybrid Theories

## 8.4 Case 3: Relative Refractive index $n/n_0 \sim 1$ and Absorption $\kappa > 0$

Now we turn to more general scatterers, with large relative indices of refraction and nonzero absorption. Hemoglobin ($1 \leq n/n_o \leq 1.2, \, 0.01 \leq \kappa \leq 0.15$) is both a strong scatterer and strong absorber and thus a good test study. The diameter sizes used to calculate the transmission were 50, 100, 250, and 500 nm. Figures 8.17, 8.18, 8.19, and 8.20 show that at 50, 100 and 250 nm diameters the hybrid theory spectra approximates Mie theory better than does Rayleigh-Debye-Gans at all wavelengths, and at the diameter size of 500 nm (figure 8.20), the hybrid model provides a better estimate to Mie theory than Rayleigh-Debye-Gans for wavelengths larger than 300nm.
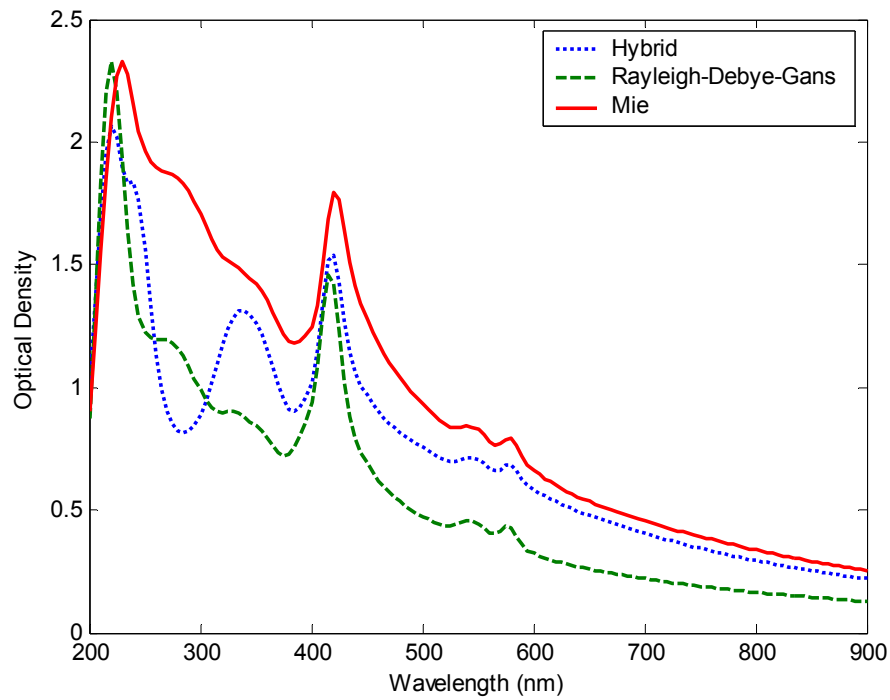
8.17: Comparison of Calculated Transmission for 50 nm Hemoglobin Spheres using RDG, Mie, and Hybrid Theories

8.18: Comparison of Calculated Transmission for 100 nm Hemoglobin Spheres using RDG, Mie, and Hybrid Theories
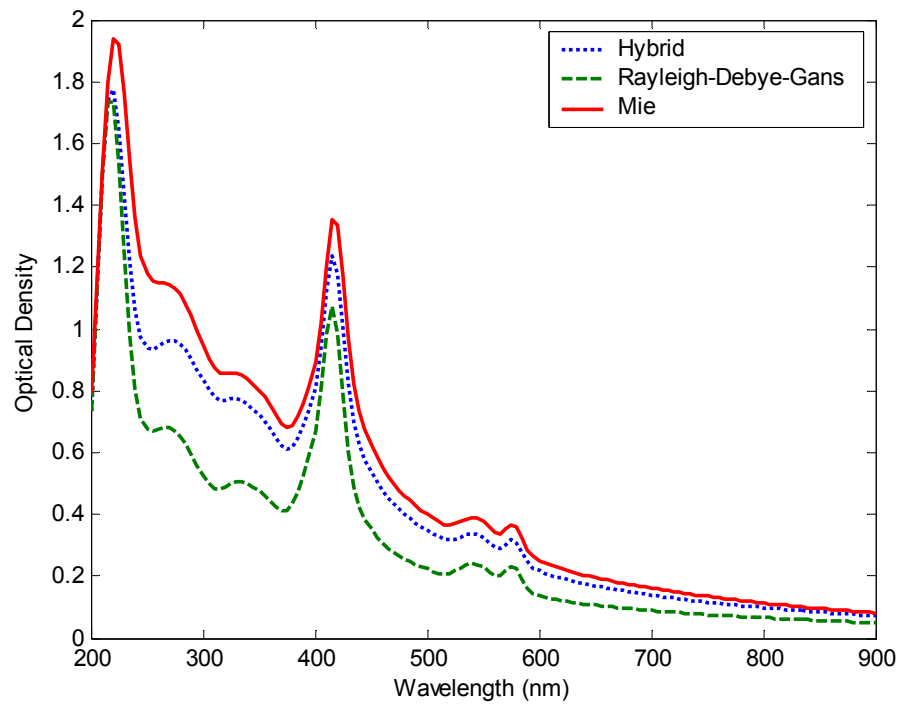
8.19: Comparison of Calculated Transmission for 250 nm Hemoglobin Spheres using RDG, Mie, and Hybrid Theories

8.20: Comparison of Calculated Transmission for 500 nm Hemoglobin Spheres using RDG, Mie, and Hybrid Theories

81

8.5 Conclusions

The hybrid model for submicron spheres has been shown to approximate Mie theory much better than Rayleigh-Debye-Gans for particle sizes smaller than the wavelength. For a wide range of relative refractive indices the improvement is particularly marked for absorbing materials. For the cases were absorption is introduced, the curves displayed that attenuation becomes more significant for the larger particles, and the hybrid theory is superior in accommodating attenuation. The results of the simulations conducted in this chapter demonstrate that the strategy of using the Mie internal field, rather than the incoming field, to energize the RDG dipoles reaps very significant benefits. One important benefit from the hybrid model was the computation time for calculating these spectra which was rapid.

Chapter Nine

Contributions and Future Work

9.1 Contributions

Mie theory is an exact solution to the wave equation for spherical scatterers [1]. This

rigorous solution is limited to spheres and although it provides a good estimate for some

characteristics of nonspherical particles, Mie theory cannot provide information on shape

and orientation. Rayleigh-Debye-Gans theory is an approximation to Mie theory and

provides, through form factors, information about nonspherical particles. The principal

limitation of Rayleigh-Debye-Gans theory is that the complex relative refractive index

must be close to one. Other theories exist for determining the light scattering behavior of

nonspherical submicron particles, such as the T-matrix and Purcell-Pennypacker

methods. In terms of real-time applications, these methods are more computationally

intensive and therefore time consuming both in code generation and computer time. The

methods available are time consuming to the extent of making them impractical for

engineering applications such as real time particle characterization.

The hybrid model presented here provides another tool for the analysis of

submicron particles for real-time computations at multiwavelength. The key to the

superior performance of the hybrid theory is the incorporation of the Mie field, rather the

incoming field, to generate the scattering produced by a particle. This hybrid model has

demonstrated vastly improved accuracy and applicability for a broader range of optical

properties than that of Rayleigh-Debye-Gans for multiwavelength particle characterization applications.

9.2 Recommendations and Future Work

Like most original work, the hybrid theory can be improved for the spherical model. As the theory stands, the truncation at the first term of the series for the internal field can be extended to include second order terms. These second order terms will influence the series for particles whose size is comparable with the wavelength. In other words, at the shorter wavelengths the hybrid model does not exactly match Mie theory or Rayleigh-Debye-Gans, but by extending the series we can include terms that will validate the model where $a/\lambda \approx 1$.

The hybrid model has been worked out for spherical particles; a proposed method of extending this model to other shapes such as ellipsoids could proceed by assuming that the internal field of the ellipsoid can be described by mapping the Mie internal field for a volume equivalent, or perhaps a circumscribing, sphere evaluated, as presented in chapter six, from the induced dipole moment using the postulated field. To account for the shape of the particle, the form factor $\int e^{i\vec{R}\cdot\vec{S}} dV$ needs to be evaluated for the ellipsoid shape, as demonstrated with a sphere in chapter six. These factors can be determined directly from table 4.1 by reinterpreting the constant vector $\vec{S}$. Although the mathematics may appear complex for the form factors, they are relatively straightforward though time consuming.

References

[1] Bohren, Craig F. and Huffman, Donald R.; Absorption and Scattering of Light by Small Particles, Wiley Science Paper Series, 1998.

[2] Van de Hulst, H.C.; Light Scattering by Small Particles, Dover Publications, Inc, New York, 1957.

[3] Garcia-Rubio, L.H.; *"Averages from Turbidity Measurements"*, ACS Symposium Series, vol 332, 11, 161-178, 1987.

[4] Garcia-Lopez, A.C.; Investigation into the Transition between Single and Multiple Scattering for Colloidal Dispersions, 2001.

[5] Kerker, Milton; The Scattering of Light and other Electromagnetic Radiation, Academic Press, New York, 1969.

[6] Singham Shermila B. and Bohren Craig F., *"Hybrid Method in Light Scattering by an Arbitrary Particle"*, Applied Optics, vol 28, No. 3, 1989.

[7] Bohren Craig F, *"Backscattering by Nonspherical Particles: A Review of Methods and Suggested New Approaches"*, Journal of Geophysical Research, vol 96, No. D3, 1991.

[8] Mishchenko Michael I., Travis Larry D., and Mackowski Daniel W., *"T-Matrix Computations of Light Scattering by Nonspherical Particles: A Review'*, J. Quant. Spectrosc. Radiat., vol 55, No. 5, 1996.

[9] Deepak Adarsh, Box Michael A.; *"Forward Corrections for Optical Extinction Measurements in Aerosol Media: Monodispersions*", Applied Optics, vol 12, No.18, 1978.

[10] Maron, Samuel H. and Prutton, Carl F.; Principles of Physical Chemistry, The Macmillan Company, New York.

[11] Veshkin, N.L; *"Screening Hypochromism of Biological Macromolecules and Suspensions"*, Journal of Photochemistry and Photobiology, B: Biology, vol 3, 625-630, 1989.

[12] Veshkin, N.L; *"Screening Hypochromism of Molecular Aggregates and Biopolymers"*, Journal of Biological Physics, vol 25, 339-354, 1999.

[13] Veshkin, N.L; *"Screening Hypochromism of Chromophores in Macromolecular Biostructures"*, Biophysics, vol 44, 1, 41-51, 1999.

[14] Wiscombe, W.J.; *"Mie Scattering Calculations: Advances in Technique and Fast, Vector-Speed Computer Codes"*, NCAR/TN-140 + STR. National Center for Atmospheric Research, Boulder Colorado, 1979.

[15] Latimer, Barber P.; *"Scattering by Ellipsoids of Revolution; A Comparison of Theoretical Methods"*, Journal of Colloid Interface Science, vol 63, 310-316, 1977.

[16] Narayanan, Smita; Aggregation and Structural Changes in Biological Systems: An Ultraviolet Visible Spectroscopic Approach for Analysis of Blood Cell Aggregation and Protein Conformation, 1999.

[17] Garcia-Rubio, L.H; Private Communication.

[18] Buehler, Christopher S.; Measurement of Orientation Distribution of Spheriod Particles by Light Scattering, 1991.

Appendices

Appendix A: Intensity Ratio and Turbidity Model

Derivation of the intensity equation for RDG and non-polarized light: Beginning

with the equation of light taken from Van de Hulst [2]

$$I(\theta,\lambda) = I_{\perp} + I_{\parallel} = (i_1 + i_2)\frac{1}{2}\frac{I_o}{k_2 r^2}$$
A.1

where

$$i_1 = |S_1(\theta,\lambda)|^2 \quad i_2 = |S_2(\theta,\lambda)|^2$$
A.2

The scattering functions are described as function of the polarizability α

$$S_1(\theta,\lambda) = -i\mathrm{k}^3\alpha$$
$$S_2(\theta,\lambda) = -i\mathrm{k}^3\alpha\cos\theta$$
A.3

were k is the propagation constant, $\mathrm{k}(\lambda) = 2\pi/\lambda_m$ and λ_m is the wavelength in the

material. The polarizability for particles with a refractive index close to 1 and

homogeneous with no approximation for the complex refractive index is

$$\alpha = \frac{3}{4\pi}\int\left(\frac{m^2-1}{m^2+2}\right)dV = \frac{3}{4\pi}\left(\frac{m^2-1}{m^2+2}\right)V$$
A.5

To account for the interference effects for each dipole, the phase factor is included to

scattering function, equation (3)

$$S_1(\theta,\lambda) = -i\mathrm{k}^3 e^{i\delta}\alpha$$
$$S_2(\theta,\lambda) = -i\mathrm{k}^3 e^{i\delta}\alpha\cos\theta$$
A.6

The scattering function can be explicitly written in terms of the polarizablity by replacing

equation A.5 into A.6

Appendix A (Continued)

$$S_1(\theta,\lambda) = -ik^3 V e^{i\delta} \frac{3}{4\pi}\left(\frac{m^2-1}{m^2+2}\right)$$

$$S_2(\theta,\lambda) = -ik^3 V e^{i\delta} \frac{3}{4\pi}\left(\frac{m^2-1}{m^2+2}\right)\cos\theta$$

A.7

Let $R(\theta,\vartheta) = \frac{1}{V}\int e^{i\delta}dV$, this is the form factor; which is replace it in equation A.7

$$S_1(\theta,\lambda) = -ik^3 V \frac{3}{4\pi}\left(\frac{m^2-1}{m^2+2}\right)R(\theta,\vartheta)$$

$$S_2(\theta,\lambda) = -ik^3 V \frac{3}{4\pi}\left(\frac{m^2-1}{m^2+2}\right)R(\theta,\vartheta)\cos\theta$$

A.8

Now that the scattering functions are defined in terms of shape, replace equation A.8 into

equation A.2.

$$i_1 = |S_1(\theta,\lambda)|^2 = \frac{9k^6 V^2}{16\pi^2}\left|\frac{m^2-1}{m^2+2}\right|^2 |R(\theta,\vartheta)|^2$$

$$i_2 = |S_2(\theta,\lambda)|^2 = \frac{9k^6 V^2}{16\pi^2}\left|\frac{m^2-1}{m^2+2}\right|^2 |R(\theta,\vartheta)|^2 \cos\theta$$

A.9

Take the equation above and replace it in equation A.1

$$I(\theta,\lambda) = I_\perp + I_\parallel = \frac{9k^4 V^2}{32\pi^2 r^2}\left|\frac{m^2-1}{m^2+2}\right|^2 |R(\theta,\vartheta)|^2 (1+\cos^2\theta)I_o \qquad A.10$$

Equation A.10 is the intensity ratio model which mathematical describes the light

scattered by an arbitrary particle in terms of a non-polarized light source. Per this

derivation, it can be seen that the wavelength dependence of these functions.

The transmission equation as described by Kerker is mathematically described as

$$\tau = N_p \ell \int_0^\infty G Q_{ext} f(D)dD \qquad A.11$$

89

Appendix A (Continued)

For a monodispersed system $f(D)dD$ is represented by a delta function, therefore its

integral equal to one. The scattering efficiency factor Q_{ext} is function of the absorption

and scattering of the particle and is described as

$$Q_{ext} = Q_{sca} + Q_{abs}.$$ A.12

The scattering efficiency factors are defined in terms of the particle scattering cross

sectional C_{sca} and it's cross sectional area G.

$$Q_{sca} = \frac{C_{sca}}{G}$$ A.13

The general equation for the scattering cross section [2]

$$C_{sca} = \int \frac{I}{I_o} r^2 \sin\theta \, d\theta d\vartheta$$ A.14

The intensity ratio in the equation above can be replaced with equation A.10 and

evaluated as

$$
\begin{aligned}
C_{sca} &= \int_0^{2\pi}\int_0^{\pi} \frac{9k^4V^2}{32\pi^2 r^2} \left|\frac{m^2-1}{m^2+2}\right|^2 |R(\theta,\vartheta)|^2 (1+\cos^2\theta)r^2 \sin\theta \, d\theta d\vartheta \\
&= \frac{9k^4V^2}{32\pi^2} \left|\frac{m^2-1}{m^2+2}\right|^2 \int_0^{2\pi}\int_0^{\pi} |R(\theta,\vartheta)|^2 (1+\cos^2\theta)\sin\theta \, d\theta d\vartheta \quad\quad \text{A.15}\\
&= \frac{9k^4V^2}{16\pi} \left|\frac{m^2-1}{m^2+2}\right|^2 \int_0^{\pi} |R(\theta,\vartheta)|^2 (1+\cos^2\theta)\sin\theta \, d\theta
\end{aligned}
$$

Substituting the C_{sca} into equation A.13 results in

Appendix A (Continued)

$$Q_{sca} = \frac{9k^4V^2}{16\pi G}\left|\frac{m^2-1}{m^2+2}\right|^2 \int_0^{\pi}|R(\theta,\vartheta)|^2(1+\cos^2\theta)\sin\theta\,d\theta \qquad \text{A.16}$$

The absorption efficiency factor is defined similarly to that of the scattering efficiency factor, equation A.13, except in terms of absorption. The absorption cross section C_{abs} is defined as

$$C_{abs} = 3kV\,\text{Im}\left(\frac{m^2+1}{m^2+2}\right) \qquad \text{A.17}$$

The absorption efficiency factor can then be expressed as

$$Q_{abs} = \frac{3kV}{G}\text{Im}\left(\frac{m^2+1}{m^2+2}\right) \qquad \text{A.18}$$

The transmission equation A.11 can be explicitly expressed in terms of the scattering and absorption components of the efficiency factor.

$$\tau = N_p\ell G\left[\frac{9k^4V^2}{16\pi G}\left|\frac{m^2-1}{m^2+2}\right|^2 \int_0^{\pi}|R(\theta,\vartheta)|^2(1+\cos^2\theta)\sin\theta\,d\theta + \frac{3kV}{G}\text{Im}\left(\frac{m^2+1}{m^2+2}\right)\right] \quad \text{A.19}$$
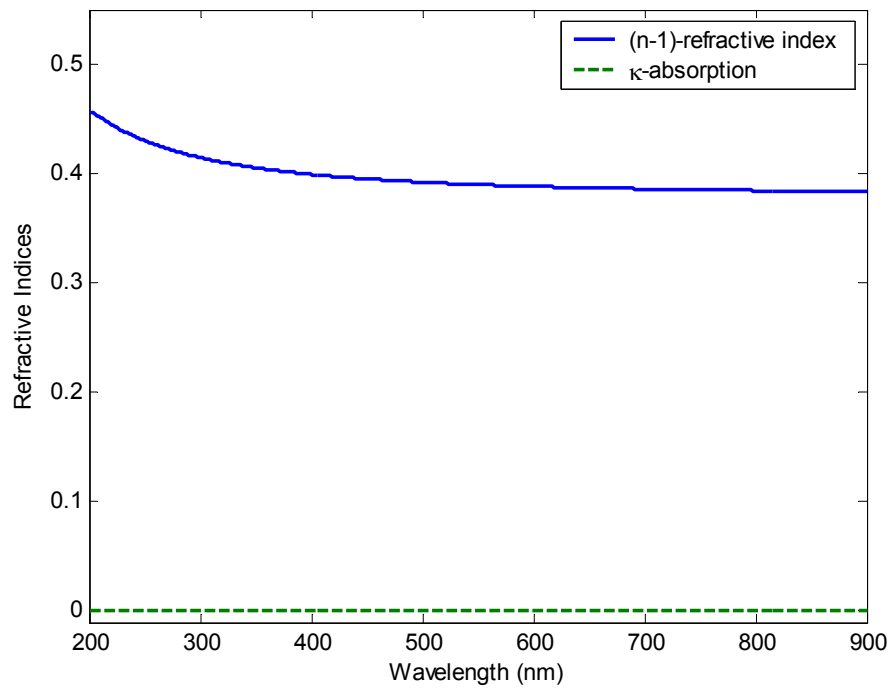
Equation A.19 is the general form of transmission equation for all form factors. Since the nomenclature of *Kerker* is being used, $|R(\theta,\varphi)|^2 = P(\theta)$ and can be replaced.

$$\tau = N_p\ell G\left[\frac{9k^4V^2}{16\pi G}\left|\frac{m^2-1}{m^2+2}\right|^2 \int_0^{\pi}P(\theta)^2(1+\cos^2\theta)\sin\theta\,d\theta + \frac{3kV}{G}\text{Im}\left(\frac{m^2+1}{m^2+2}\right)\right] \quad \text{A.20}$$

Appendix B: Optical Properties
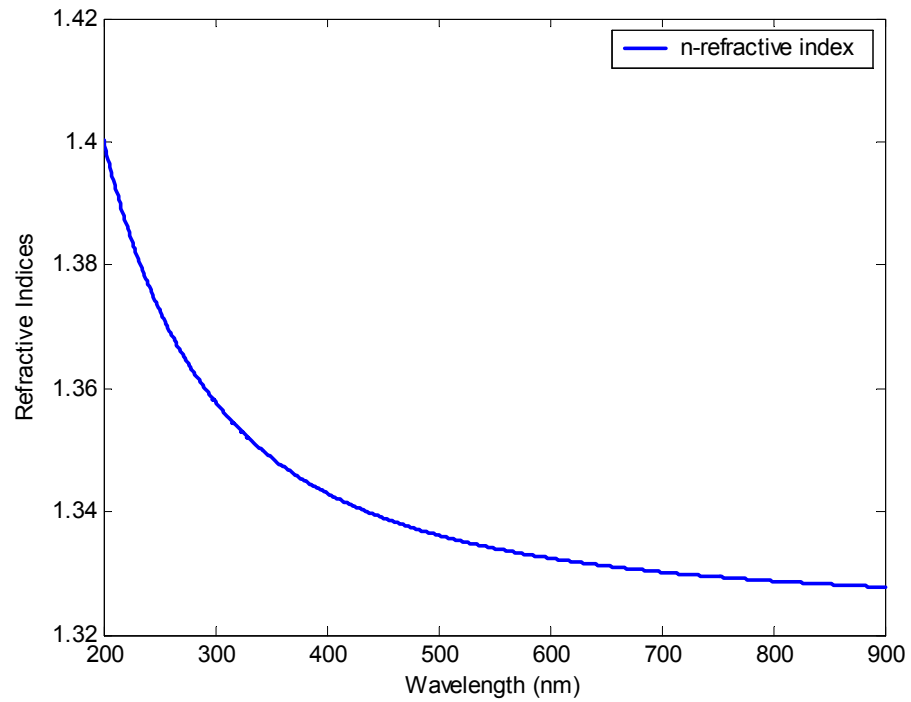
Figure B.1: Optical Properties for Water

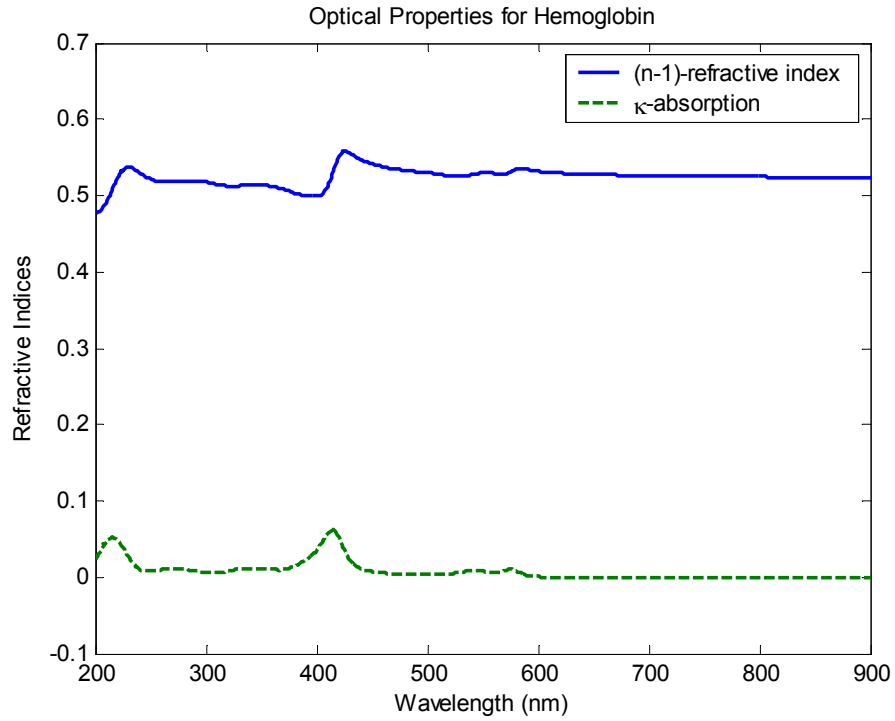*Figure B.2: Optical Properties for Soft Body*

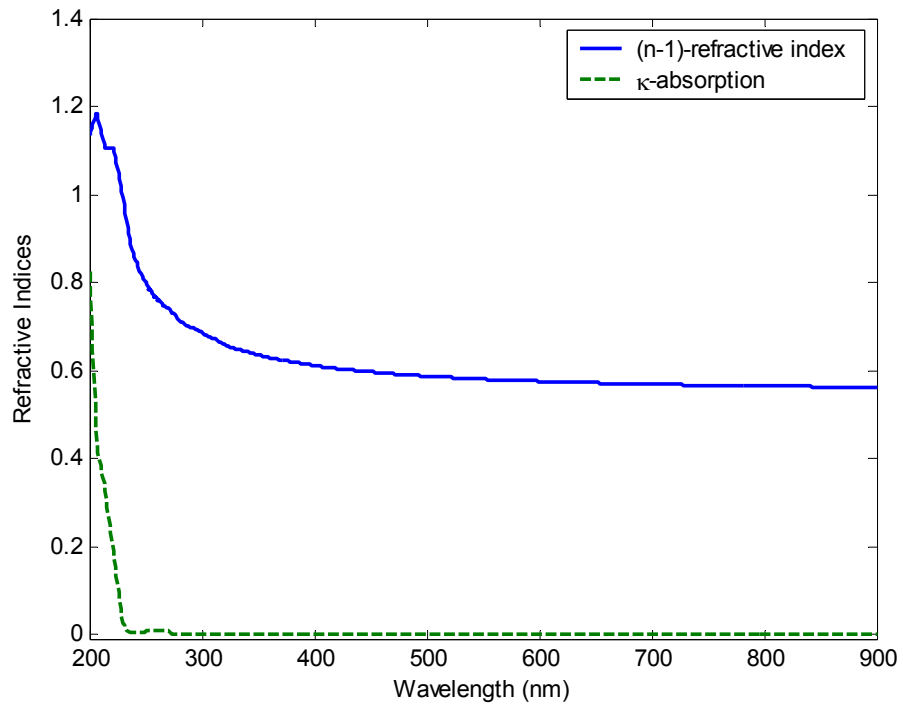*Figure B.3: Optical Properties for Hemoglobin*

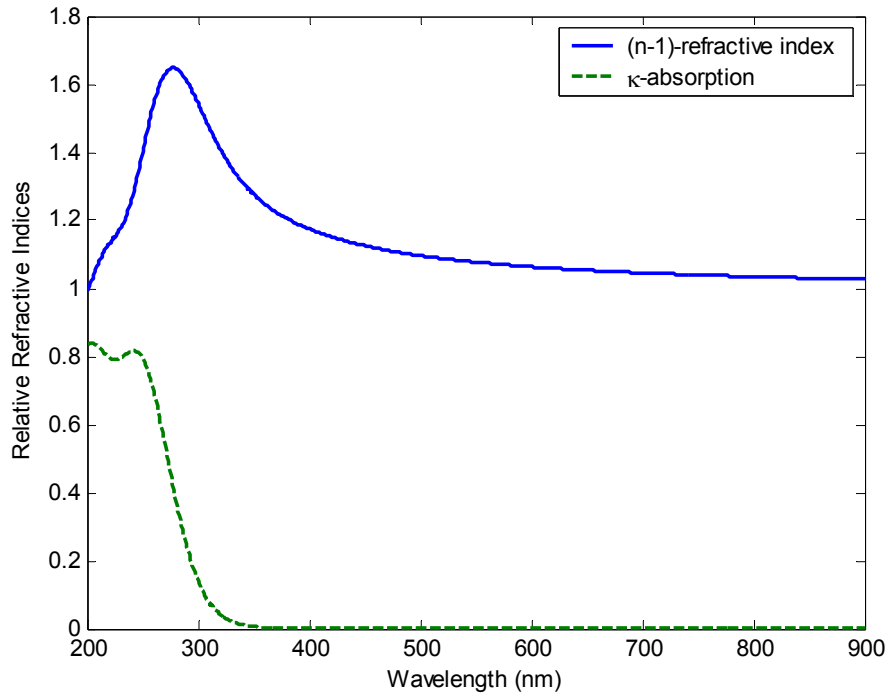*Figure B.4: Optical Properties for Polystyrene*

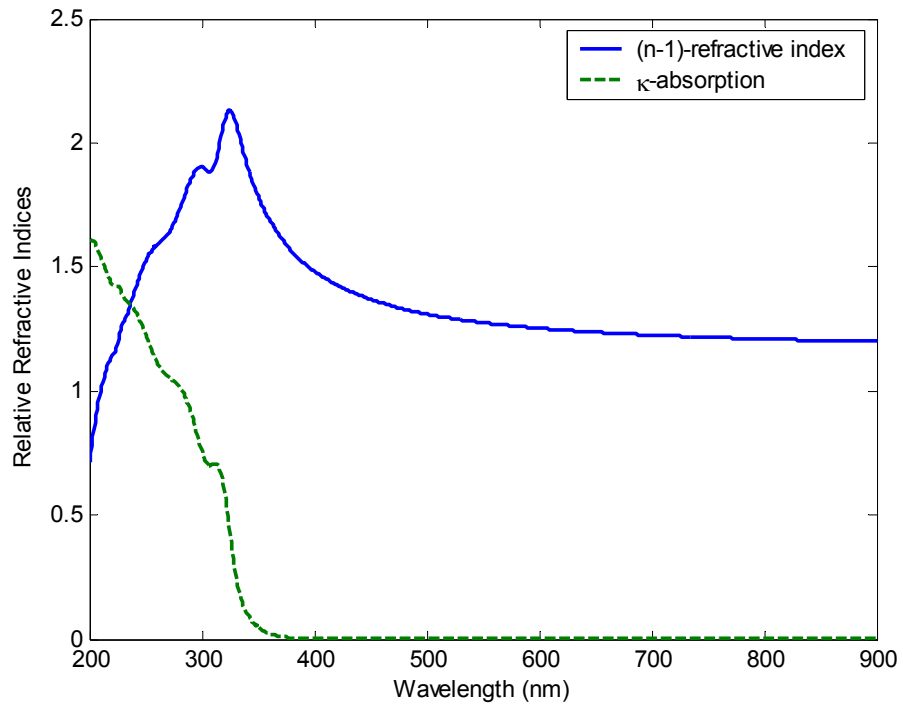Appendix B (Continued)

Figure B.5: Optical Properties of AgCl

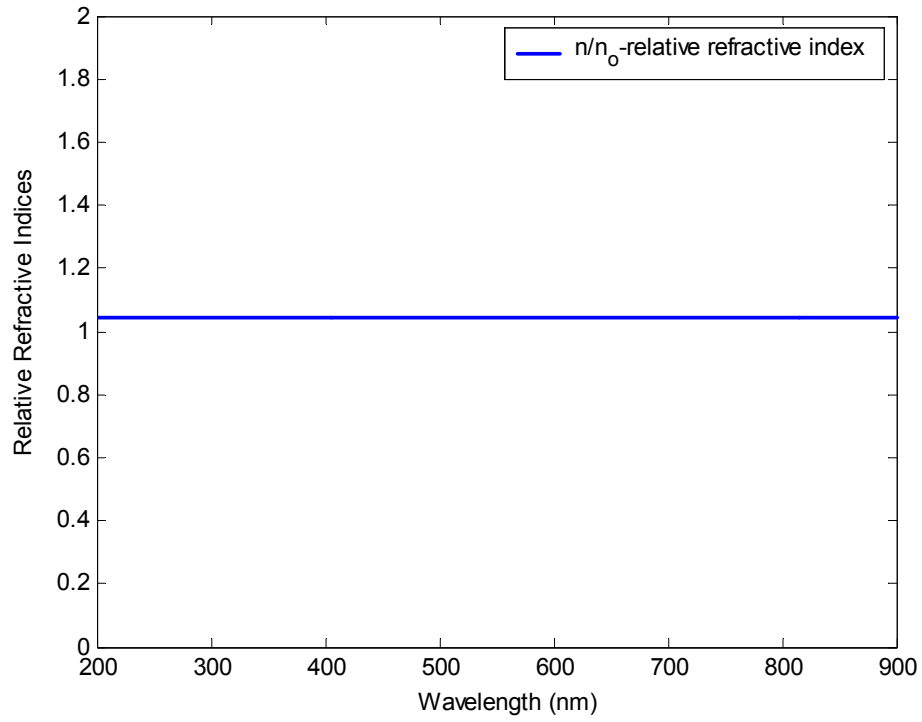*Figure B.6: Optical Properties of AgBr*

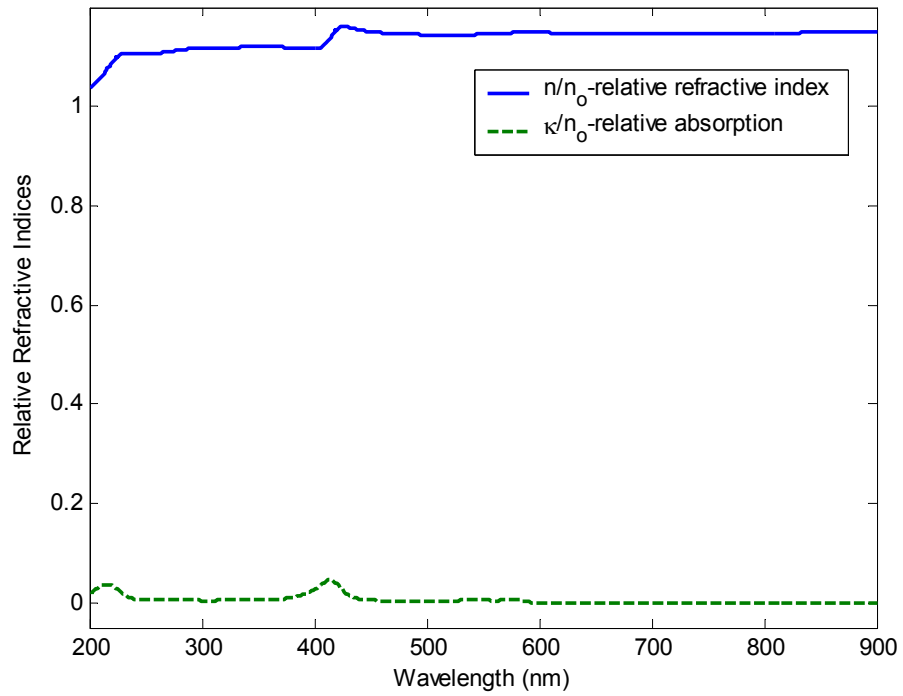*Figure B.7: Relative Refractive Index of Soft Body in Water*

Figure B.8: Relative Refractive Index of Hemoglobin in Water

Appendix B (Continued)
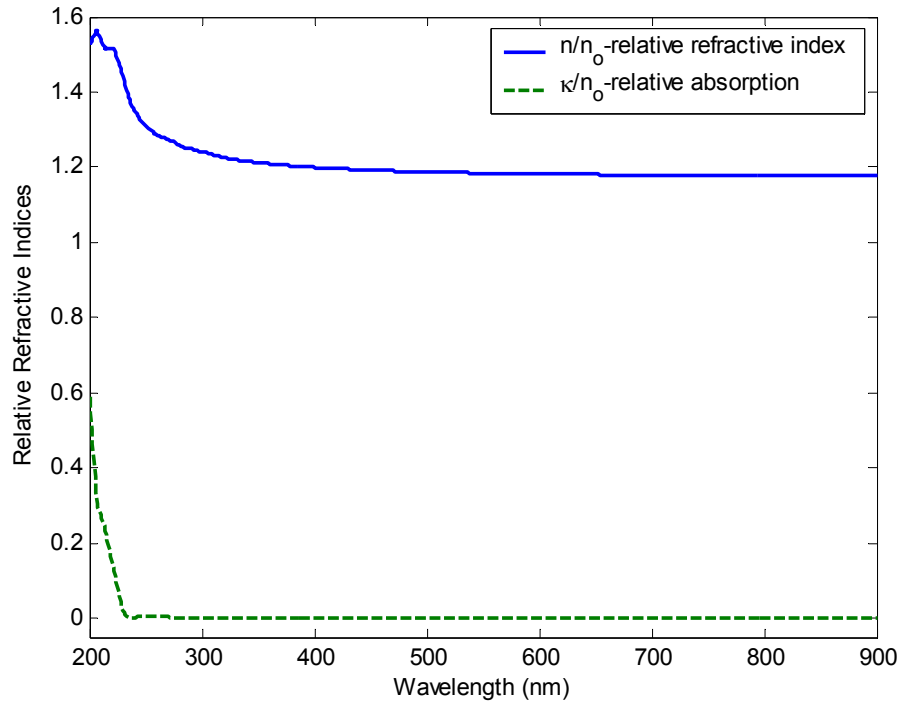

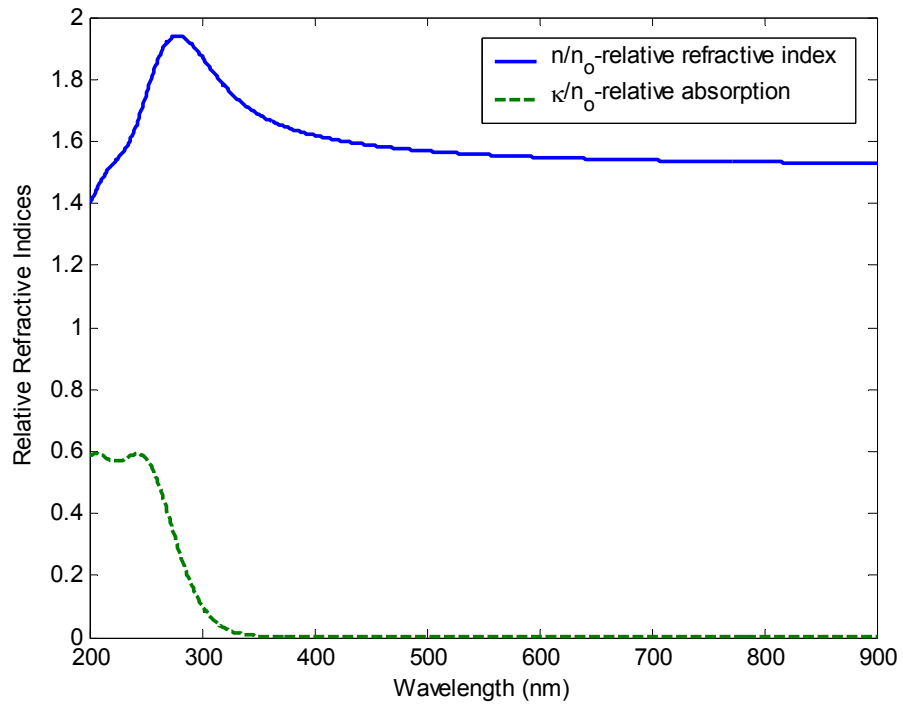*Figure B.9: Relative Refractive Index of Polystyrene in Water*

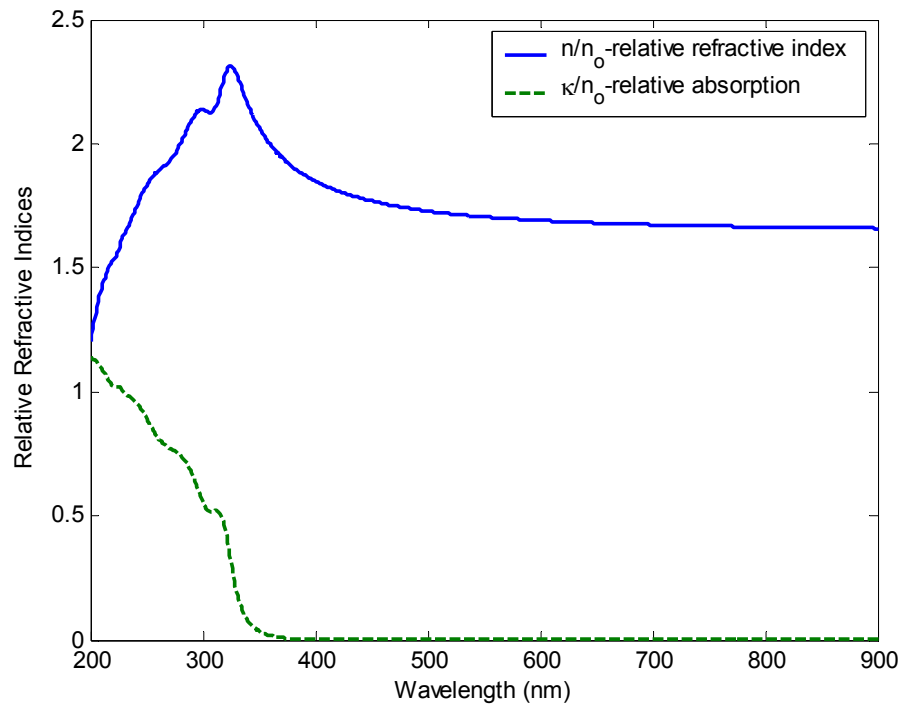*Figure B.10: Relative Refractive Index AgCl in Water*

96

Figure B.11: Relative Refractive Index of AgBr in Water

Appendix C: Validation for Rayleigh-Debye-Gans Theory

A validation study for the Rayleigh-Debye-Gans theory was conducted, here RDG was programmed and tested against Mie theory. The range of particle diameters was chosen between 25 nm -500 nm. The simulation parameters used to define the suspensions for the transmission calculations are: light source wavelength 200-900nm, particle concentration 1E-4 g/cc, particle density 1g/cc.

C.1 Validation of Rayleigh-Debye-Gans Theory

The limits of applicability of RDG theory are established by the approximations made in its derivation (each volume element behaves as a Rayleigh scatterer and there is no phase shift through the particle) which require that $n/n_0 \cong 1$ and $d \leq \lambda$, where d is the diameter of the particle. Because our analysis is for the Uv-vis-NIR (Near infrared) spectrum (190-900 nm), it is impossible to simultaneously satisfy both conditions at every wavelength. Prior to any detailed study it is important to validate the software implemented for Rayleigh-Debye-Gans theory as a function of the wavelength, and to explore the behavior of the calculated spectra relative to a reference material.

Under the conditions of applicability of RDG, both Mie theory and RDG theory should yield the same results. Polystyrene is a reference material with known wavelength-dependent optical properties that is used in the manufacturing of spherical particles used as standards for particle analysis. Comparison of the turbidity spectra calculated with RGD and Mie for polystyrene particles suspended in water should provide a good indication of when the spectra deviate, and the theories no longer agree to an acceptable level.

Appendix C (Continued)

The diameter sizes chosen were 25 nm, 50 nm, 100 nm, and 500 nm. The calculated spectra have been plotted on a semilog axis to better illustrate the differences between theories. Figures C.1 and C.2 demonstrate the expected close approximation of Rayleigh-Debye-Gans to Mie theory for small sized particles. Figures C.3 and C.4 show divergences of Rayleigh-Debye-Gans approximation from Mie as the particle size increases while maintaining the optical properties within the limits of the theory. Appendix B shows the optical property requirements of RDG are met as functions of wavelength for polystyrene. These results demonstrate that the programs developed for Rayleigh-Debye-Gans theory yield the expected values when compared with Mie theory and that the software developed can be reliably used for the simulations reported herein.
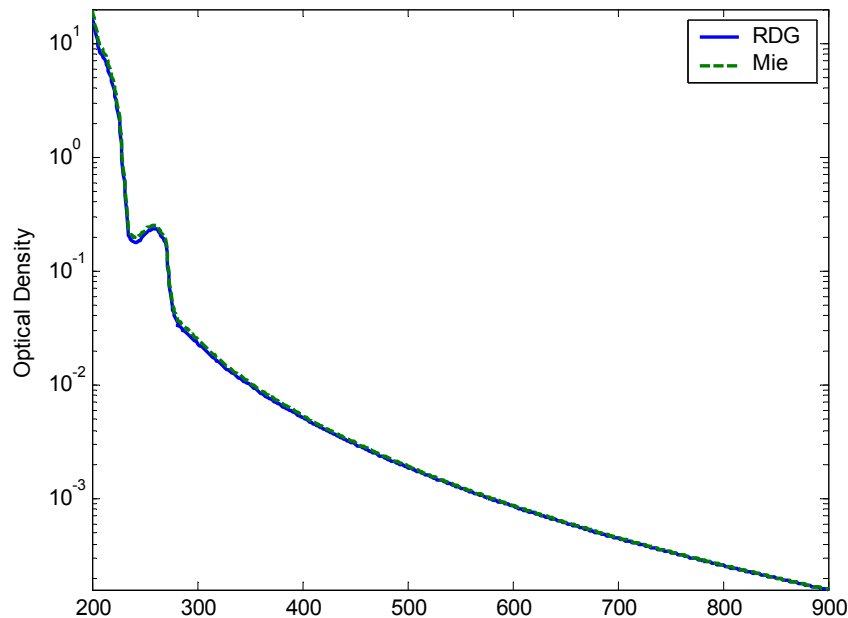
Figure C.1: Calculated Transmission of Mie and Rayleigh-Debye-Gans for a Suspension of 25 nm Polystyrene Spheres
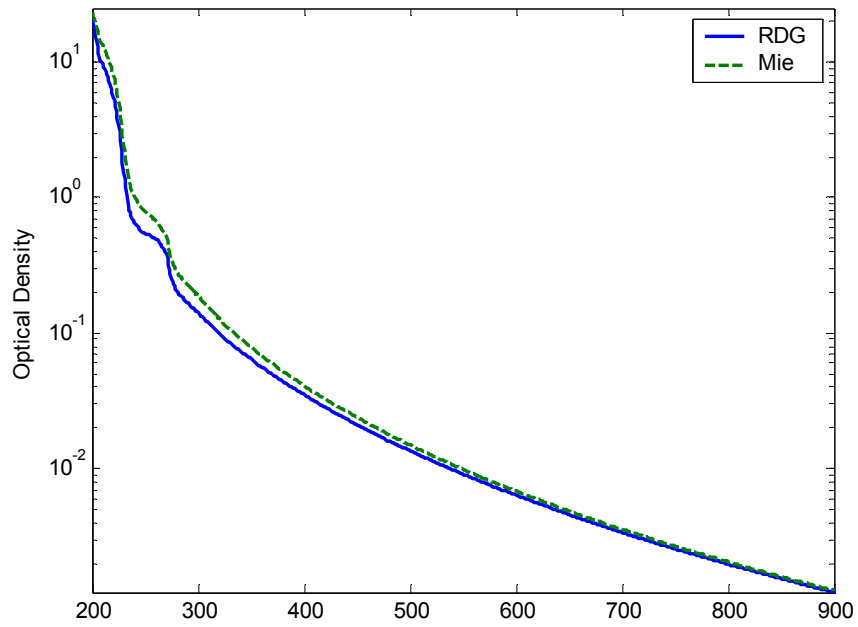
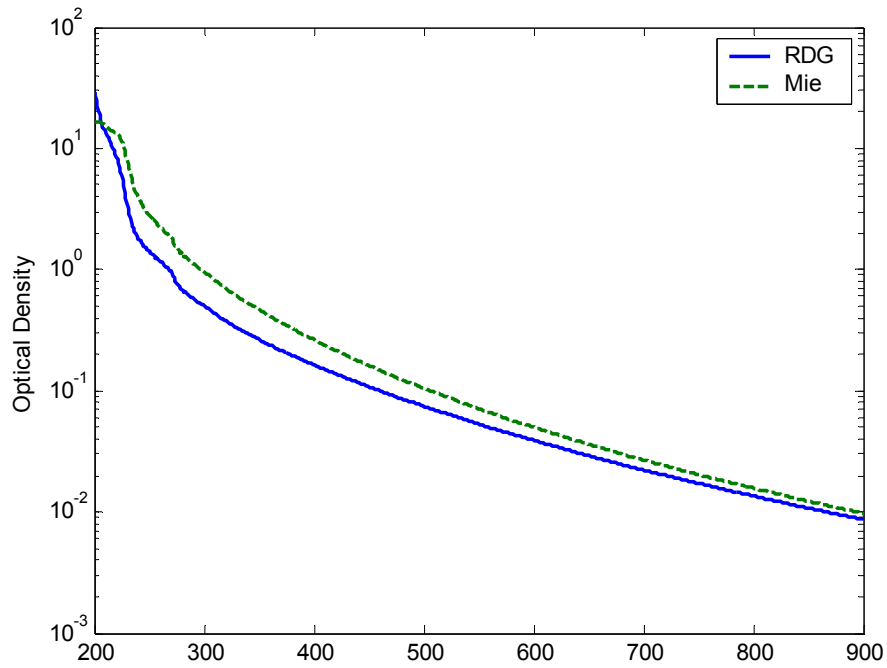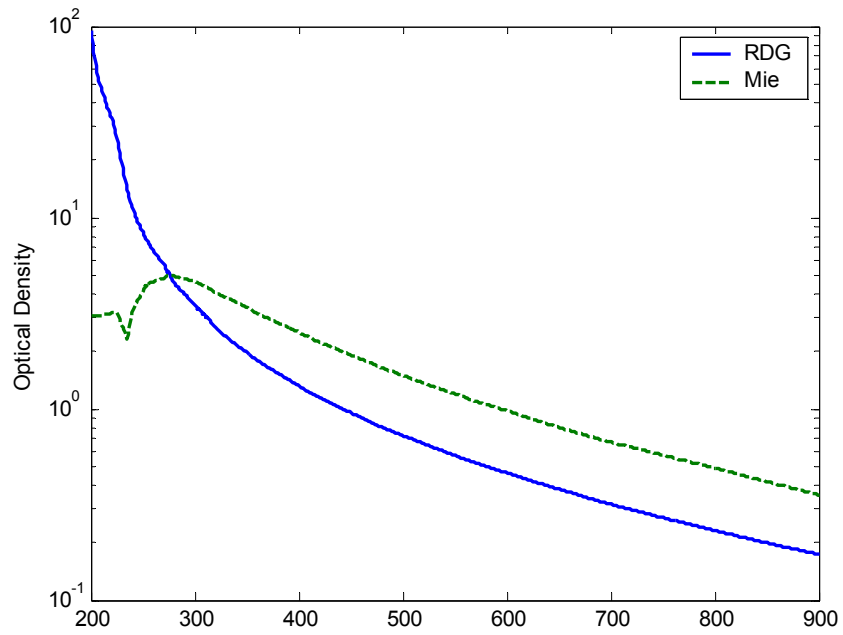*Figure C.2: Calculated Transmission of Mie and Rayleigh-Debye-Gans for a Suspension of 50 nm Polystyrene Spheres*

Figure C.3: Calculated Transmission of Mie and Rayleigh-Debye-Gans for a Suspension of 100 nm Polystyrene Spheres

Figure C.4: Calculated Transmission of Mie and Rayleigh-Debye-Gans for a Suspension of 500 nm Polystyrene Spheres

Appendix D: Estimation of Absorption Coefficient and Hypochromism Model

The absorption coefficient κ is the imaginary value of the refractive index. A mathematical derivation given by Maron [10], on the absorption of radiation as a function of thickness and concentration of absorbing material, describes how the absorption coefficient can be obtained. The decrease in intensity of incident light of any wavelength passing through an absorbing substance is given by Lambert's law. The law states that the rate of decrease of intensity with thickness of absorbing material is proportional to the intensity of the light at point l,

$$\frac{-dI_x}{dl} = \kappa I_t \qquad \text{D.1}$$

where I_t is the intensity at thickness l and κ is the absorption coefficient characteristic of the medium. The original intensity I_o, is given at $l=0$ and the intensity at any point l can be found from the equation above. Thus we can obtain

$$\int_{I_o}^{I_t} \frac{dI_t}{dl} = \int_{l=0}^{l=l} -\kappa dl$$

$$\ln \frac{I_t}{I_o} = -\kappa d \qquad \text{D.2}$$

$$\frac{I_t}{I_o} = e^{-\kappa d} \qquad \text{D.3}$$

Accordingly, $\ln I_t$ falls off linearly and I_t exponentially, with the distance l the light travels through the absorbing medium. In the case of absorbing solutes the decrease in intensity with l is proportional only to I_t and the concentration of the solution C.

$$-\frac{dI_t}{dl} = \varepsilon I_t C \qquad \text{D.4}$$

Appendix D (Continued)

where ε is the molar absorption coefficient which is a proportionality constant determined

by the nature of the absorbing solute and the wavelength used. Integrating the equation

above using the same limits as those in equation D.2 results in the following expression:

$$-\int_{I_o}^{I_t}\frac{dI_t}{I_t} = \int_{l=0}^{l=l}\varepsilon C dl$$

$$\ln\frac{I_t}{I_o} = -\varepsilon C l$$

D.5

$$\frac{I_t}{I_o} = e^{-\varepsilon C l}$$

D.6

Equation D.5 and D.6 are the expression of Beer's law for absorption of light by

solutions. These two laws can be combined to form Beer-Lambert law which says the

absorbance is directly proportional to the pathlength and the concentration. This law is

stated as equation D.5, however the absorbance and the complex refractive index are

coupled through the absorptivity

$$\varepsilon = \frac{4\pi\kappa}{\lambda}$$

D.7

Through a transmission measurement and the use of equations D.5 and D.7 the

absorption coefficient can be calculated. This only holds for homogeneous solutions,

otherwise scattering has to be considered.

Appendix D (Continued)

D.1 Hypochromism Model

Hypochromism was quantified using the model developed by Vekshin [11,12]. Vekshin's model describes screening of chromophores when stacked along the molecular chain axis, see figure below.
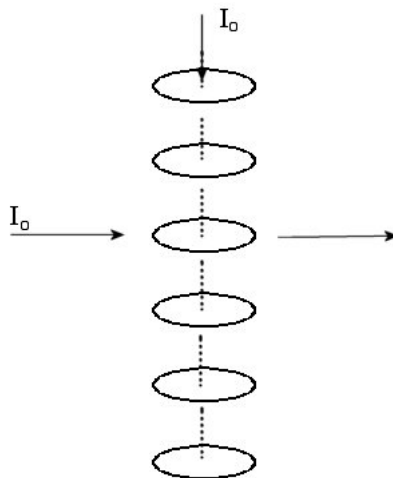
Figure D.1: Stack Arrangement of Chromophores along Chain Axis

Experimentally the hypochromism value h at a given wavelength is defined by:

$$h = 100\% \frac{\varepsilon - \hat{\varepsilon}}{\varepsilon}$$

D.8

where ε is the extinction coefficient for the situation of single chromophore in units of $1/M\,cm$ and $\hat{\varepsilon}$ is the average extinction coefficient to account per 1 chromophore. From the screening model [12,13]

$$\hat{E} = \frac{s}{2.3qk}\left(1 - \left(1 - 2.3\frac{Eq}{s}\right)^{k}\right) [=]\mathring{A}^2$$

D.9

This equation predicts the hypochromic extinction coefficient in a solution of stack chromophores (cluster) if the values $E, s, q,$ and k are known. E is in units of molecular

104

Appendix D (Continued)

extinction coefficients ($Å/molecule$) which is function of wavelength, $\hat{E}$ is the average

extinction coefficient, s is the effective geometric area of a chromophore ($Å^2$), q is the

orientation factor, and k is not to be confused with the wave number but rather is the

quantity of chromophores.

Transforming Vekshin's model from units $1/M\,cm$ to $Å$ results in rewriting the

above equation to

$$\hat{\varepsilon}_m = \frac{s}{2.3qk} N_A \left[1 - \left(1 - 2.3\frac{Eq}{s6.022E4} \right)^k \right] \qquad \text{D.10}$$

where N_A is Avogadro's number. Equation D.10 can now be used to correct the

imaginary component of the refractive index by first calculating the extinction coefficient

using equation D.7. The extinction coefficient is then transformed to molar units

$$\varepsilon_m = \frac{\varepsilon M_w}{V} \qquad \text{D.11}$$

where M_w is the molecular weight of the particle and V is the unit volume transformation

of 1000 cm³/L. The number of chromophores k, is solved through the volume fraction or

concentration of the sample

$$k(\lambda) = \frac{v_f \lambda}{d} \qquad \text{D.12}$$

where v_f is the volume fraction, λ is the wavelength, d is the diameter of the sample. The

probability of absorption of a photon by a molecule P can be presented as

$$P = 2.3\frac{q\dot{E}}{s} \qquad \text{D.13}$$

Appendix D (Continued)

$$\dot{E} = \frac{\varepsilon_m V * (1E8)^2}{Na}$$

D.14

where $\dot{E}$ is the calculated value from equation D.9. Vekshin's screening equation can

therefore be written in the following form

$$\hat{\varepsilon}_m = \frac{N_A s}{V \, 1E8^2 \, k \, \dot{E} \, q} \left[1 - (1 - p)^k \right]$$

D.15

where the extinction coefficient for one chromophore is calculated by

$$\hat{\varepsilon} = \frac{\hat{\varepsilon}_m V}{M_w}$$

D.16

From this, the hypochromicity can be calculated using equation D.8. The corrected

imaginary part of the refractive index κ_c can be solved for using the following equation

$$\kappa_c = \frac{\hat{\varepsilon} \lambda}{4\pi}$$

D.17

About the Author

Alicia C. Garcia-Lopez was born in Hamilton, Ontario Canada. She came to the United States in 1984 and attended the local schools in Tampa, Florida. Alicia attended University of South Florida and received her bachelors in Chemical Engineering in 1998 and her masters in Chemical Engineering in 2001. Alicia's keen interest in the science and mathematics combined with interest in problem solving and the desire to learn new subjects lead her to pursue a PhD in Electrical Engineering. Her other interests and hobbies enjoyed, besides pursuing a PhD, are learning foreign languages, hiking, camping, cycling, climbing, running and traveling.